Forschungszentrum Karlsruhe
Technik und Umwelt

Wissenschaftliche Berichte
FZKA 6567

Investigation of In-vessel Core Degradation for the European Pressurised Water Reactor with SCDAP/RELAP5 mod 3.2

W. Hering

Institut für Reaktorsicherheit
Programm Nukleare Sicherheitsforschung

März 2001

Forschungszentrum Karlsruhe GmbH
Postfach 3640, 76021 Karlsruhe

Mitglied der Hermann von Helmholtz-Gemeinschaft
Deutscher Forschungszentren (HGF)

ISSN 0947-8620

Forschungszentrum Karlsruhe
Technik und Umwelt

Wissenschaftliche Berichte
FZKA 6567

Investigation of In-vessel Core Degradation for the European Pressurised Water Reactor with SCDAP/RELAP5 mod 3.2

W. Hering

Institut für Reaktorsicherheit

Programm Nukleare Sicherheitsforschung

Forschungszentrum Karlsruhe GmbH, Karlsruhe
2001

Abstract

In the Forschungszentrum Karlsruhe (FZK) the Institute for Reactor Safety (IRS) performed accident analyses for the European Pressurised Water Reactor (EPR) by plant calculations with SCDAP/RELAP5 mod 3.2 (S/R5) and RELAP5 (R5). The calculations were performed up to spring 2000 with an EPR agreed by to Siemens/KWU.

S/R5 calculations have been performed for a surge line rupture (SL), a loss-of-offsite power (LOOP), and a 46 cm² small break loss of coolant accident (SBLOCA). Furthermore, LOOP reflood calculations were performed at various core states varying between 1900 K and 2880 K peak core temperature.

Generally all calculations were performed up to contact of an in-core molten pool with the EPR specific heavy reflector. The code fails during relocation into the water-filled lower plenum. Actually, the simulation of the following accident phase, including estimation of fuel coolant interactions, is not possible with S/R5. The state of the corium in the molten pool as well as hydrogen source term have been calculated for various cases of the scenarios mentioned above.

Untersuchung der Schadensausbreitung im Reaktordruckbehälter für den Europäischen Druckwasserreaktor mit SCDAP/RELAP5 mod 3.2

Kurzfassung

Im Institut für Reaktorsicherheit (IRS) des Forschungszentrums Karlsruhe (FZK) wurden bis Frühjahr 2000 Unfallanalysen für den European Pressurised Water Reactor (EPR) mit SCDAP/RELAP5 mod 3.2 und RELAP5 durchgeführt. Das EPR Inputdeck enthielt alle Anlagenverbesserungen entsprechend der Vorgaben von Siemens/KWU.

Mit S/R5 wurden Unfallanalysen für folgende Szenarien durchgeführt: Abriss der Druckhalterleitung (SL), Ausfall der Wechselstromnetze (LOOP), und kleines Leck (46cm² SBLOCA). Ferner wurden für das LOOP Szenario Rechnungen zum verzögerten Wiederfluten der Kernes durchgeführt, wobei der Flutzeitpunkt variiert wurde zwischen 1900 K und 2800 K Maximaler Kerntemperatur.

Im allgemeinen rechnete S/R5 bis zum Kontakt des Schmelzepools im Kern mit dem EPR spezifischen “Heavy reflector”. Der Code versagt während der nachfolgenden Verlagerung in das wassergefüllte untere Plenum. Derzeit ist eine Simulation der dabei auftretenden Phänomene wie z.B. die Schmelze Wasser Wechselwirkung mit SCDAP/RELAP5 nicht möglich. Daher wurden die Rechnungen nicht weitergeführt. Es wurden der Zustand des Coriums im Kern, die Temperaturen der Einbauten des Reaktordruckbehälters und der Wasserstoffquellterm für verschiedene Fälle der o.g. Szenarien berechnet.

Table of Contents

List of Figures

List of Tables

Symbols/Abbreviations

AEAT	AEA, Technology, Oxfordshire, UK
ACCU	Accumulator, Druckspeicher
AMM	Accident Management and Mitigation
BDBA	Beyond Design Basis Accident
BDOP	Basic Design Optimisation Phase
BOC	Begin of Cycle
CB	Core Barrel
CSC	Control rod drive support columns
DBA	Design Basis Accident
DC	Downcomer
ECC	Emergency Core Cooling
EFWS	Emergency Feedwater System
EOC	End of Cycle
EPR	European Pressurized Water Reactor, http://www.siemens.de/kwu/e/foa/n/products/s11.htm

FE	Fuel Element
FEM	Finite Element Methode
FLECHT	Full Length Emergency Cooling Heat Transfer (Westinghouse), USA
FLECHT-SEASET	Full Length Emergency Cooling Heat Transfer - Separate Effects and System Effects Test (Westinghouse)
FZK	Forschungszentrum Karlsruhe, Technik und Umwelt, http://www.fzk.de/FZK2
HR	Heavy Reflector, EPR
HS	RELAP5 heat structure
INEEL	Idaho National Engineering and Environmental Laboratory, Idaho Falls, USA
IRS	Institut für Reaktorsicherheit, http://hikwww4.fzk.de/irs/organisation/IRS1/irs1_home.html
IRWST	In-containment Refuelling Water Storage Tank
ISS	Innovative Systems Software, USA, http://www.relap.com/.
KWU	Kraftwerk Union, Erlangen, Power Generation Group of Siemens AG, Germany, http://www.siemens.de/kwu
LBLOCA	Large Break Loss Of Coolant Accident
LCSP	Lower Core Support Plate
LOCA	Loss Of Coolant Accident
LOFT	Loss Of Fluid Test (Idaho National Engineering Laboratory, USA)
LOOP	Loss of On-site and Off-site Power (station black-out)
LWR	Light Water Reactor
MAAP	Modular Accident Analysis Program
MFWS	Main Feed Water System
MHSI	Medium Head Safety Injection
MSIV	Main Steam Isolation Valve
MSRV	Main Steam Relieve Valve
MSSV	Main Steam Safety Valve
NEPTUN	DBA Reflood test facility at PSI, http://pss100.psi.ch/~aubert/NEPTUN.html
PCT	Peak Core Temperature
PSA	Probabilistic Safety Assessment
PSD	Primary system depressurisation
PSF	Projekt nukleare Sicherheitsforschung, FZK, http://psf-nt-server.fzk.de/psfhome.htm
PSI	Paul Scherrer Institut, Würenlingen, Schweiz, http://pss100.psi.ch/~aubert/LTH.html
PWR	Pressurised Water Reactor
PZR	Pressurizer system
QUENCH	Research programme at FZK, focussed on investigations on material behaviour during LWR reflood conditions: http://imf1-wt-server.fzk.de/quench/

RS	Reactor shut down, reactor scram
RCP	Reactor Coolant pump
RELAP5	old: Reactor Excursions and Leak Analysis Program, presently: Reactor Leak and Analysis Program, for LWR transients and SBLOCA, http://www.nrc.gov/RES/RELAP5/
RCS	Reactor coolant system
RCSL	Reactor Control, Surveillance and Limitation System
RPV	Reactor Pressure Vessel
SBLOCA	Small break LOCA
SCD	Severe Core Damage
SCDAP	Severe Core Damage Analysis Package, (USNRC code, developed at INEEL), http://relap5.inel.gov/scdap/home.html
SCDAP/RELAP5	Coupled SCDAP and RELAP5 code to simulate reactor conditions up to SFD conditions
SDTP	SCDAP Development and Training Program of ISS http://www.sdtp.org/
SFD	Severe Fuel Damage
SG	Steam Generator
SAMG	Severe accident mitigation guidelines
SIS	Safety Injection System
TMI-2	Three Mile Island Unit 2, Mitigated SFD accident, http://www.libraries.psu.edu/crsweb/tmi/tmi.htm
UH	Upper head
UCP	Upper core plate
UP	Upper Plenum
UPS	Upper Plenum Structure model, dedicated models in S/R5 mod3.2
USP	Upper support plate
USNRC	United States Nuclear Regulatory Commission, http://www.nrc.gov, USNRC-Codes (Research): http://www.nrc.gov/RES/rescodes.html

(Remark: URL-Addresses valid January 2001)

1 INTRODUCTION

As part of the trilateral contract between German utilities, Siemens Power generation group and Forschungszentrum Karlsruhe (FZK) in-vessel accident analyses were performed for the European Pressurised Water Reactor (EPR) at Institute for Reactor Safety (FZK/IRS). The EPR is under development of the bilateral consortium of Framatome (France) and the Power Generation Group of Siemens AG (Germany). The analyses were performed using the USNRC best estimate code system SCDAP/RELAP5 mod 3.2 (S/R5) /1/. The results of the analyses are used for comparison with those calculated by MELCOR /2/ and MAAP /3/.

In total three different accident scenarios plus one series of reflood calculations were investigated as indicated in Table 1.1. These scenarios are considered to be representative to investigate accident sequences leading to severe core damage:

1. rupture of the largest pipe connected to the hot leg of main coolant pipe was selected: surge line rupture (SL, section 3),
2. a small break loss of coolant accident scenario with a 46 cm² leak in the cold leg (SBLOCA, section 4),
3. a station black-out scenario, called Loss of Offsite Power (LOOP, section 5), and
4. delayed core reflood in case of LOOP scenario (section 6), an extension of previous work /4/. For reflood analyses the PSI-reflood model and the improved FZK-Chen-correlation /5/ were activated.

Table 1.1 Brief summary of all starting conditions for the different scenarios which were analysed with S/R5 to allow for comparison with other code calculations.

Initial events	Leak size (cm²)	Leak-Position	2nd side cooldown	2nd side manual cooldown	EFWS	RCS depress	ECC-activation
Surge line rupture	951	hot leg 1	6.0 MPa	No	Yes	3 valves	No
SBLOCA	46	cold leg	6.0 MPa	Yes / No	No/Yes	No	No
Loss of off-site power	----	----	6.0 MPa	Yes / No	No	3 valves	No
LOOP re-flood	----	----	6.0 MPa	Yes / No	No	3 valves	4 LHSI or 4 MHSI

Main focus of the analyses is to determine the in-vessel damage progression including core and adjacent RPV structures such as heavy reflector (HR), upper core plate (UCP), upper plenum structures (UPS) as well as the lower core support plate (LCSP). Furthermore, reactor specific data are to be extracted for the QUENCH experiments at FZK/IMF. At least the long-term behaviour of the melt in the lower plenum has to be investigated by the dedicated SCDAP/RELAP5 FEM tool COUPLE.

2 PLANT REPRESENTATION

To investigate the EPR in-vessel conditions under severe core damage accidents the main components of the nuclear island shown Figure 2.1 have to be simulated using USNRC severe core damage code system SCDAP/ RELAP5 mod 3.2 (S/R5) /1/.

Essentially, S/R5 is composed of three parts, RELAP5 (R5), SCDAP (SCD), and Couple (CP), which allow to simulate the most significant components of the reactor coolant systems. The behaviour of the fluid in the primary, secondary, and (partially) containment system (Figure 2.3) is described by R5 1-D, 2-phase, 2-fluid thermohydraulic models including dedicated models for technical devices (pump, valve, separator ...). For all primary system and some secondary system pipes calculation of thermal and mechanical behaviour of fluid enclosures is realised. The most relevant parts of the EPR reactor control, surveillance and limitation (RCSL) system is simulated by R5 trip logic. The decay power representing UO_2 with 50% MOX loading plus 5% uncertainty is simulated by a R5 general table (Figure 2.8) and distributed over the core using fixed axial and radial power profiles (section 2.3).

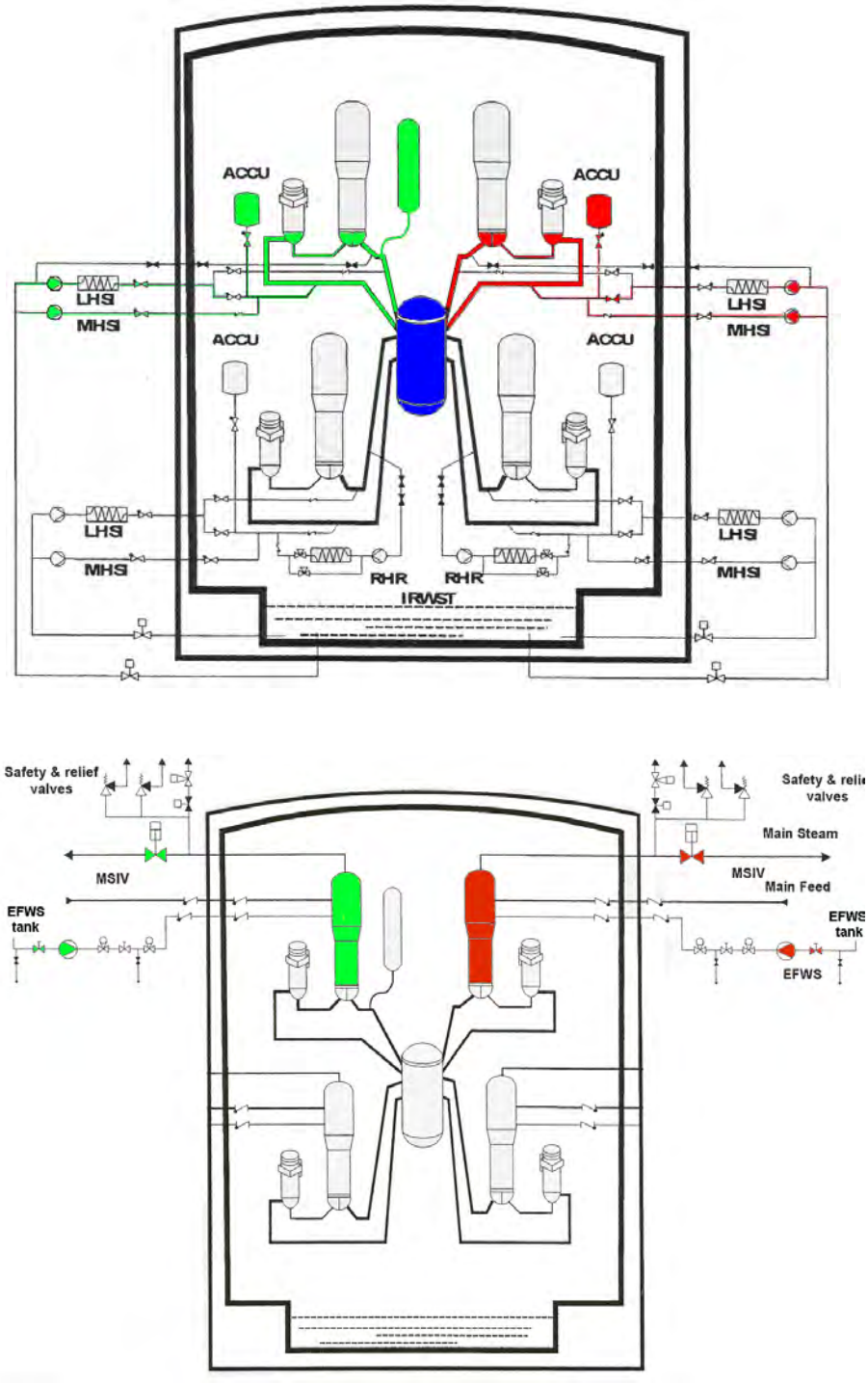

Figure 2.1 Simulated parts of the EPR nuclear island: primary systems (top) and secondary systems (bottom)

Presently the MOX property database in the MATPRO /1/ library is not completely validated, so that pure UO_2 material property data had to be used. In Figure 2.2 the S/R5 representation of reactor pressure vessel (RPV) structures is shown on the left side. R5 heat structures were used for upper dome wall, upper support structure, support columns, upper core plate (UCP), lower core support structure, and lower head wall. The new upper plenum structure (UPS) model of S/R5 was used for the UCP (section 2.4.1). The UPS allows to calculate melting of steel structures and melt relocation to the lowest supporting structure. At least the user can trigger steel melt relocation into the core region so that the steel melt can be added to the debris or molten pool.

The core behaviour including its radial enclosure, the heavy reflector (HR) and the core barrel (CB) is simulated by SCD components such as fuel rod, control rod, and shroud, respectively. The active core section is divided radially into five radial rings and 14 axial zones. In this study global ring to ring radiation heat exchange in the core was removed, because of an error reported by ISS /6/ in the radiation absorption module. The consequence of this code error, which occurs only if multitude fluid channels are imbedded in one radiation enclosure leads to an increased radiation absorption in the steam compared to reality, so that the core outlet temperatures are over-predicted.

To simulate the behaviour of debris or molten material in the lower plenum the Couple (CP) code was used with a fine mesh derived from stand-alone analysis /7/. In the present study no long term debris behaviour in the lower plenum could be studied due to code failure.

2.1 Reactor coolant system

In all scenarios investigated, one of the four loops behaves different compared to the others due to PZR connection, leak position, or EFWS activation. The three loops with nearly identical behaviour were simulated by one three-fold loop (Triple loop), so that the reactor coolant system could be represented by a 2 loop-model: one single loop and the triple loop.

2.1.1 Primary system

All pipes, the pressurizer and the RPV downcomer are connected to R5 heat structures (HS) to get information about heat-up behaviour during different phases of the accident. At the outside of the heat structures adiabatic boundary conditions and at the inner side standard convective heat transfer conditions are considered. To simulate realistically the pressure loss at various structures such as LCSP, UPC, and CSC in the upper plenum friction factors were derived from pressure differences delivered by Siemens/KWU and validated during steady state simulation.

2.1.1.1 Accumulator

Four accumulators are modelled each with a volume of 47 m^3 to avoid scaling problems in the accumulator injection lines for the Triple Loop. The water inventory amounts to 32 m^2 at 4.5 MPa. The surge line loss coefficient is given by $\zeta/A^2 = 1000\ m^{-4}$ /9/. With an cross section area of 0.038 m^2 a loss coefficient of about ζ=1.44 is calculated. The surge lines were not closed after accumulator emptying so that the driving gas nitrogen enters the primary system.

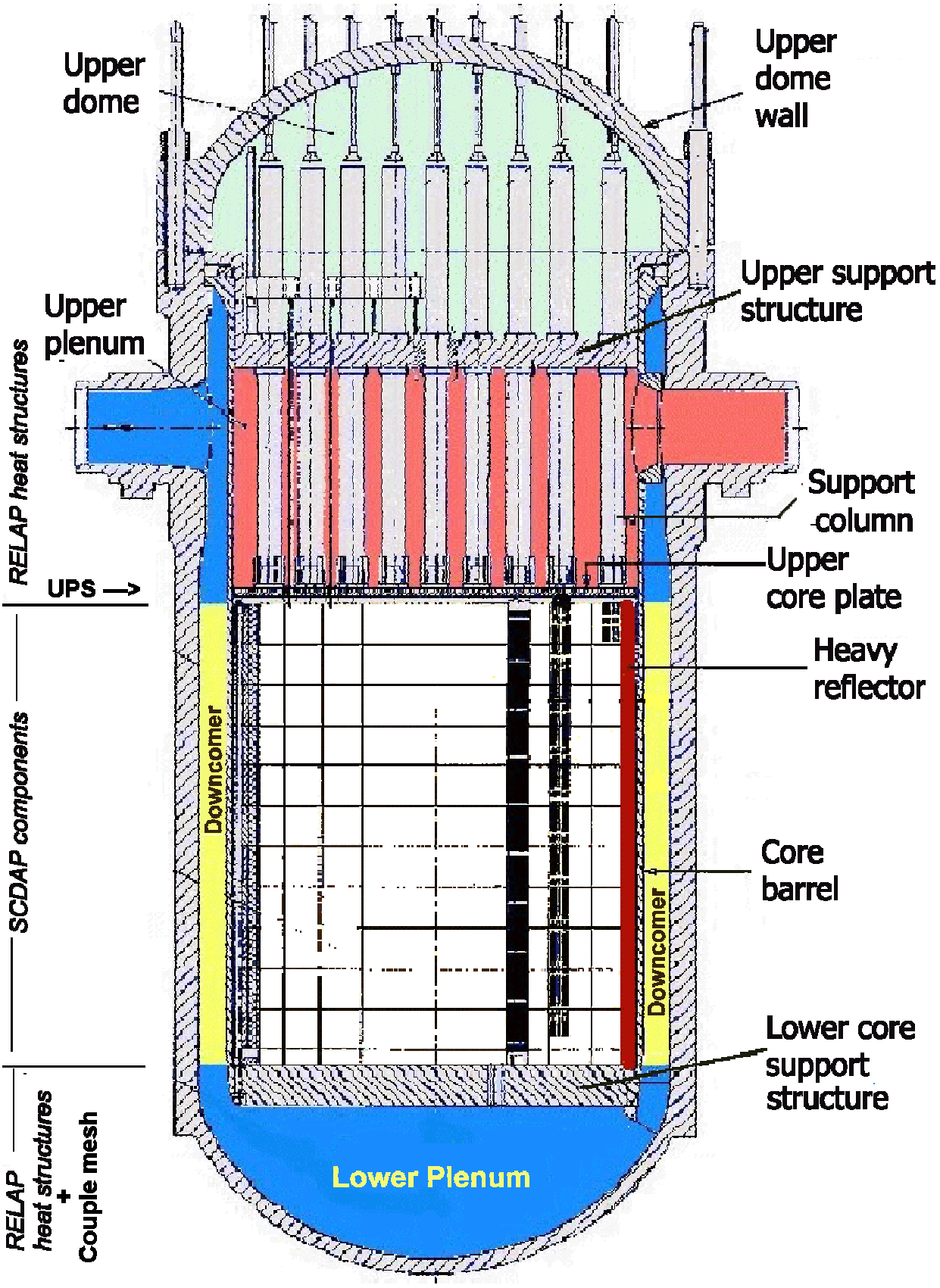

Figure 2.2 Schematics of the EPR reactor pressure vessel including all modelled internals as well as their representation by SCD components (core, HR, CB, cylindrical part of RPV wall), R5 heat structures, and the Couple FEM-mesh in the lower plenum.

The numerical problems occurring if more than one accumulator is connected to one RELAP5 volume were solved by connecting either the surge line of the three accumulators to different volumes along the cold leg of the triple loop or by using a threefold accumulator model.

2.1.1.2 Pressurizer

The pressurizer (PZR, Figure 2.3 #8xx) simulation is based on a nodalisation used for LOCA and DBA transient analyses at Siemens/KWU /8/. The PZR normally is connected to the single loop for LOCA and LOOP scenarios. The model consists of a detailed nodalisation for the surge line (net flow cross section 951 cm²) and the pressurizer tank including the wall as R5 heat structures.

In case of a surge line rupture scenario the junction to the primary circuit is realised by a valve, which is closed when the leak valves are opened (section 3). The simulation of the safety valves on top of the PZR (Figure 2.3) have been adapted to one pressure control valve (#814) which is closed following the reactor control, surveillance and limitation (RCSL) system to simulate the behaviour of the volume control system in the pressurizer in case of different scenarios. The three primary system safety valves with different activation pressure levels are simulated by two valves, because one valve is sufficient to control the system pressure in case of a scenario leading to system overpressure (e.g. LOOP) and in case of primary system depressurisation (PSD) all three valves are activated simultaneously.

To correctly represent the desired maximum steam flux of 83.3 kg/s for each safety valve the net cross section of the first motor-valve (#824) was adapted to 0.0028 m². It opens at 17.6 MPa and closes below 16.6 MPa. The opening time was assumed to be 10 s.

The second motor-valve (834) with a net cross section of 0.006 m² simulates the two dedicated safety valves with activation pressures of 18.0 MPa and 18.5 MPa opens automatically at 18.0 MPa. In the scenarios discussed in this study it is only activated in case of primary depressurisation (PSD). Both valves stay open after activation by the PSD command.

2.1.1.3 Main Coolant pump

The main coolant pumps, based on the original Siemens-RELAP5 (Siemens-R5) input deck, have been adapted to the EPR 4900 MW_{th} conditions. So the head as well as the mass flow rates have been adjusted during several steady state optimisation calculations. The steady state data were supplied from Siemens/KWU based on Siemens-R5 and MELCOR calculations.

2.1.1.4 Steam generator

The steam generator (SG) is divided into primary side volumes, composed of the inlet plenum, the heater tube bundle, and the outlet plenum, and the secondary side volumes which are discussed in section 2.1.2.1. The length of the heater tube bundle were extended to fit the primary/ secondary side heat transfer area of 8350 m². The pressure loss coefficients at heater tube entrance and exit were adapted to Siemens/ KWU data.

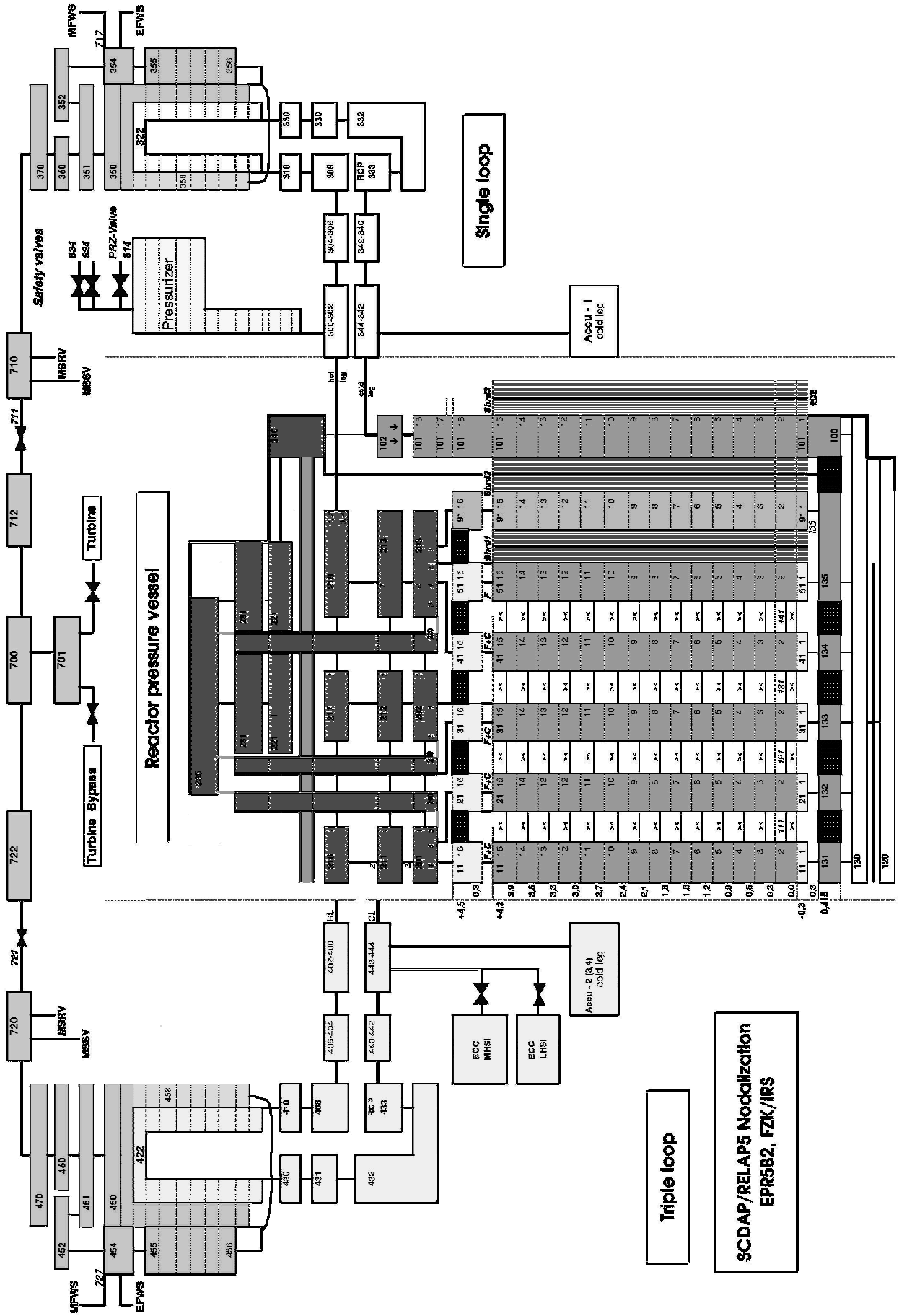

Figure 2.3 Reactor coolant system nodalisation based on two loop approach.

2.1.1.5 Safety Injection System

As part of the safety injection system (SIS) the emergency core cooling (ECC) system mainly is composed of four Medium Head Safety Injection (MHSI) and four Low Head Safety Injection (LHSI) systems. In this study the behaviour of the core is under consideration only so that all ECC systems could be connected to the cold leg of the Triple Loop. The injection systems are modelled using time dependent volumes and junctions to allow simulation of pressure dependent injection rates as shown in Figure 2.4 /4/. The results of reflood calculations with S/R5m32 are documented in section 2. No delay is simulated between actuation and onset of pump feed in.

2.1.2 Secondary system

The type of secondary system simulation was maintained from the Siemens-R5 input deck used for calculation with S/R mod 3.1 /4/. The secondary system components shown in Figure 2.3 can be divided into two categories:

- Normal operation:
  only required to achieve steady state conditions, i.e. main feed water system (MFWS), main steam line components (MSRV, MSIV, and MSSV valves), turbine and turbine by-pass to the condensor, which simulates the pressure boundary condition.
- Transient analyses:
  steam generator, emergency feedwater system, time dependant pressure boundaries, etc. are mainly required for transient analyses.

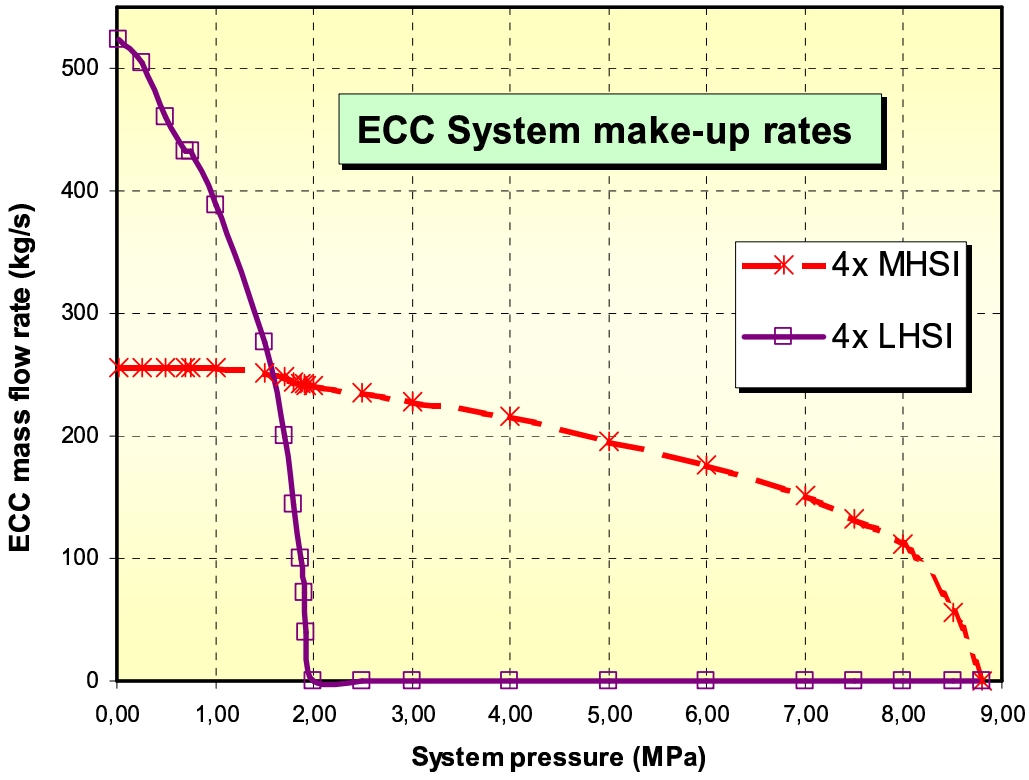

Figure 2.4 Water injection rate of MHSI (dashed line) and LHSI (solid line) system.

2.1.2.1 Steam generator

The maximum secondary system pressure is limited by steam generator (SG) relief valves to 9.15 MPa. Therefore, the SG safety valves which open at 10.0 MPa need not be considered here. A controlled secondary side depressurisation with a cool-down rate of 100 K/h down to 6.0 MPa is initiated automatically by the reactor control, surveillance and limitation (RCSL) system if the primary pressure drops below 11 MPa (section 2.5). This is realised using the time dependant back pressure volume for the safety valves. Furthermore, manual depressurisation to 0.2 MPa is simulated 1800s after reactor scram signal by opening the SG valves. The outlet of SG safety valves are connected to the environment.

The secondary side SG volumes are extended axially according to the increased length of the heater tube bundle to increase secondary side water inventory required to achieve sufficient time margins before SG dry-out occurs. Furthermore, the boiler cavity was split into a pipe connected to the riser part of the heater tubes (358) and one to the downcomer part (350). The lowest volumes of both pipes are connected to secondary side SG downcomer as sketched out in Figure 2.3. This reflects more realistically the orifice in the wall separating riser and downcomer section of the heater tube bundle.

2.1.2.2 Emergency feedwater system

In this study the EFWS is necessary for SBLOCA scenario only assuming that at least one X-diesel is available to generate sufficient electric power for one EFWS pump. The simulation of the EFWS pump rate is controlled proportional to the secondary side water level in the SG. This is realistic because the EFWS is deactivated if the water level exceeds 16.0 m. EWFS is activated by the trip logic for the SBLOCA scenario with a delay of 50 sec. The fluid temperature was set to 323 K at the SG entrance.

2.1.2.3 Containment volumes

The containment pressure is set stationary to 0.2 MPa for the whole transient. The containment model is composed of several volumes which allows the coupling of different leak or valve positions to one containment boundary pressure. This inhibits unphysical boundary conditions e.g. in case of the SBLOCA scenario when the leak and the primary system depressurisation both expel steam directly into the containment. No heat structures are connected to the containment volume because of R5 difficulties in case of condensation.

2.2 Core representation

The reactor core (Figure 2.3) is divided axially into 16 zones, 14 zones representing the active core, each 0.3 m high. In radial direction five rings (Figure 2.5) plus a bypass channel in the heavy reflector allow detailed analyses even in the late phase of severe core damage accidents. Cross flow junction located between adjacent rings at each elevation allow a certain 2-D flow redistribution in the core i.e. in case of flow path blockages due to debris or molten pool.

The number of fuel rods and control rods represented in each ring by one representative SCDAP component are listed in Table 2.1. In this study the input deck Ex5C2 was used which has a

2.1.2.1 Steam generator

The maximum secondary system pressure is limited by steam generator (SG) relief valves to 9.15 MPa. Therefore, the SG safety valves which open at 10.0 MPa need not be considered here. A controlled secondary side depressurisation with a cool-down rate of 100 K/h down to 6.0 MPa is initiated automatically by the reactor control, surveillance and limitation (RCSL) system if the primary pressure drops below 11 MPa (section 2.5). This is realised using the time dependant back pressure volume for the safety valves. Furthermore, manual depressurisation to 0.2 MPa is simulated 1800s after reactor scram signal by opening the SG valves. The outlet of SG safety valves are connected to the environment.

The secondary side SG volumes are extended axially according to the increased length of the heater tube bundle to increase secondary side water inventory required to achieve sufficient time margins before SG dry-out occurs. Furthermore, the boiler cavity was split into a pipe connected to the riser part of the heater tubes (358) and one to the downcomer part (350). The lowest volumes of both pipes are connected to secondary side SG downcomer as sketched out in Figure 2.3. This reflects more realistically the orifice in the wall separating riser and downcomer section of the heater tube bundle.

2.1.2.2 Emergency feedwater system

In this study the EFWS is necessary for SBLOCA scenario only assuming that at least one X-diesel is available to generate sufficient electric power for one EFWS pump. The simulation of the EFWS pump rate is controlled proportional to the secondary side water level in the SG. This is realistic because the EFWS is deactivated if the water level exceeds 16.0 m. EWFS is activated by the trip logic for the SBLOCA scenario with a delay of 50 sec. The fluid temperature was set to 323 K at the SG entrance.

2.1.2.3 Containment volumes

The containment pressure is set stationary to 0.2 MPa for the whole transient. The containment model is composed of several volumes which allows the coupling of different leak or valve positions to one containment boundary pressure. This inhibits unphysical boundary conditions e.g. in case of the SBLOCA scenario when the leak and the primary system depressurisation both expel steam directly into the containment. No heat structures are connected to the containment volume because of R5 difficulties in case of condensation.

2.2 Core representation

The reactor core (Figure 2.3) is divided axially into 16 zones, 14 zones representing the active core, each 0.3 m high. In radial direction five rings (Figure 2.5) plus a bypass channel in the heavy reflector allow detailed analyses even in the late phase of severe core damage accidents. Cross flow junction located between adjacent rings at each elevation allow a certain 2-D flow redistribution in the core i.e. in case of flow path blockages due to debris or molten pool.

The number of fuel rods and control rods represented in each ring by one representative SCDAP component are listed in Table 2.1. In this study the input deck Ex5C2 was used which has a

MAAP specific radial core nodalisation. The main difference compared to previous input deck (Ex5B2) is the rather large centre channel and a slightly modified arrangement of control rod drives (AIC). Radiative heat exchange is modelled between fuel rods, absorber rods, and if present a shroud, based on the real arrangement in the fuel element.

In the fifth ring the HR is taken into account as a third component modelled by a SCD shroud component. The inner edges of the HR were taken into account in increasing the average thickness of the SCD shroud component to 0.261 m. It is subdivided into 3 zones, the inner HR with original material properties (0.04 m), a central zone, which includes the HR cooling borings by adapted material properties (0.15 m), and the outer zone which simulates the remaining part of the HR and the core barrel (0.06). The outer surface of this shroud component is in contact with the downcomer which is surrounded by a R5 heat structure to simulate the reactor pressure vessel (RPV) wall.

Table 2.1 Distribution of core components on the five different radial rings

		Ex5B2			Ex5C2		Rods:	
5 Channel Core		BE	AIC		BE	AIC	264	24
1	Center	9	5		37	17	*9768*	*408*
2	Average_1	36	12		32	12	*8448*	*288*
3	Average_2	64	24		52	16	*13728*	*384*
4	Outer_1	76	40		56	28	*14784*	*672*
5	Outer_2	56	8		64	16	*16896*	*384*
Total		241	89		241	89	63624	2136

For the calculation presented here, ring to ring radiation heat exchange in the core was removed, because of an error reported by ISSC /4/ in the radiation absorption module. Due to averaging over all fluid temperatures of one level in the radiation enclosure a wrong virtual fluid temperature is calculated for radiation absorption. This leads to an increased energy deposition in the fluid so that the fluid temperature increases. As a consequence, the convective heat loss of the rods is reduced in the upper part of the core so that core outlet temperature and temperatures of upper plenum structures became overestimated.

Even simulating ring to ring radiation based on reduced ring to ring view factors leads to a more pronounced lateral core melt spreading, which may explain the calculated heavy reflector failure at rather high core levels reported.

On the other hand, sudden temperature increase in one ring e. g. caused by clad oxidation or melt relocation remains localised in the ring. As a direct consequence the hydrogen production rate is lowered. A detailed comparison is under way but a realistic modelling of in-core radiation exchange requires experimental data which are not yet available. The RPV internals above and below the core, the upper core plate (UCP) and the lower core support plate (LCSP) are modelled as R5 heat structures with 5 section in radial direction to meet the radial core discretization.

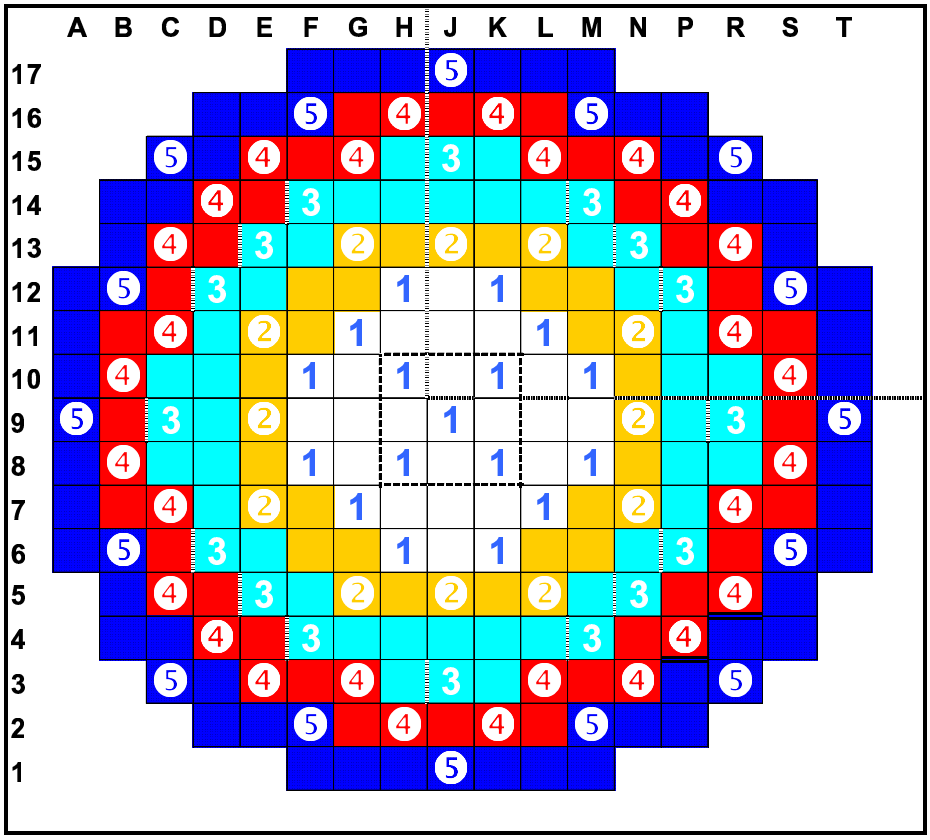

Figure 2.5 Five ring radial nodalisation of the EPR core including positions for fuel elements with the absorber rods.

2.3 Power distribution

The local decay power released in the fuel rods is calculated from the decay heat (Figure 2.8) and distributed over the whole active core using an axial (Figure 2.7) and a radial power profile (Figure 2.6). In this study a begin of cycle (BOC) situation is assumed. As axial power profile a simple chopped cosine shape is used. In radial direction the power is distribute over the five rings as indicated in Figure 2.6. Both types represent "Begin of Cycle" (BOC) conditions.

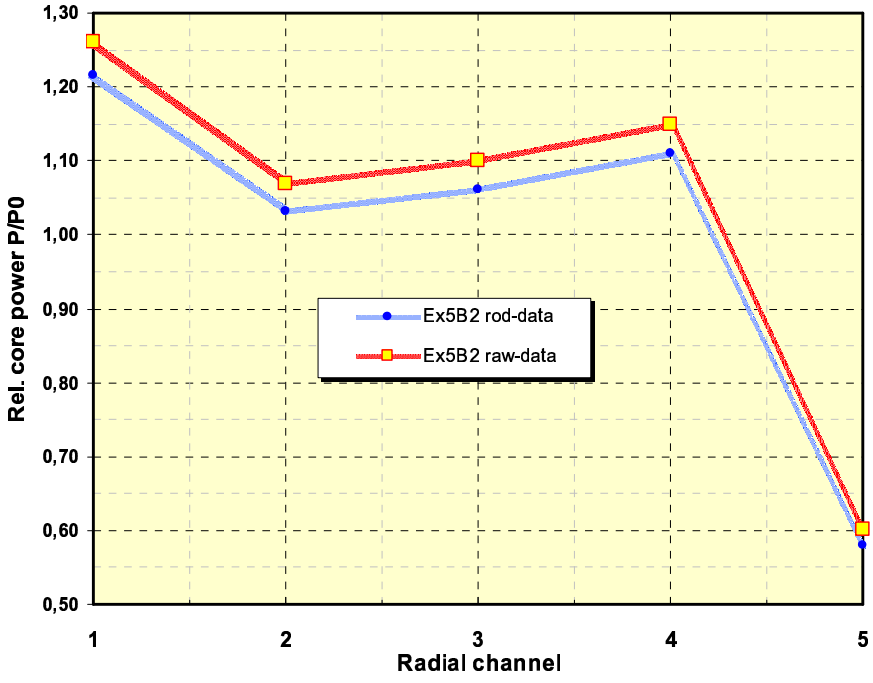

Figure 2.6 Radial power distribution across the five channels in the core

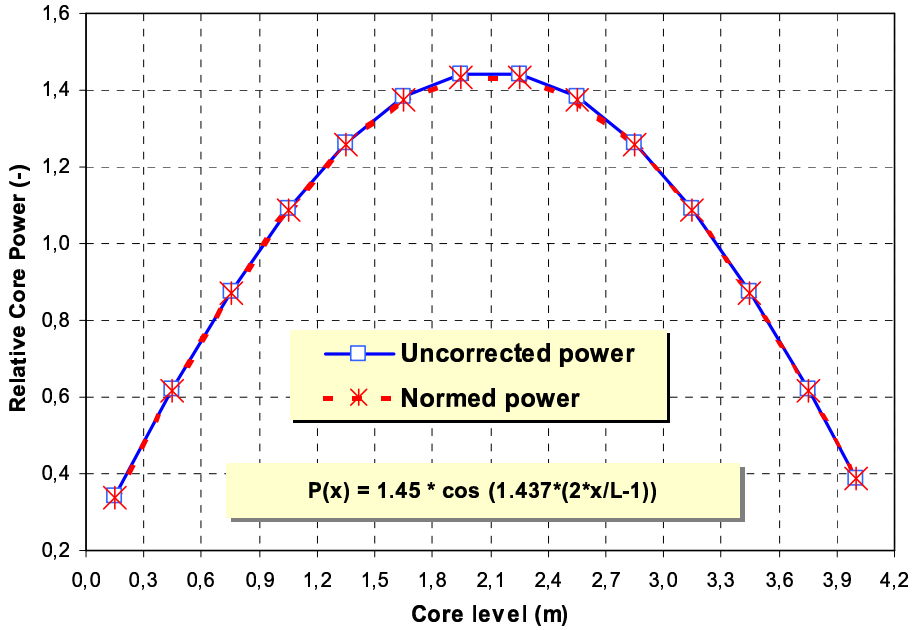

Figure 2.7 Axial power profile used for EPR analyses with S/R5 mod 3.2

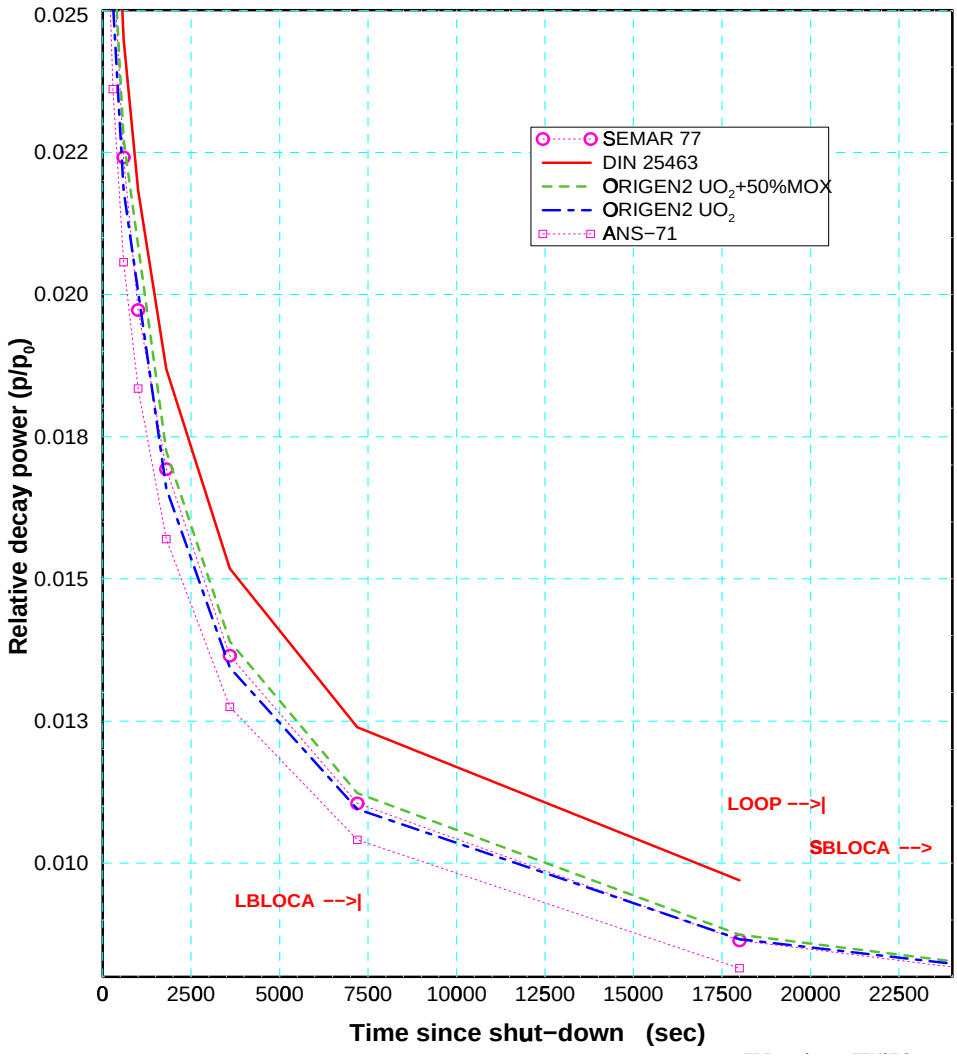

Figure 2.8 Decay heat curves used in the present study are derived from ORIGEN calculations assuming 50 % UO_2 + 50% MOX.

2.4 Upper plenum

For the EPR upper plenum discretization three rings were selected to allow as possible as realistic calculation of the heat-up of upper plenum structures. In axial direction it is divided into a lower zone of 0.48 m elevation, a middle one of 0.60 m, and an upper one of 1.2 m as can be seen in Figure 2.3. The upper plenum (UP) is enclosed by the upper support plate (USP) on top, the upper part of the core barrel at the outside, and the upper core plate (UCP) at the bottom (Figure 2.9). Inside the upper plenum 89 control rod support columns (CSC) extend from the UCP up to the upper head (UH) cavity.

Under normal operation no direct connection exists between the upper head and the upper plenum. As a consequence of the shape of the USP, water may remain on top for a quite long time cooling the structure efficiently. To overcome this rather unrealistic scenario a narrow pipe was added at the outermost ring allowing water to escape from UH into the upper plenum.

2.4.1 Upper plenum internals

In each ring one representative CSC is simulated by a pipe (Figure 2.9) with heat structures to simulate the material of tube walls. It is assumed that the control rod drive is completely inserted as foreseen after reactor scram, so that additionally 50 mm thick stainless steel rod is added to the structure.

In the inner ring, above core channels 11 and 21, 17 support columns with an individual outer diameter of 0.23 m and an inner diameter of 0.2 m were simulated by one heat structure. In the 2nd ring, above core channel 31, 24 support columns and in the 3rd ring, above core channels 41 and 51, 48 support columns are simulated.

The left side of the heat structures, the inner surface, is connected to pipes simulating the flow path from the core outlet to the UH. The right side is connected to adjacent upper plenum volumes. R5 heat structures only allow 1-D heat conduction so that in axial direction, no heat is transported to the USP structure.

In the upper head two nodalisation variations were used so far. The early version uses three axial levels, two for the lower zones with the CSC and one for the volume connected to the RPV head. The simplified version uses only one volume for the whole upper head. No significant difference in the thermal behaviour of the upper head or the USP was found so far.

In S/R5m32 a dedicated "Upper Plenum Structure" (UPS) model is available to tackle 2-D heat conduction, melting and melt relocation to the lowest UPS element /1/. In the present version UPS was only used for upper core plate (UCP) simulation because of two reasons:

1. at the moment no radiative heat exchange between UPS and RELAP heat-structures or even SCDAP components is possible, and
2. previous analyses showed that only melting of the UCP and at least lowest section of the CSC may happen.

If radiation becomes available in a future code version an improved description of the upper plenum is feasible. However, the 2-D flow in the upper plenum around the support columns is difficult to predict with a 1-D code since the fluid mainly follows the fluid path predetermined by the input.

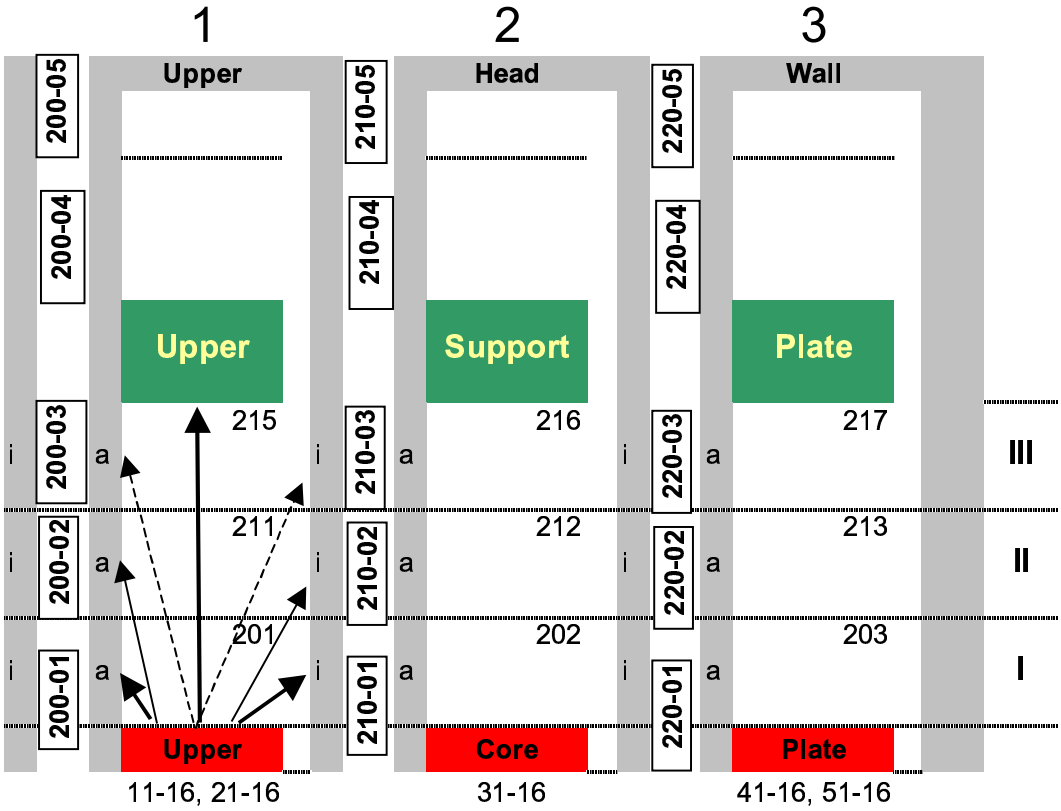

Figure 2.9 Upper plenum 3-ring scheme with upper core plate, control rod drive tubes, and upper support plate. The arrows show possible radiation paths.

2.4.2 Radiation heat transfer

In high pressure scenarios the major source for the upper plenum structure heat-up is the convective heat transfer, radiative heat transfer is negligible especially in scenarios in which the boil down phase lasts for longer time. In low pressure scenarios, however, the convective heat transfer is reduced so that radiative heat exchange has to be considered too.

In Figure 2.9 the simulated radiation exchange paths are shown for the innermost volume. The heat source is the UCP which radiates mainly to the USP and the lowest segment of the CSC. View factors were calculated by hand based on crossed string methodology /1/. For the upper head an additional heat exchange volume was developed, however, surface temperature remains rather low during late phase of the sequences so that it could be removed. Heat up of RPV upper head wall is mainly due to limited convective heat transfer.

Since it is not feasible to simulate adequately the 3-D arrangement of the control rod support tubes a simplified cylindrical scheme was used, which allows to couple outer surface of each tube to the inner and the outer hydraulic volume. In a first approach the control rod support columns (CSC) were assumed to be arranged cylindrically so that outside surface facing laterally to the

adjacent channel participates radiation exchange with this enclosure. In total three radiation enclosures were formed as indicated in Figure 2.9.

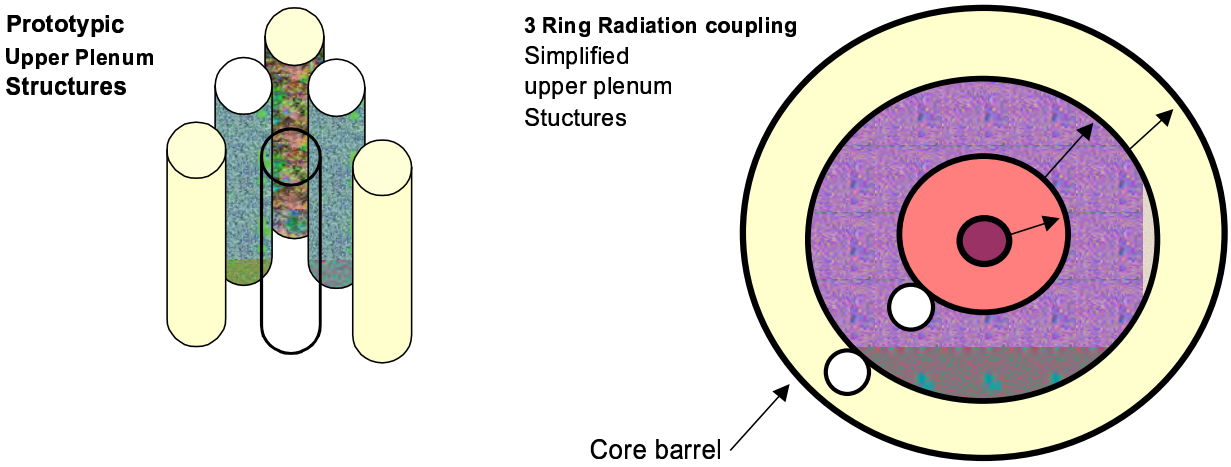

Figure 2.10 Real 3-D geometry in the upper plenum (left) and 2-D simplification used for radiative heat exchange calculation (right).

Based on the orientation and the real surfaces view factors were estimated. In Table 2.2 for each channel the surfaces of the radiation enclosure are listed. The surface areas with high view factors and high surface temperatures are printed bold. An emissivity value of 0.75 was applied to all surfaces taking into account oxide or corrosion layers on the surface. Radiation exchange computed for the upper head volume was removed since the surface temperatures remain rather low so that not significant contribution was found.

Table 2.2 Enclosure surfaces assumed for upper plenum heat exchange calculations.

Ring	Bottom	Inner Surface	Top	Outer Surface
Center	UCP: **01+02**	CSC-1: z=**01**, 02, 03	USP: **01**	CSC-2: z=**01**, 02, 03
Average	UCP: **03**	**CSC-2: z=01, 02, 03**	USP: **02**	CSC-3: z=**01**, 02, 03
Outer	UCP: **04+05**	CSC-3: z=**01**, 02, 03	USP: **03**	CB: z=**01**, 02, 03

2.5 Lower plenum simulation

For the simulation of the molten corium relocated into the lower plenum the FEM tool COUPLE is merged to S/R5. This code allows cylinder symmetrical description of the RPV wall, the fluid and the corium debris. The basic description with the nodalisation scheme shown in Figure 2.11 was derived from stand-alone calculations with already filled plenum /7/.

In the present version the old input style was maintained since the new input (S/R5m32) style handling is still faulty. The initial corium loading was replaced by SCDAP controlled core slump. A coupling to S/R5 containment volume is foreseen to simulate external cooling if an efficient steam condensation formulation in the containment volumes becomes available (S/R5 mod 3.3). In the present version the code slows down drastically if condensation occurs.

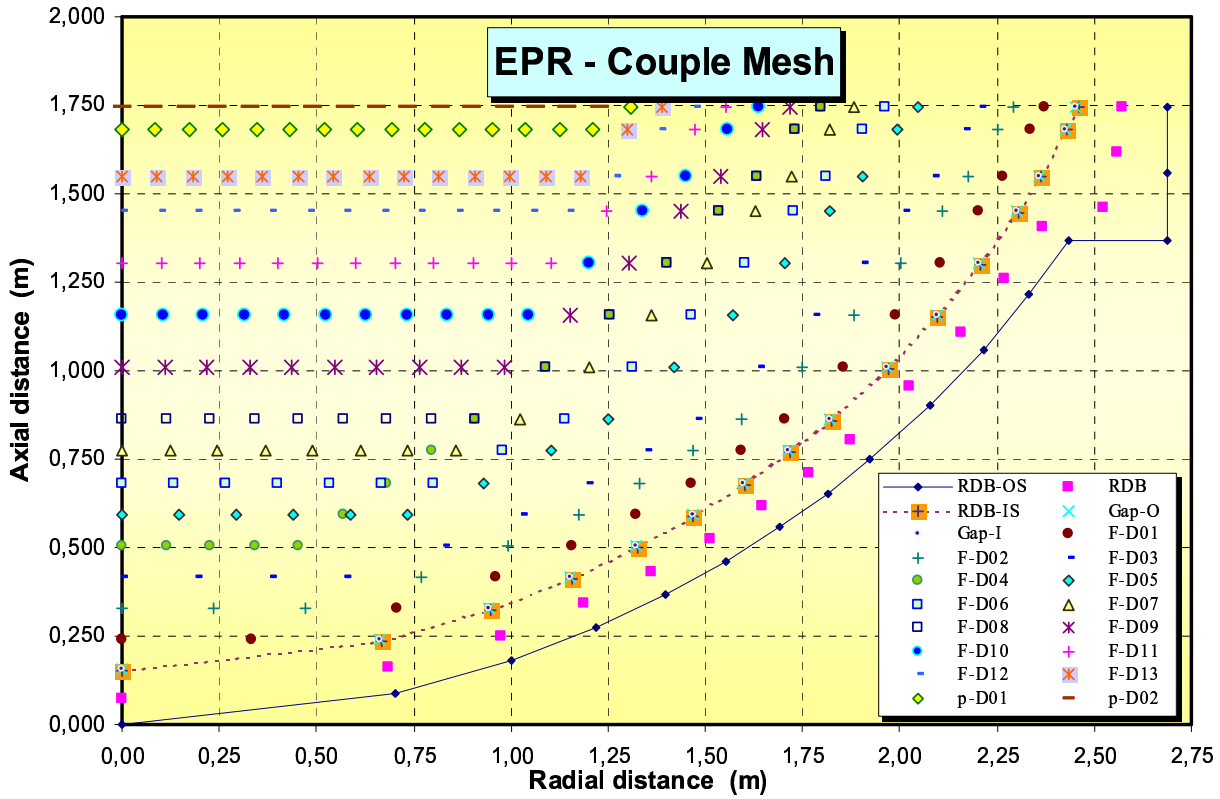

Figure 2.11 COUPLE FEM mesh used for melt behaviour analysis in the lower plenum

In Figure 2.11 the outermost corner positions of each COUPLE element (cylindrical ring) is shown. The nodes used to simulate the RPV wall are marked by lines. At the inner surface the COUPLE gap model is used. The upper plane of the mesh fits to the lower face of the lower core support plate (LCSP). Melt is placed in the centre of the scheme, no relocation along walls is taken into account even in case of relocation through downcomer (DC).

2.6 Reactor Control, Surveillance and Limitation System

The EPR input deck also includes most important parts of the reactor control, surveillance and limitation (RCSL) system as shown in Table 10.3 in the Appendix. On the left side the trips are shown with respect to their relevance (Loop, auxiliary, result). The centre column gives the control topic and the left the relations between the conditions and/or trips. In total three groups are used: calculation control which is not part of the RCSL but required for starting and controlling the calculation, primary and secondary system control. Bold numbers indicate trips used for control of RELAP components.

The list reflects some optimisation during the basic design optimisation phase (BDOP). The control logic was extended by a local RCP shut down conditions to allow the pumps in case of SBLOCA to continue forced convection beyond reactor scram signal. Also no isolation of the accumulator by closing the surge line check valve is realised for each loop individually.

The primary system depressurisation is activated if the vapour temperature in the lowest R5 volume of the upper plenum exceeds 926 K. To avoid activation by short temperature spikes, which is often observed in fluid temperature plots, the signal has to be true for 30 s.

On the secondary side the activation and control of the emergency feedwater system (EFWS) was simplified avoiding oscillation due to the originally realised on/off pump control. The EFWS make-up flow is now controlled by the target water level in the secondary side of the steam generator allowing a smooth SG refill. The EFWS signal is activated just after scram signal and locked in case of LOOP scenario. Secondary side pressure control follows the requirements for automatic and manual depressurisation.

2.7 Code and Input specification

2.7.1 S/R5 code version

The code version used for these calculation is based on INEEL SCDAP/RELAP5 mod 3.2 with some improvements developed at FZK/IRS to simulate the QUENCH facility /13/. For the EPR analyse the most significant modifications are error corrections necessary to simulate material relocation in more than ten axial nodes, removal of wrong limitation in the RELAP5 radiation module (upper plenum), and activation of improved reflood model based on the PSI model and the FZK-Chen-correlation for the transition phase. The same code version was used for Phebus-FP and QUENCH analyses.

2.7.2 User defined input parameters

The majority of the best estimate models are only accessible by the user by code modification. However, for some processes or phenomena no reliable models are available, or the validation database cannot be covered with completely, e.g. the cladding failure criteria, user defined parameters are required.

2.7.2.1 Clad and crust failure criteria

The used clad rupture criteria is based on strain limitation. For all calculations a rupture strain of 20 % was used. The oxide scale failure temperature was set to 2350 K if less than 60% of the cladding is oxidised, derived from code validation using CORA and PHEBUS tests.

The failure criteria of the molten pool crust was set to early crust failure, so that lateral crust failure at HR contact is calculated.

2.7.2.2 Oxidation correlation

In the low temperature range (< 1853 K) experimental correlation for oxide layer growth and weight gain are used from of Cathcart /21/ and in the high temperature range those measured by Urbanic and Heidrick /22/. The influence of a non-condensable gas layer next to the outer clad surface (N_2, H_2) which may hinder oxidation was taken into account (Limit on).

2.7.2.3 Cladding shattering model

For the reflood scenarios the global shattering model of S/R5m32 was extended by a local shattering model based on recent QUENCH results. The basic physical idea is that at the phase transition from tetragonal phase (> 1478 K) to monoclinic phase the protective oxide layer becomes partially transparent for the oxygen ions so that higher diffusion velocities are possible.

The density change of 7 % (Figure 2.12) amounts to a chance in lattice linear size of app. 40 %. In real situation the oxide at the interface to the α-Zr(O) may show a certain variation in the oxygen concentration, so a temperature range from 1560 K to 1150 K was selected. In single effects test in the QUENCH rig crack formation was observed above an oxide layer thickness of 150 µm

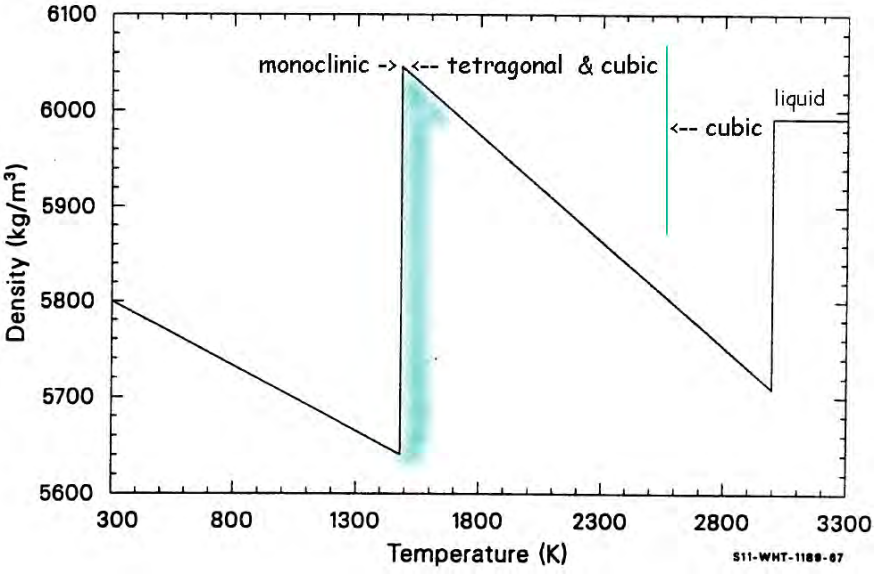

Figure 2.12 Density jump at phase change from monoclinic to tetragonal (< 2973 K)

Therefore the model tracks all nodes above 1150 K which exceed 100µm oxide layer thickness. Actually nodes already containing debris are skipped by the shattering logic. It is assumed that the metal content is scarce.

The process of a partial or complete removal of the protective oxide scales is defined as shattering which is calculated to occur if:

1. cladding temperature between 1150 K and 1560 K,
2. the remaining metallic Zircaloy layer is below 150 µm, and
3. a fast temperature gradient (> 4K/s) occurs for at least five time steps.

If all conditions are given, the protective thickness of the oxide scale of the fuel rod cladding is reduced to 2.54µm. Actually the model is not applicable to water, control rod guide tubes, or shroud components so that at lower temperatures, when these rods are supposed to be still intact app. 5% more hydrogen can be produced. This value may vary because of slightly smaller oxide scales at water rod and guide tubes, so that they may be below shattering threshold.

For comparison, the original model is initiated by a user trip and reduces artificially all protective oxide scales to a initial value of 0.25µm. Since this happens at the same time all over the core the resulting hydrogen production rate is rather overestimated and less physical sound.

3 SURGE LINE RUPTURE

The results of S/R5 mod 3.2 calculations for the scenario “Surge line rupture” (section 3) and “SBLOCA” (section 4) will be discussed with respect to information required for analyses of upper plenum structural behaviour (BERDA/IVAN), debris and/or molten pool composition prior to failure of core enclosure, and source term for hydrogen production and release. The results will be used for comparison with those obtained by integral code systems (e.g. MAAP/3/, MELCOR/2/).

In the surge line rupture (SL) scenario a complete two-ended rupture of the surge line is assumed. The surge line with a cross section of 951 cm² is the largest pipe connected to the main coolant circuit located in the hot leg. The scenario, a typical large break LOCA, is dominated by large coolant loss during blowdown and core heat-up phase. The scenario is characterised by low pressure and low coolant inventory in the primary system.

3.1 Thermohydraulic phase

In Figure 3.1 some integral variables such as decay heat (a), system pressure (b), leak outflow rate (c), and hydrogen production (d) are shown to identify the different phases of the SL scenario. The calculation starts with steady state conditions and at 0.1 s the leak valve is opened. Together with the leak valve opening, the connection between SL and main coolant line is closed and a second leak valve at SL is opened to discharge the pressurizer to the containment. This allows to balance the steam mass and water mass in the containment, but will not be discussed here. For both leaks standard R5 outflow conditions were used.

The reactor scram is triggered by the pressure low signal at 1.2 s and at 12.4 s the RCP is stopped due to high void at the pump inlet. Due to the large leak size, the pressure (Figure 3.1 b left scale) and hence the peak core temperature (Figure 3.1 a right scale) drops fast to saturation temperature. The leak outflow rate (Figure 3.1 c) reaches a peak value of app. 2.8 Mg/s (pure water) which drops down to 500 kg/s app. 120 s (2 min) later. App. 2 min later primary system pressure reached 4.5 MPa (Figure 3.1b left scale) and the accumulators start to inject (Figure 3.2e).

Between one and 3 min the heat is transferred in the SG from the secondary side (Figure 3.2 a) to the primary side, since the secondary system pressure and hence the saturation temperature is higher than those of the primary system. After 3 min that heat transfer mechanisms ceases because of low primary system pressure. From that time no secondary system measure can affect primary system so that the discussion of the scenario can be focussed on primary side events.

Boil off is accelerated by the low system pressure (< 1 MPa) and the release of the stored heat in the core and the massive RPV structures. After 15 min only 2.0 m collapsed water remains and the fading evaporation fails to remove sufficiently all decay heat from the uppermost part of the core. The boil-down period last up to 20 min voiding upper head, upper plenum and the core.

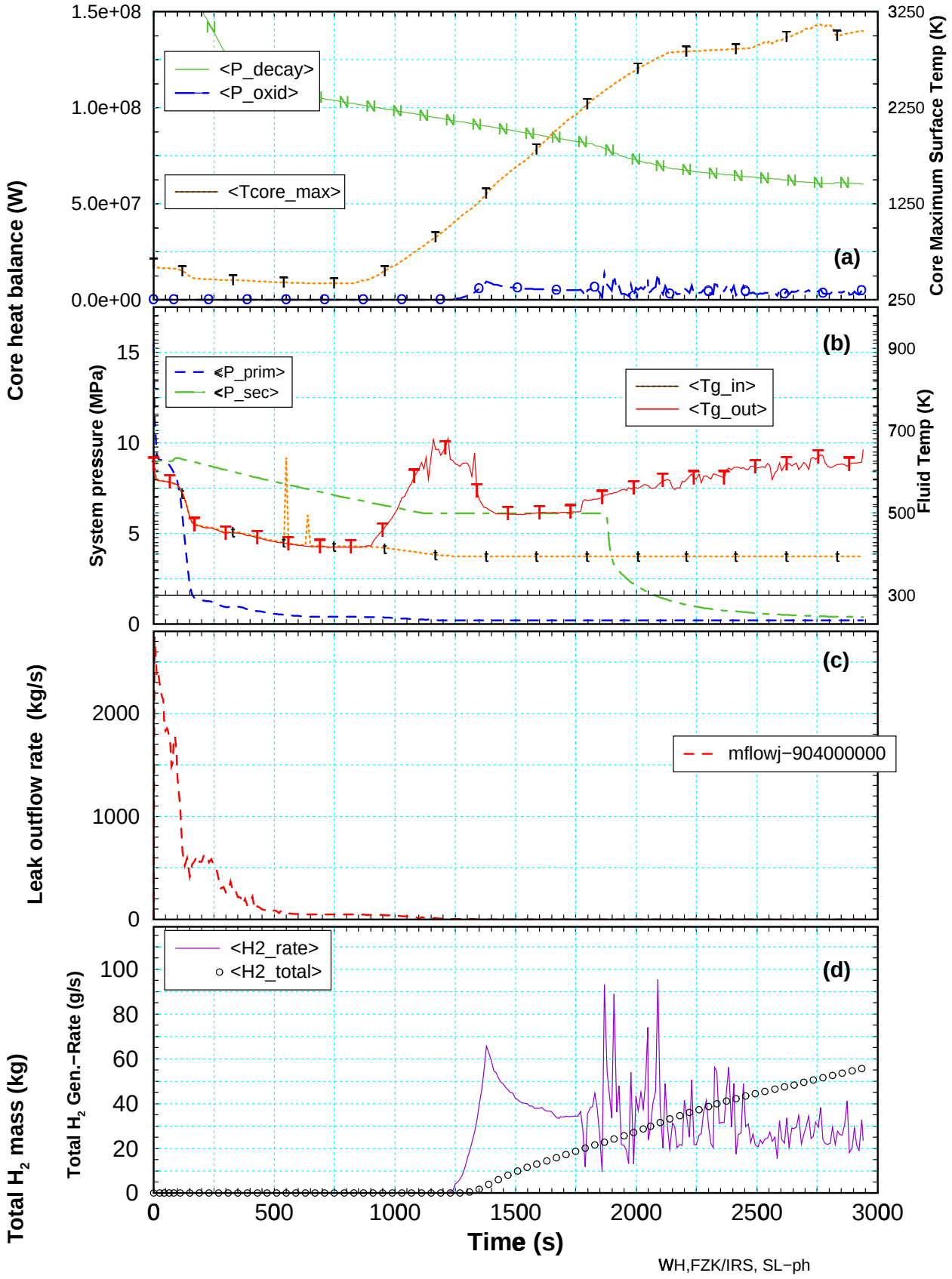

Figure 3.1 Overview of the surge line rupture Scenario: (a) power balance (left scale) and peak core temperature (PCT, right scale), (b) system pressure (left scale) and core entrance and exit vapour temperatures (right scale), (c) leak outflow rate, and (d) hydrogen release and total mass in the core (circles).

3.2 Core heat-up

Between 15 min and 20 min the water level drops down to 0.7 m in the core, and the PCT rises up to app. 1000K. Due to the low water level in the core only limited amount of steam is produced. Oxidation starts as expected above 1000K (Figure 3.1d) at 21 min but 1 min later calculated hydrogen release decreases. With the onset of oxidation the core outlet temperature given in Figure 3.1b, right scale, drops too. The reason can be found by analysing the cladding behaviour in the core.

Between 1375 s and 1401 s (23 min) the whole core fluid cross section decreases by app. 10 % as can be seen in Figure 3.4d. In the temperature range from 1340 K to 1350 K the outer diameter of all fuel rod cladding of the four inner rings have increased from app. 9.6 to 10.8 mm nearly blocking the fluid path. The outermost channel followed somewhat slower but at app. 30 min the core is homogeneously blocked at around 2.55m. This core-wide blockage hinders steam supply to the upper third of the core.

The spikes in the hydrogen source term after 1883s (31 min) shown in Figure 3.1d are caused by first release of metallic melt as indicated in Figure 3.4a +b. At that time the cladding temperature in centre ring of the core exceeds 1500 K (Figure 3.3a). Due to the low steam concentration no oxidation hardening is calculated so that ballooning is calculated to a large extend at rather low temperatures. In case of ruptured cladding the liquid Zircaloy dissolved some UO_2 which relocates above melting temperature of Zircaloy (app. 2030K) far below the oxide scale failure criteria (section 2.7.2.1). Oxidation process is stopped due to lacking metal and hence hydrogen production reduced so that the core outlet temperature drops to app. 550 K between 1400 s and 1800 s (Figure 3.1b). As a consequence the heat-up rate in the core is reduced (Figure 3.3 a,c,e).

Up to 30 min the oxidation of intact fuel rods only delivers app. 25 kg hydrogen, however this is half of the whole hydrogen mass calculated in this scenario. The other half originated from debris oxidation because relocated melt forms rather metallic U-O-Zr debris. The hindered oxidation however leads to rather low fluid temperatures at core exit so that a detailed discussion of upper plenum structures heat-up is not necessary here. The centre part of the upper core plate just reaches 750 K at end of calculation (Figure 3.3h).

Up to the 2941s (50 min) only 58 kg hydrogen were produced with a peak hydrogen release of less than 100 g/s (Figure 3.1 d). The oxide scales are rather low, less than 60 µm. As will be discussed later, this is the lowest hydrogen value for this scenario. The hydrogen mass varies between 58 kg and 250 kg as can be seen in Figure 7.1, mainly influenced by the steam availability.

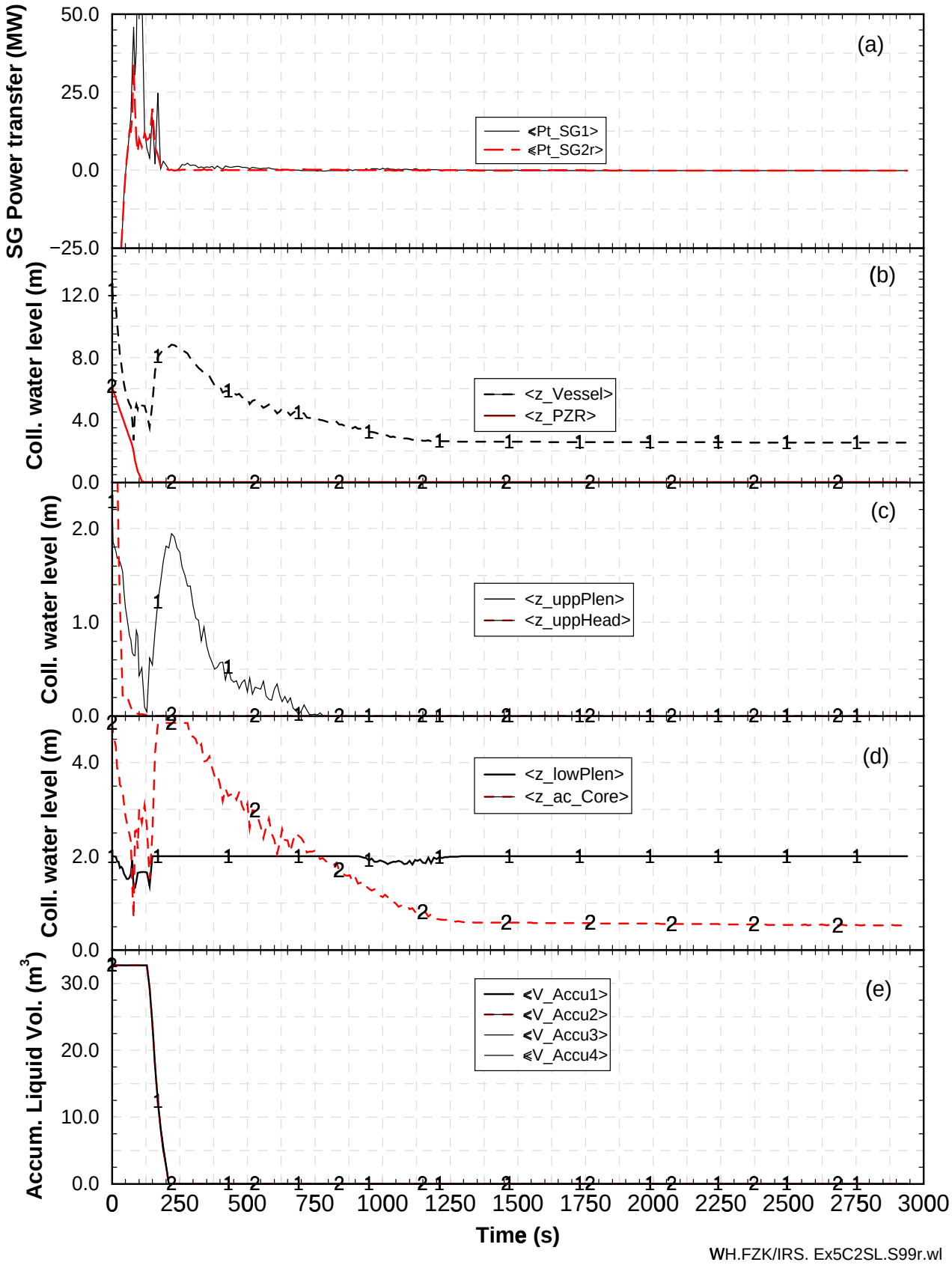

Figure 3.2 Primary system water and power inventory (a) heat flux across SG tubes to 2nd system, (b) collapsed water level in pressurizer, reactor vessel, (c) top plena, (d) bottom plena, and (e) water volume in the accumulators.

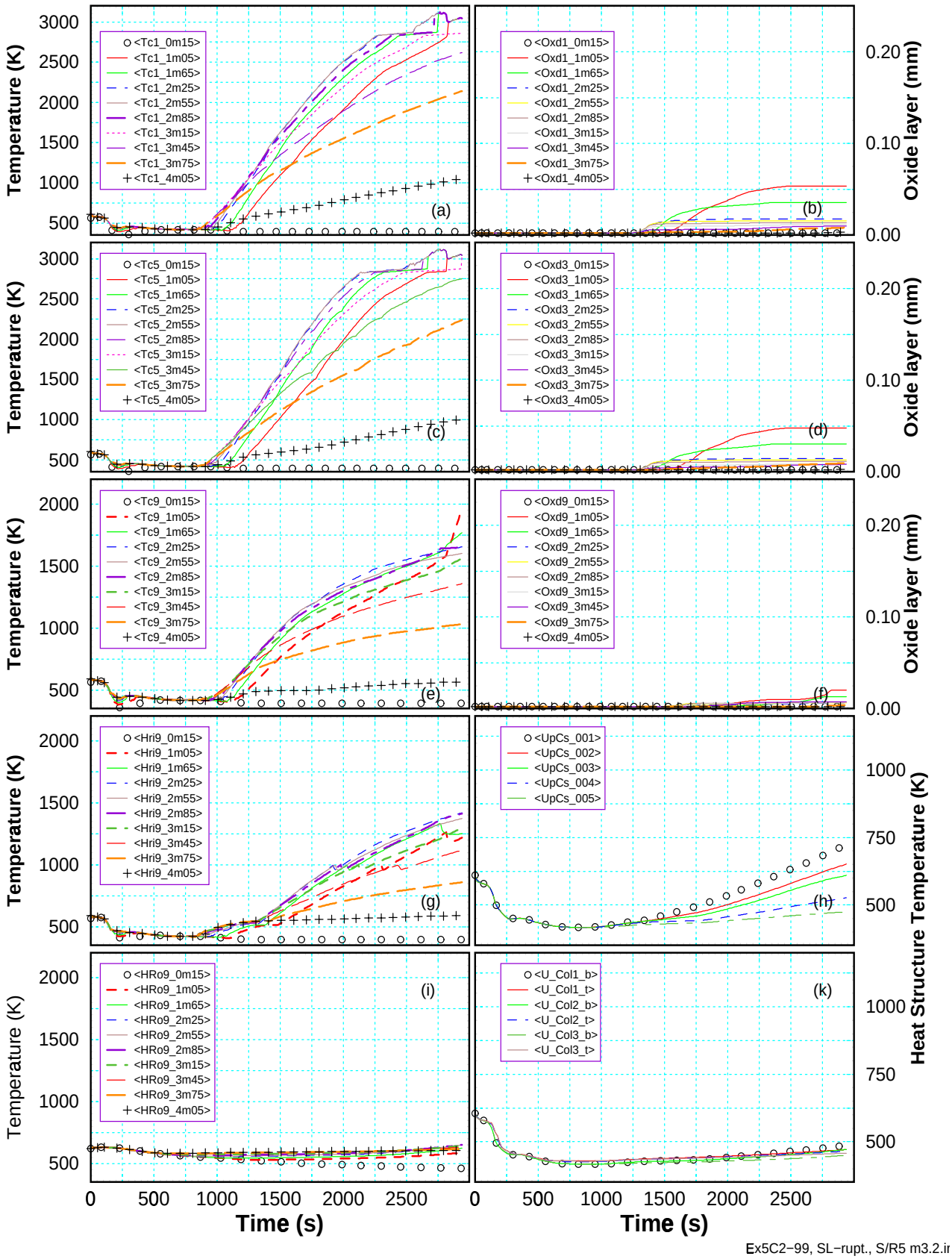

Figure 3.3 „Dry“ surge line rupture scenario: core temperatures (left column) and oxide scales (right column) for the inner ring (a, b), the centre ring (c, d) and the outermost ring (e, f), heavy reflector inner surface (g), and outer surface (i) temperatures and upper core structure (h) and control rod guide tube temperatures.

Table 3.1 List of events calculated for the SL scenario.

	Type (General)	**Time (min)**	**Primary System Pressure (MPa)**	**PCT (K)**
1	Reactor scram	1.2 sec.	15.5	T_{sat}
2	RCP stopped	12.4 sec	---	T_{sat}
3	Evaporation of SG 2nd side	---	---	T_{sat}
4	Accumulator injection period	2-4	0.2	T_{sat}
5	Onset of core heat-up	15	0.2	T_{sat}
6	Fast cool-down of SG 2nd side	30		T_{sat}
7	Primary side depressurisation	---	---	T_{sat}
8	Onset of hydrogen production	20.5	0.2	1000
9	Onset of clad failure (balloon., rupture)	21	0.2	1205
	Type (Local) Localisation by: R=ring, Z=axial zone	Time (min)	Position in the core R-Z	PCT (K)
10	Onset of absorber melt relocation	28	R1 – Z9	
11	Clad oxide failure -> first U-Zr-O melt	30	R1 – Z9	
12	Onset of large debris formation	36	R3 – Z9	
13	Melting of upper core plate (R1-R5)	---	--- — ---	
14	Onset of molten pool formation	41	R3 – Z8	
15	Debris/Molten pool crust contacts heavy reflector	---	--- – ---	
16	End of calculation (numerical error)	48		
	Duration of phases	**min**		
16	Thermohydraulic phase (8 - 4)	16.5		
17	Initial core degradation phase (14-10)	20.5		
18	In-core molten pool spreading (16-14)	9.0		

3.3 Core degradation

In the dry SL scenario the chemical energy of the Zirconium water reaction only contributes with less than 10 % to the total power released in the core. So the maximum heat-up rate of app. 2.5 K/s (Figure 3.3 a at 3.15 m) is mainly dominated by the decay heat and the low convective heat transfer to the steam. After 1524 s (25 min) the core heat-up rate sinks below 2 K/s.

App. 5 min later first metallic melt relocation is calculated as can be seen in Figure 3.4 a for the UO_2 and in Figure 3.4 b for Zircaloy at 2.55 m core elevation. In this figures the mass is balanced for one elevation over the whole core. The initial mass of UO_2 amounts to app. 10 Mg for one 0.3 m long axial node. The mass removed from the intact fuel rods is mainly added to debris, which is not balanced in Figure 3.4. Only a small amount is calculated to form localised blockages increasing the initial mass.

The metallic melt relocation continues for more than 10 min until a molten pool of corium is formed. At 2470 s (41 min) a molten pool is formed at 2.25 m core elevation by debris melting. In Figure 3.4c the radial and axial spreading as well as the growth (-T-) of the molten pool is given, however, it is difficult to clarify it. Therefore, the spatio-temporal behaviour of the molten pool is shown using the axial and radial position of its lower crust in Figure 3.5.

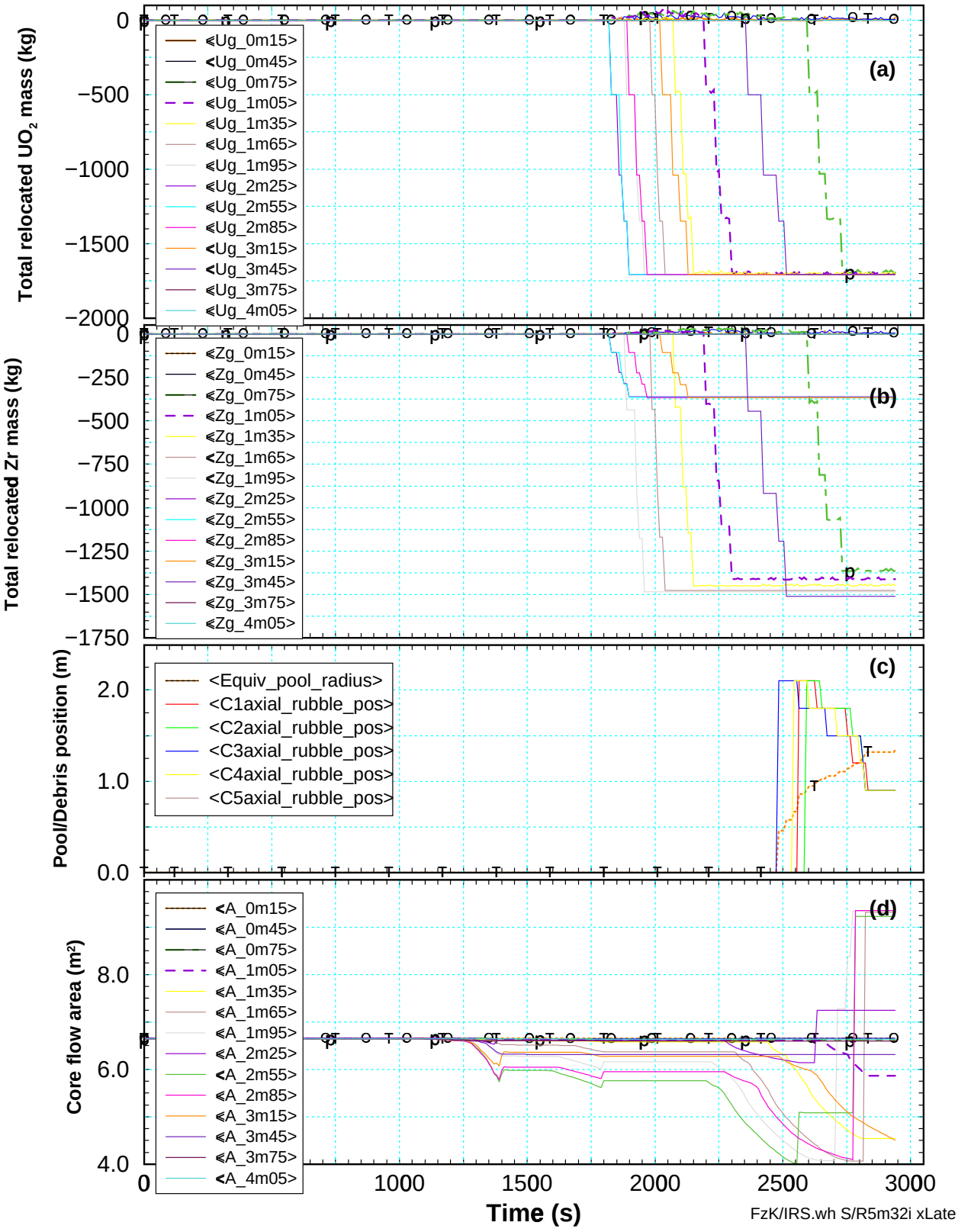

Figure 3.4 Late phase metallic melt relocation for SL scenario: (a) UO_2 mass redistribution, (b) Zry mass redistribution, and (c) axial position of porous debris (crust) and (d) equivalent pool size.

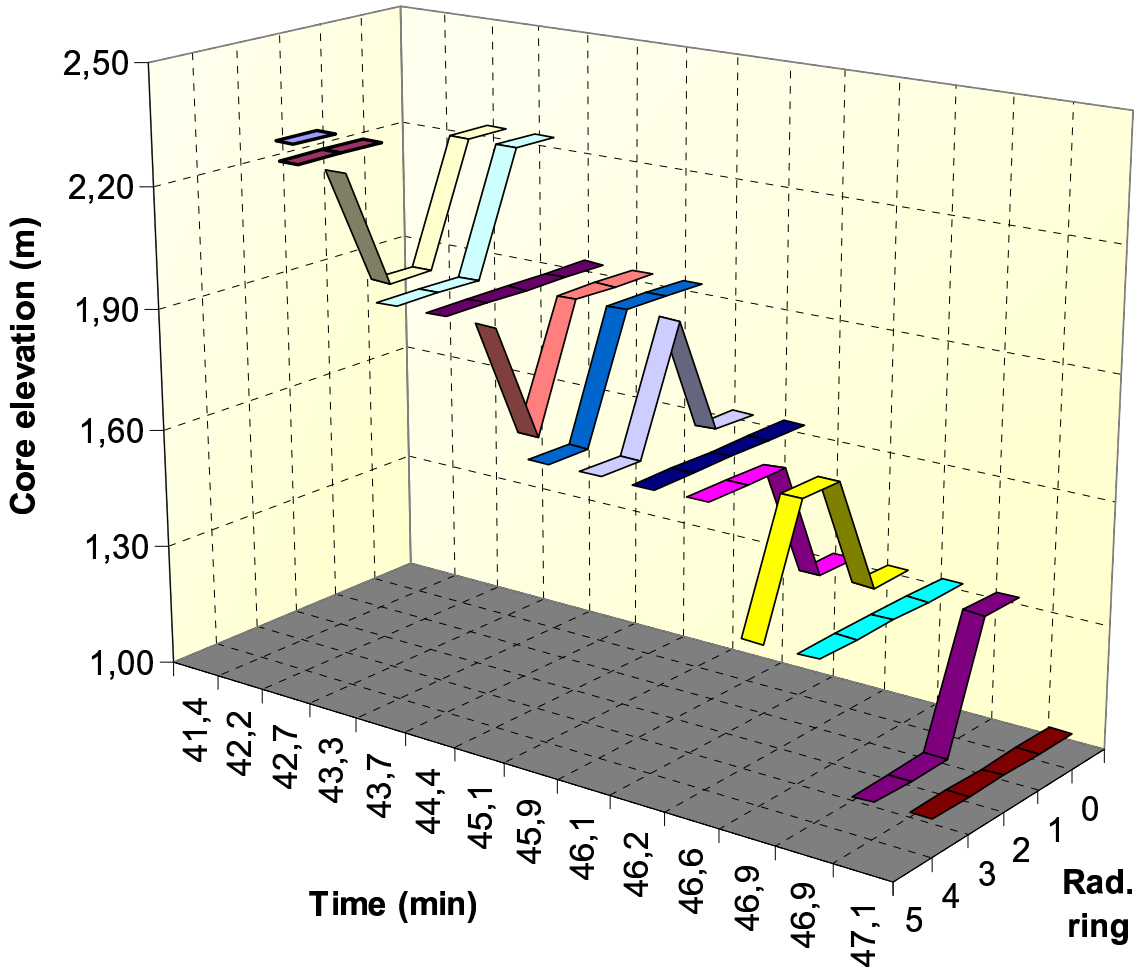

Figure 3.5 Axial and radial position of the lower crust of the molten pool in the SL scenario for times at which relocation events were calculated between 41 min and 48 min. The crust is situated on top of porous debris one zone below.

Within 80 s (up to 42.7 min) the molten pool spreads over nearly the whole core cross section except for the outermost ring. At that time, a large part of the core above the molten pool becomes voided (Figure 3.4d) due to melting and slumping of ZrO_2 and UO_2 as indicated in Table 3.2 left. The free cross section of the core increase from 4.0 m² to 8.0 m².

As can be seen the third ring of the core has the tendency to relocate first to lower levels, perhaps due to the radial decay power profile (Figure 2.6) and the limited convective cooling. Also rather flat molten pool configurations were calculated (e.g. at 43.7 min or at 46.9 min in Figure 3.5) which may be explained similarly. Starting from an axial elevation of 2.25 m the molten poor reaches a level of 1.0 m at 2824 s (47 min), the final state of this calculation.

3.4 Final state

The calculation was terminated because of numerical problems leading to small time steps. Since relocation into the lower plenum has not yet been calculated the values in Table 3.2 show the whole corium mass in the core region.

At the end of the calculation, the molten pool volume increased to 5 m³ with an average temperature of 3046 K. The nuclear heat generation amounts to app. 60 MW whereas chemical power only contributes by 6 %. The mass in the molten pool is composed of 40.8 Mg UO_2, 657 kg ZrO_2 , and no metallic Zry. The liquefied mass in the porous debris amounts to 4.7 Mg. The molten pool has an effective radius of a half sphere with a diameter of 2.68 m (5.6 m²), which compares with the core diameter of 3.72 m (10.8m²). If the nodalisation geometry is considered as shown in Table 3.2, the molten pool axially extends over two zones, a pan-cake type configuration leads to diameter of 3.3 m (8.4 m²). In the latter case app. 78% of the core is blocked.

Table 3.2 In core state calculated for the SL Scenario at app. 48 min into the transient

Ax-Node (m)	#	Ring 1	Ring 2	Ring 3	Ring 4	Ring 5
4.05	14	I	I	I	I	I
3.75	13	I	I	I	I	I
3.45	12	I	I	I	I	I
3.15	11	L	L	V	L	I
2.85	10	V	V	V	V	I
2.55	9	V	V	V	V	I
2.25	8	V	V	V	V	I
1.95	7	V	V	V	V	P
1.65	6	V	V	V	V	P
1.35	5	**xxMxx**	**xxMxx**	**xxMxx**	**xxMxx**	P
1.05	4	**xxMxx**	**xxMxx**	**xxMxx**	**xxMxx**	P
0.75	3	**P**	**P**	**P**	**P**	I
0.45	2	I	I	I	I	I
0.15	1	I	I	I	I	I

3.5 Discussion

The general characteristics of this scenario is the low pressure level and the low remaining water inventory in the primary system. As a consequence, no secondary side measure e.g. bleed and feed may influence the course of the accident because natural convection is not very efficient. On the other side, the evaporation rate is rather low leading to low steam mass flow rates of less than 0.6 kg/s up to 38 min and after this time less than 0.2 kg/s. This is the lower end of the mass flow rate calculated for the SBLOCA scenario discussed in section 4.1. As a consequence, calculated hydrogen mass is the lowest in this scenario, showing the lower end of the scale (see section 7.1).

Another limiting parameter is the simulation of the outflow conditions, which hinders water being expelled from the core. Also the simulation of realistic outflow conditions has to be checked, because a lower mass flow rate strongly influence the water inventory in the core, and hence the hydrogen production by increasing the steam availability.

4 SMALL BREAK LOCA

The small break loss of coolant accident (SBLOCA) scenario with a leak size of 46 cm² in single loop cold leg (CL) was selected for code comparison between MAAP 4.02 used at Framatome, MELCOR 1.8.3 used at Siemens/KWU and SCDAP/RELAP5 used at FZK/IRS. The SBLOCA scenario assumes failure of the on-site power supply for the safety injection system and the emergency diesel engines. Only one X-diesel remains active maintaining one steam generator secondary side at saturation temperature.

Therefore, the single loop behaves quite different from the lumped loop (loop 2), as described in /14/. Also between the code large time differences were observed, mainly caused by different calculation of the momentum and thus the heat exchange in the single loop hot leg during reflood-condensor mode (section 4.1.3). So far several calculations with older S/R5 versions (S/R mod3.1.irs and S/R5 m32β) were performed and discussed in /14/. The actual calculation with S/R5m32 show comparable results with S/R5mod3.1 and MELCOR calculations.

4.1 Thermohydraulic phase

The scenario conditions, mainly the small leak size and the availability of the EFWS in loop 1 extends the thermohydraulic phase up to app. 18700s as seen in Figure 4.1. The thermohydraulic phase can be subdivided into the blow-down phase at system pressure > 4.5 MPa up to 1882 s, the accumulator refill and nitrogen release phase up to 7500 s, the natural circulation phase from 4800 s (80 min) up to 18700 s (310 min), and the core heat-up phase starting at 15000 s (250 min). The duration of the different phases is summarised in Table 4.3.

4.1.1 Blow down

The main results of the calculation are shown for the primary system in Figure 4.2 and for the secondary side in Figure 4.3. After opening of the leak assumed at 0.1 sec primary system pressure decreases for 30 s until it sinks below 13 MPa, causing reactor scram (RS) as indicated in Table 4.1. Up to this time the leak flow rate is dropped from initial 470 kg/s to 100 kg/s at 1200 s due to secondary side depressurisation caused by the automatic secondary side cool-down with 100 K/h (Figure 4.1b). The primary system pressure reaches 6.0 MPa at 1130 s and at 1831 s (30.5 min) manual depressurisation of the SG secondary side reduces primary side pressure the accumulators can start to feed water into the cold legs.

4.1.2 Accumulator refill

At that time, the water level in the core has dropped by 1.5 m (solid line in Figure 4.2d), so that large amount of the accumulator water in Loop 1 is lost through the leak. After complete release of water the driving gas nitrogen is injected into the cold legs of the primary system increasing the non-condensable mass fraction (Figure 4.2c). In Loop 1 the non-condensable gas nitrogen leaves the system rather quickly through the leak so that 30 min later no nitrogen was present.

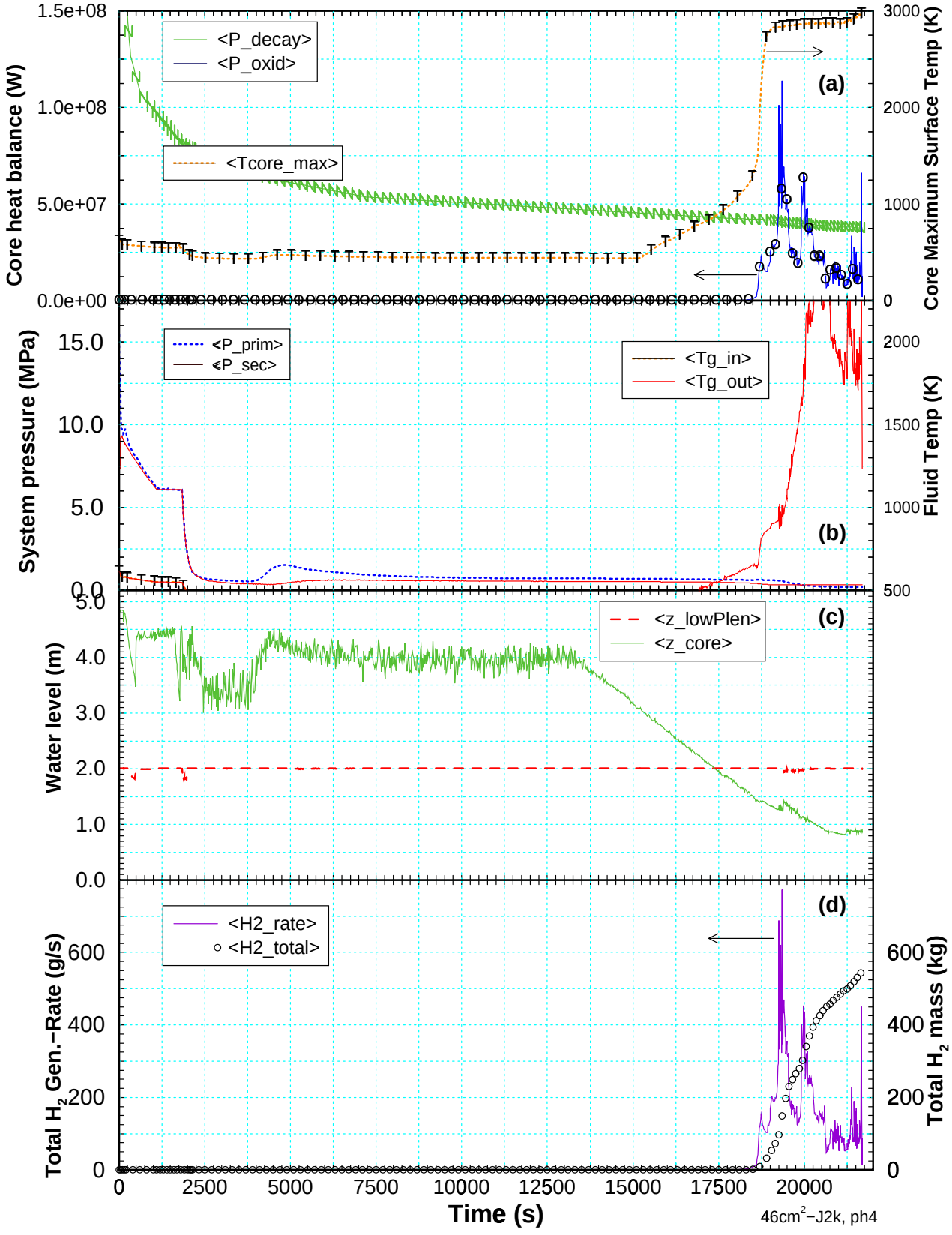

Figure 4.1 Overview of SBLOCA phases: (a) power balance (left scale) and peak core temperature (PCT, right scale), (b) system pressure (left scale) and vapour temperatures at core entrance and exit (right scale), (c) core and lower plenum water level, and (d) hydrogen release (left) and total hydrogen mass (right) produced in the core (circles).

Table 4.1 List of events calculated for the 46 cm² SBLOCA scenario.

Type (General)	Time (min)	Primary System Pressure (MPa)	PCT (K)
Reactor scram	30.5 sec	15.5	T_{sat}
RCP stopped	30	---	T_{sat}
Accumulator injection period	31-35	4.5 – 1.2	T_{sat}
SG2 secondary side evaporated (no EFWS)	63	5.5---	T_{sat}
Fast cool-down of secondary side	32		T_{sat}
Onset of core heat-up	250	0.2	T_{sat}
Manually activated primary side depressurisation	---	---	T_{sat}
Onset of hydrogen production	297	0.2	1000
Onset of clad failure (ballooning, clad rupture)	310	0.2	1205
Type (Local) Localisation by: R=ring, Z=axial zone	Time (min)	Position in the core R-Z	PCT (K)
Onset of absorber melt relocation	312	R1 – Z11	
Onset of melt relocation forming localised debris	318	R1 – Z12	
Onset of large debris formation	334	R3 – Z9	
Melting of upper core plate (R1-R5)		--- — ---	
Onset of pool formation	335	R1 – Z11	
Debris/Molten pool crust contacts heavy reflector	362	R5 – Z8	

In Loop 2 the nitrogen strays for about 90 min because it can only vanish through the water in the lower plenum and in the core. At that time no non-condensable gas was found in the hot leg (Figure 4.2b) indicating that the water in the pump leg and the SG2 prevented such a migration. The RPV is completely filled, so that the nitrogen could only penetrate though the upper part of the downcomer into the Loop 1.

As a consequence the mass flow rate through the leak increases because the RPV is filled up to the hot leg pipe positions (Figure 4.4c) and the nitrogen entrains water as indicated by spikes as can be seen Figure 4.2d.

4.1.3 Natural convection

At 3754 s (63 min) the SG 2 is emptied (Figure 4.3b) and 10 min later no more heat is transferred to its secondary side as can be seen in Figure 4.3a. The EFWS constantly refills SG 1 (Figure 4.3d) maintaining a water level of app: 15.5 m (Figure 4.3b) up to the end of the natural convection phase at 18760 s (313 min). During this period in the hot leg of loop 1 the reflood-condensor mode efficiently removes heat from the core. As can be seen in Figure 4.4 a, b the first phase up to 11000s is dominated by water entrainment into the hot leg because the water level in the upper plenum is still at app. 1.2 m (Figure 4.4c). When the water level drops below 1.2 m only steam can enter the hot leg with a velocity of app. 10 m/s whereas the condensed water lows with -4.5 m/s downwards to the core. The standard R5 inter-phase friction formulation was used.

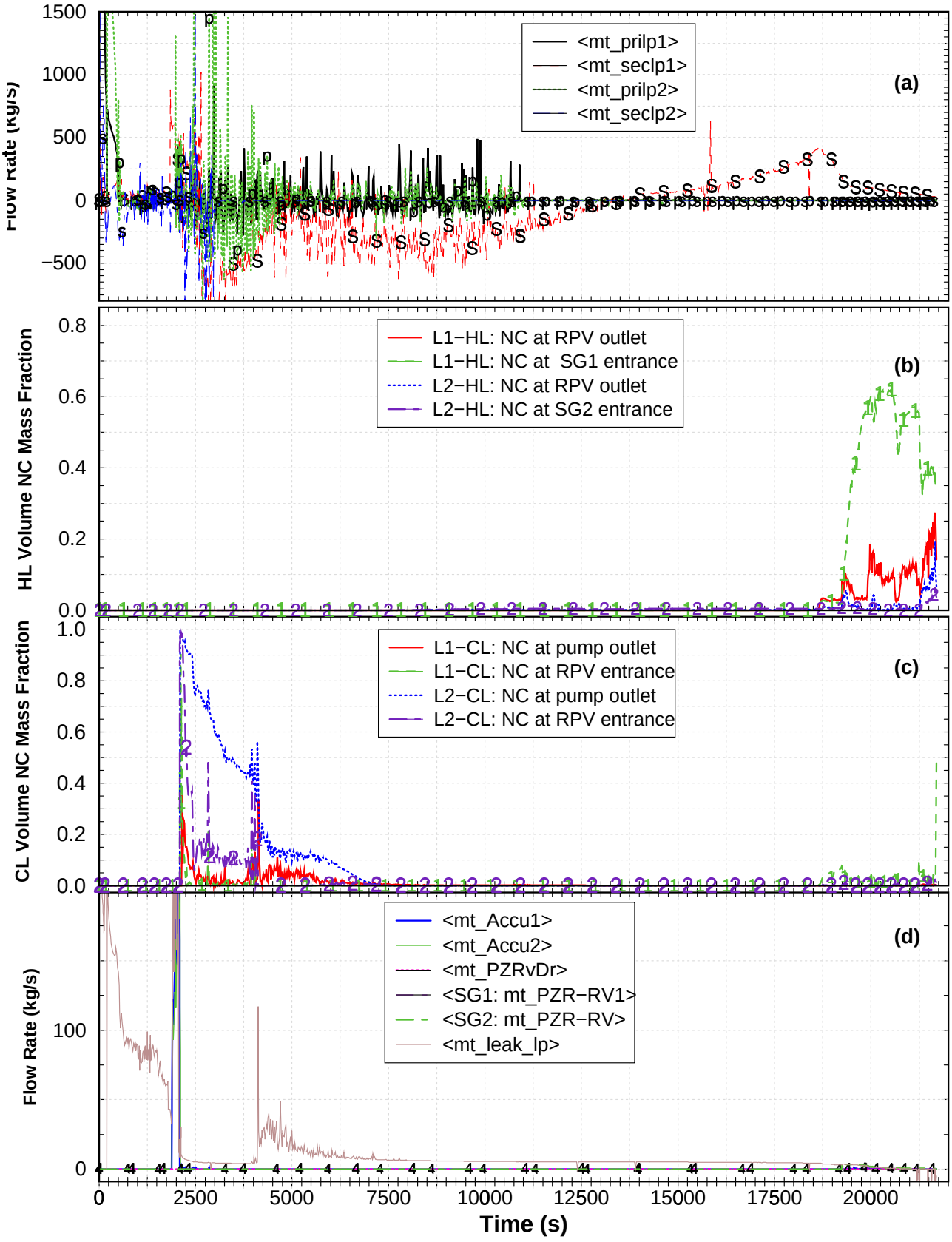

Figure 4.2 SBLOCA primary system behaviour: (a) mass flow rates, non-condensable quantities in (b) hot leg and (c) cold leg, (d) mass flow rate through leak, pressurizer, and accumulator stand-pipe.

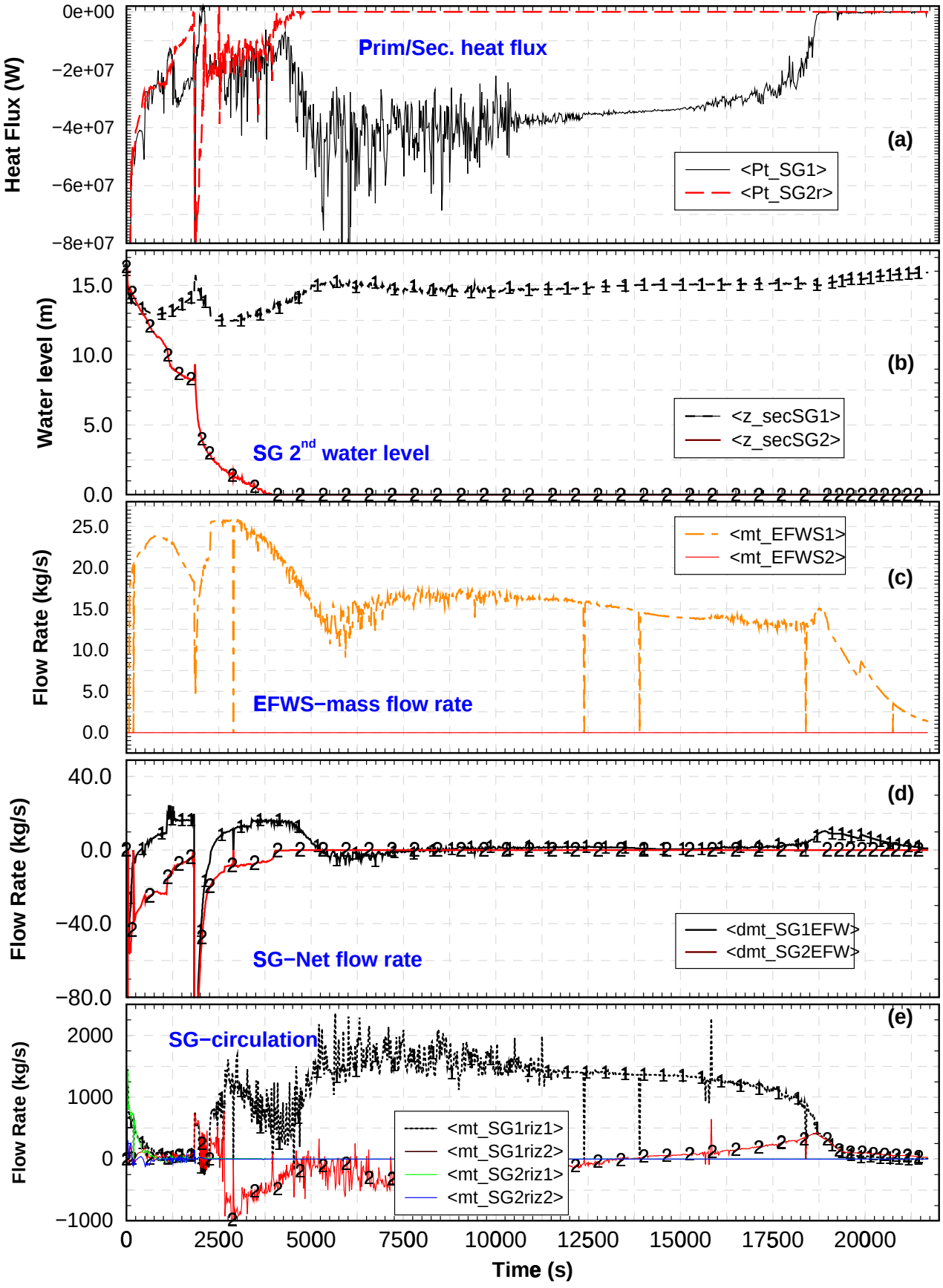

Figure 4.3 SBLOCA secondary side conditions: (a) total heat flux to the SG 2nd side, (b) SG water level, (c) EFWS injection rate for both loops, (d) SG mass in-/out-flow balance, and (d) SG internal circulation.

For this scenario the original 1-D SG nodalisation has been improved to consider the unsymmetrical thermal loading of the SG tubes. Under normal reactor operation the temperature profile along the SG tubes can be simulated with only one secondary fluid element, because of fluid behaviour is controlled by forced convection driven by the main feedwater pump and the evaporation of water.

In this situation the internal water circulation in the SG starts with evaporation, droplet separation, re-flow through the SG downcomer. In case of emergency feedwater supply (< 28 Kg/s) the different behaviour of the riser and downcomer side of the SG tubes becomes detectable. The standard SG nodalisation was extended (Figure 2.3) to simulated both branches, the riser and the downcomer part independently. This is important because only at the riser side of the SG tubes heat is transferred to the water condensing steam. As a consequence an internal re-circulation driven by rising steam bubbles is established during natural convection phase as can be see in Figure 4.3e.

The upper curve in Figure 4.3e shows the rising steam and water mixture and the lower (negative mass flow values) the down-coming water in the other half of the SG. The difference is the vapour mass released through safety valves. The amount of steam is app. the same as the injected emergency feedwater shown in Figure 4.3. In SG2 the mass fluxes are zero after dry-out occurred at app. 63 min. An overview of the different water levels is added in Figure 4.4c.

4.2 Core heat-up

At around 13420 s (223 min) the boil-down starts leading to core heat-up when the core water level drops below 3.2 m at 15236 s (254 min). Up to 17800 s (297 min) the heat-up rate remains below 0.25 K/s, only driven by the decay heat (Figure 4.1 a). At 18000 s the decay heat amounts to 42 MW, 0.9 % of nominal power.

At around 17800 s (297 min) the peak core temperature exceeds 1000 K and the SCDAP oxidation model becomes active. At 18720 s (312 min) the core outlet fluid temperature exceeds 926 K. In this scenario an activation of the primary system depressurisation is assumed which reduces the primary system pressure from 0.6 MPa to 0.2 MPa. Thus reduces the saturation temperature and the enhanced evaporation increases oxidation as can be seen in the hydrogen spikes in Figure 4.1d. The heat-up rate which starts with app. 0.3 K/s increases constantly due to the exothermal reaction up to its maximum of app. 9 K/s at 18672 s (311 min).

At that time the hydrogen production rate reaches 0.8 kg/s (Figure 4.1 d), which releases app. 112 MW, this is app. 3 times the decay heat as can be seen in Figure 4.1 a.

Cladding rupture caused by ballooning is calculated for the inner ring at 18617 s (310 min) at a core elevation of 3.45 m when the cladding temperature exceeds 1436 K. In the outer ring the failure is delayed until 328 min. In detail the growth of the oxide layers is shown in Figure 4.5 on the left side together with the relevant cladding temperatures (right side). Generally the core is axially divided by the progressing evaporation as well as the pressure control measures. Especially at 1.65 m the cladding temperature drops slightly at 19000 s due to primary depressurisation which increases the evaporation rate so that oxidation heat is removed more efficiently.

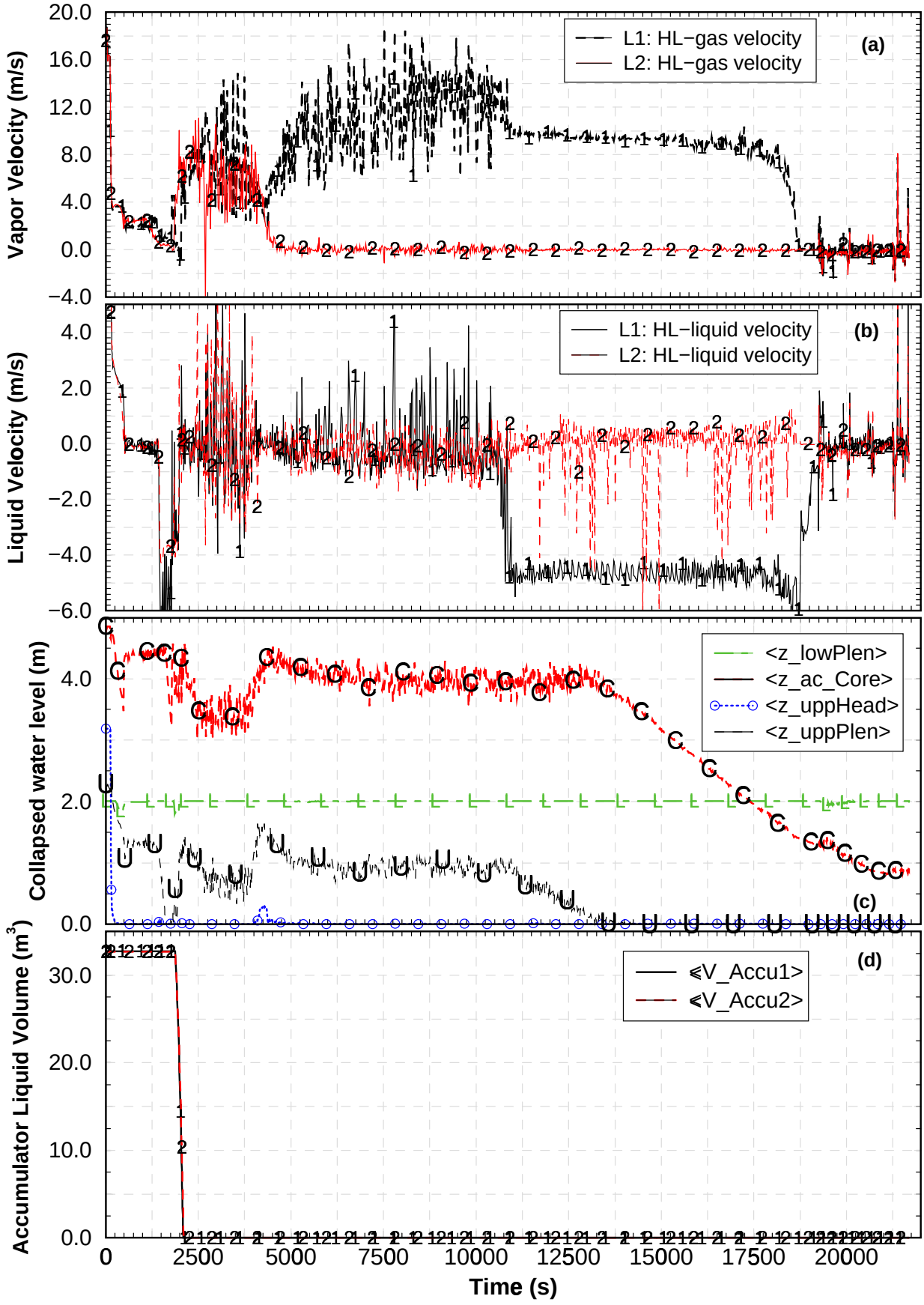

Figure 4.4 SBLOCA: Gas (a) and liquid (b) velocity in the hot-legs of Loop 1 and Loop 2, (c) water levels in the upper head (-0-), upper plenum (U), (c) core (C) and lower plenum (L), and (d) accumulator water inventory.

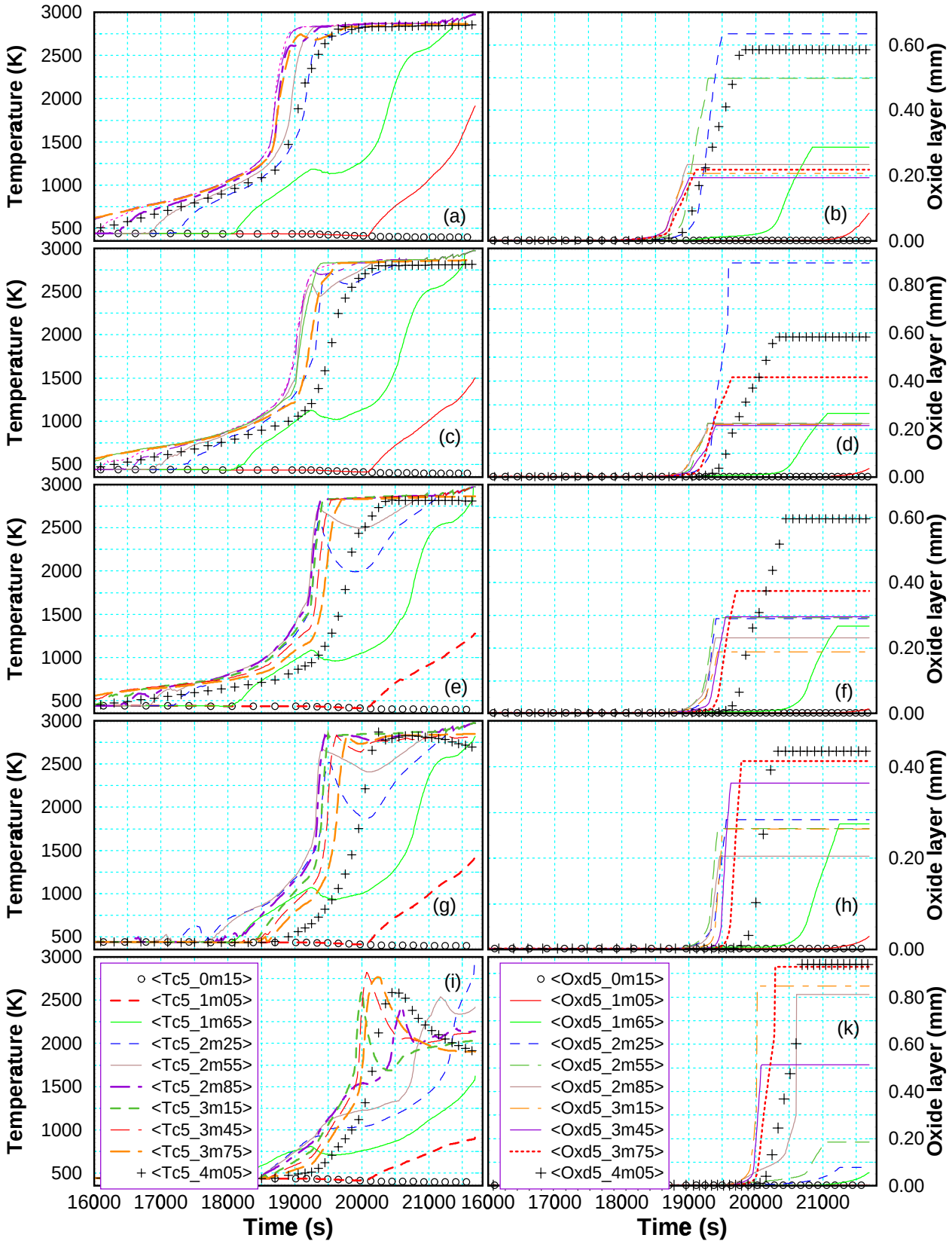

Figure 4.5 Calculated cladding temperatures (left side) and oxide scales (right side) for the SBLOCA scenario: (a, b) centre ring, (c, d) ring 2, (e, f) ring 3, (g, h) ring 4, and (i, k) outermost ring 5.

As a consequence of the improved convective cooling temperature drops at this elevation in the whole core. A complete cladding oxidation is calculated only for the uppermost two nodes in the outermost ring (Figure 4.5h). All other nodes show oxidation up to 0.65 mm until melting temperature of β-Zry is reached and pellet-clad interaction starts. At that time no more metallic Zry is available for oxidation. The lowest node which significantly contributes to hydrogen production of intact fuel rod claddings is at 1.05 m.

4.3 Temperatures of RPV internals

4.3.1 Radial core enclosure

As mentioned earlier, for this analysis the radial radiative heat transfer calculation is restricted to each ring. In the outermost radiation to the HR simulated by a shroud component is considered. This causes a time delay of app. 20 min between first escalation in the central ring (Figure 4.6 a) and in the outermost channel (Figure 4.6c).

Up to the 20800 s, the calculated HR temperatures exceed melting temperature in the inner half of the HR (Figure 4.6e, g) above 2.85 m. In the outer half, only the uppermost node reaches melting conditions. In inner half simulates the edges facing to the fuel elements. The CB (Figure 4.6i) remains below 900 K.

At 21700 s the inner HR surface (Figure 4.6e) and centre temperature (Figure 4.6 g) show a sudden unrealistic temperature increase between 1.05 m and 1.65 m core elevation. Within one time step the HR temperatures jump from below 750 K to more than 2700 K. One possible cause this unphysical behaviour may be that the late phase failure model of the shroud component was not tested for such massive structures like the HR. The main reason for this code error is still questionable (section 10).

4.3.2 Upper plenum internals

In the column of Figure 4.6 the temperatures of RPV internals above and below the core are shown. For the upper support structure (USS) and the three rings of the upper dome wall (Figure 4.6b) temperatures of less than 650 K were calculated. The USS temperatures show an increase of < 280 K/h caused by heat conduction from the upper plenum. If the thermohydraulic conditions are maintained melting would occur app. 10 h after reactor scram.

In the upper plenum, the top and middle section of the control rod support tubes (CSC) shown in Figure 2.3 are heated up to app. 1200 K (Figure 4.6d), the lower section (Figure 4.6 f) to 900 K. Based on the heat-up rates calculated in this phase of the accident (< 0.15 K/s) melting would occur app. 6 h after reactor scram.

For the upper core plate (UCP) two models were used, a SCDAP upper plenum structure (UCP) component and a RELAP5 heat structure. In Figure 4.6 h the temperature history of the RELAP5 heat structures is given, which show some discrepancy compared to the UCP results due to different boundary conditions caused by lacking radiation coupling of the UPS component.

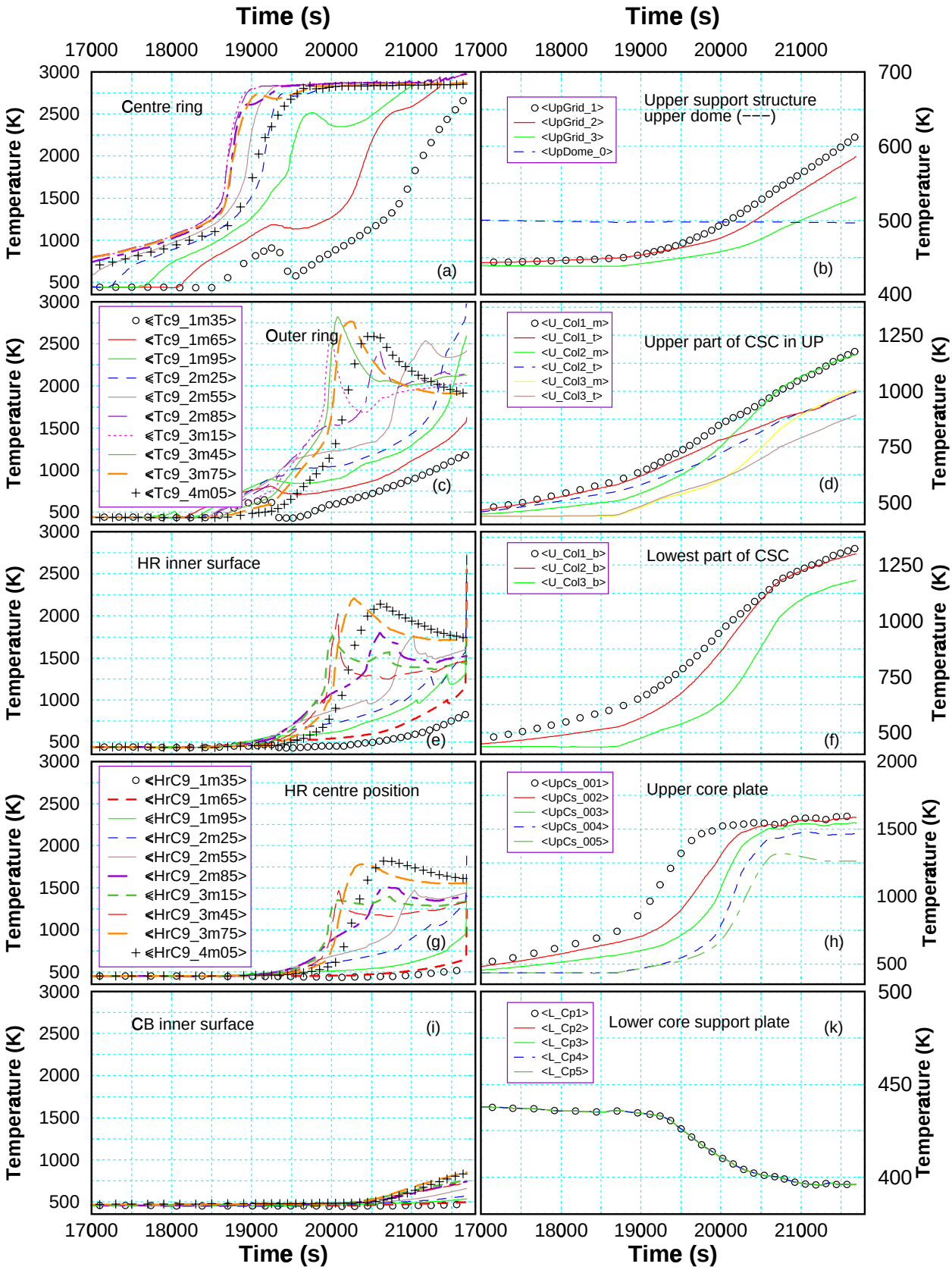

Figure 4.6 Calculated temperatures for the SBLOCA scenario: fuel rod cladding: centre ring (a) and outermost ring (c), heavy reflector: at inner surface (e), in the centre (g) and at the outer surfaces (i), upper core support plate (b), support columns top and middle zone (d), bottom zone (f), upper core plate (h), and lower core plate (k).

4.3.3 Lower core support plate

As discussed in section 2.2 the lower core support plate is a massive stainless steel structure with four borings for each fuel element. At the end of the calculation the core water level is at 1.2 m so that the massive lower core support plate (LCSP, Figure 4.6 k) is kept at saturation temperature.

4.4 Core degradation

4.4.1 Control rod

First component to fail releasing metallic melt is the Silver-Indium-Cadmium (SIC) control rod in the centre ring. It fails at 18739 s (312 min) releasing the liquid alloy between 3.15 m and 4.05 m core elevation. At 21556 s (359 min) the control rod in ring 5 is calculated to fail in 1.65 m core elevation, just below the just recently formed molten pool.

4.4.2 Fuel rod

After oxide layer failure at 18617 s first metallic melt relocation occur and after some subsequent relocation events first debris is formed at 19089 s (318 min) in 3.45 m elevation in the centre ring. In the next 1200 s a sequence of metallic melt relocation remove up to 3 Mg UO_2 and Zr as can be seen in Figure 4.7a, b.

The accumulation of melt starting at 20000 s increases the cohesive debris at 3.15 m and reduces convective cooling so that it starts melting, forming the nucleus of the in-core molten pool 100 s later (Figure 4.8). As a consequence the net core flow area is reduced as shown in Figure 4.7d until molten pool is formed as can be seen in the Equiv_pool radius in Figure 4.7c. The flow area reduction due to molten pool formation is not included, because S/R5m32 uses late phase models for the components if a molten pool exists in this axial level. So flow blockage caused by the large molten pool shown in Figure 4.9 cannot be found here either.

4.5 Debris and molten pool behaviour

In Figure 4.7c the direct results of S/R5 shown axial and lateral spreading of the pool however, the interpretation may become laborious. Therefore, a simplified 3-D schematics is extracted from these data showing the position of the lower crust of the molten pool. After formation of a single node molten pool primarily axial spreading is calculated in the next 10 min. After 20574 s (343 min) the molten pool spreads out radially into the fourth up to 20663 s. The lowest core level is reached in the centre ring at 21355 s (356 min). The molten pool grows by melt accumulation until end of the calculation. At 21962 s (362 min) contact mode between molten pool crust and heavy reflector is calculated starting melt release into the downcomer. However, an instantaneous and complete melt through is not realistic, stand alone analyses indicates a certain time delay of app. 30 min /14/.

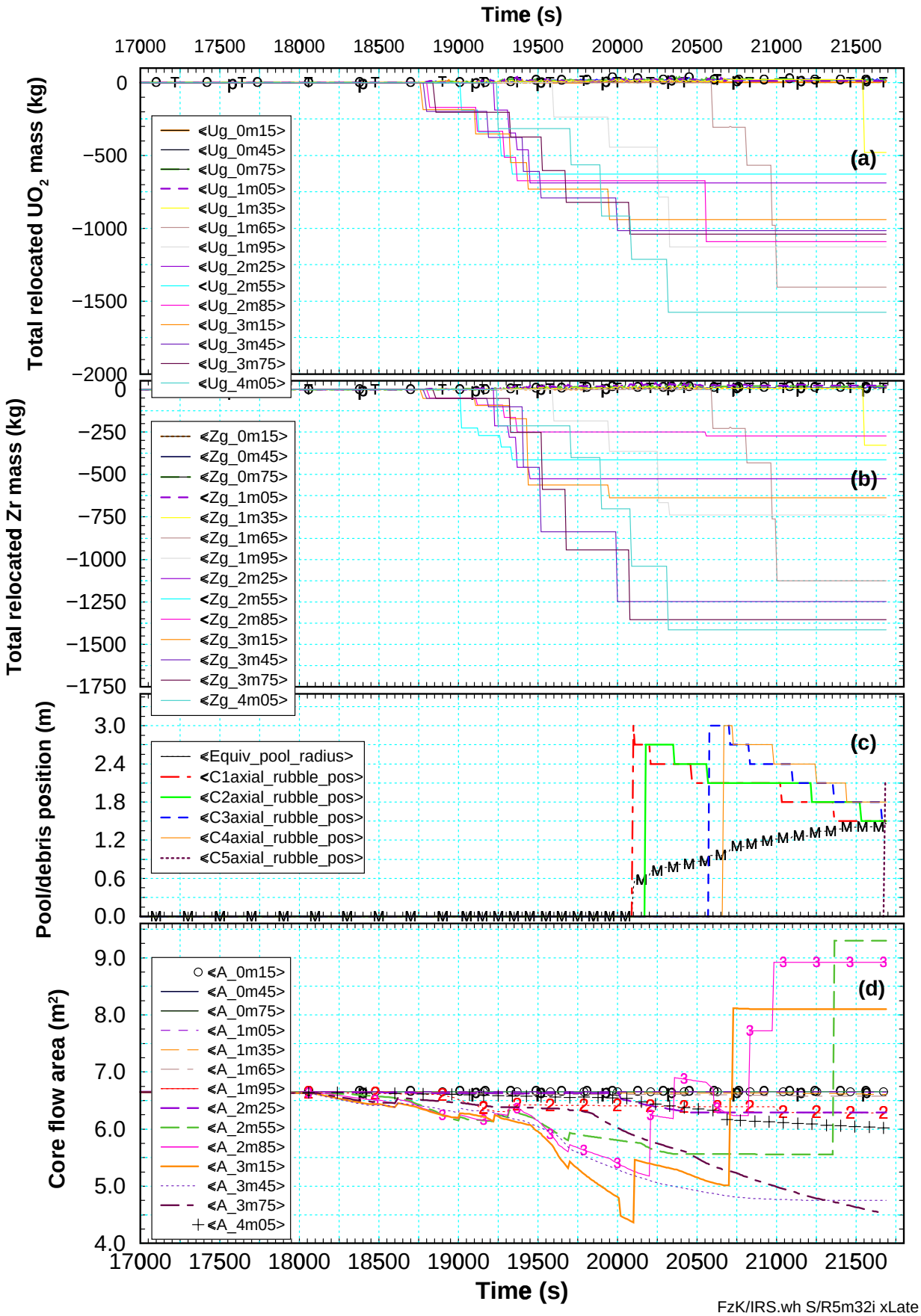

Figure 4.7 Late phase metallic melt relocation for SBLOCA scenario: (a) UO_2 mass redistribution, (b) Zr mass redistribution, (c) axial position of porous debris (crust) and equivalent pool size, and (d) net flow area in the core.

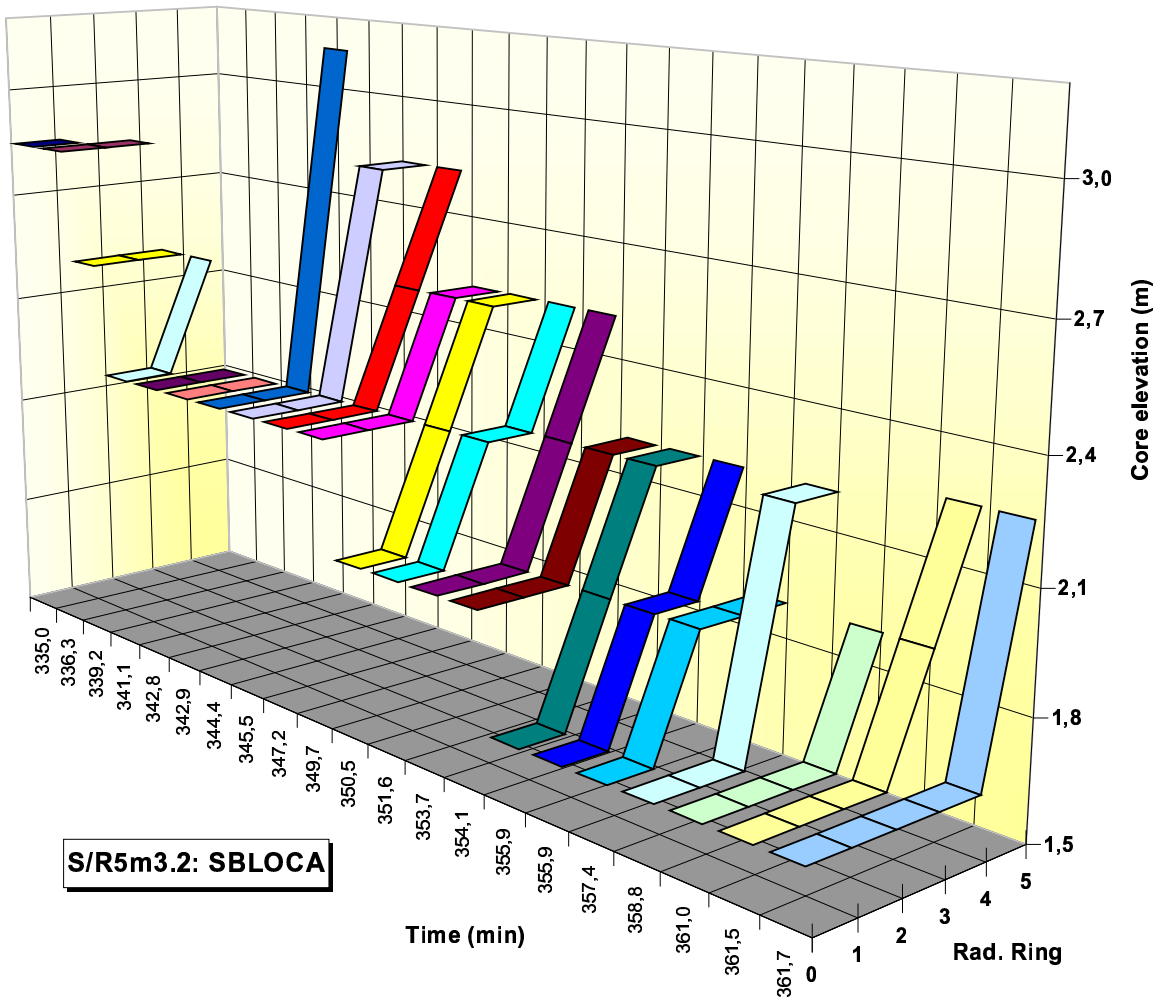

Figure 4.8 Axial and radial position of the lower crust of the molten pool in the SBLOCA scenario for times at which relocation events were calculated between 335 min and 362 min. The crust is situated on top of porous debris one zone below.

4.6 Final state

The schematics shown in Figure 4.9 describes the final state of this calculation. On the left side the nodalisation levels are indicated, in the centre the RPV is sketched, and on the right side the calculated mass distribution is given.

As pointed out above, the debris- and molten pool region spreads out radially over the whole core in 2.25 m core elevation and contains a liquid mass of app. 62 Mg composed of UO_2, Zr, ZrO_2 and some liquefied debris. The axial extension of the molten pool is 3 zones (app. 1 m). This is roughly twice as much material compared to the initial mass distribution (app. 10 Mg / 0.3m neglecting absorber and steel mass) and hence the decay heat inventory is twice as high. Above the molten pool a voided region extends up to 3.45 m. Above this region some debris (P) with liquefied material (L) or even some intact fuel rod are calculated. This scenario is strongly biased by the TMI-2 accident where intact regions were found above the voided region. However, in the ongoing accident this is not very realistic and requires some improvements (S/R5mod3.3).

As mentioned in section 4.3.2 the upper core plate (UCP) is modelled by SCDAP upper plenum structure (UPS) elements used to identify onset of melting and RELAP5 heat structures as radiation surfaces for upper plenum heat exchange calculation. So the mass is scaled and therefore not added to the debris or molten pool. However, the code indicates that the UCP is oxidised and nearly completely molten.

In the lower section the melt calculated to be relocated in the downcomer and frozen in the second axial zone of the downcomer (below the water level). This shortcoming is not yet understood, one possible hypothesis is that the code was tested with large amount of melt relocation through the downcomer into the lower so that an early freezing was never observed. Also shroud components used to simulate the heavy reflector behaviour may not be appropriate for this case. To corroborate these hypothesis the calculation may be repeated with SCDAP/ RELAP5 mod 3.3 including an updated shroud model.

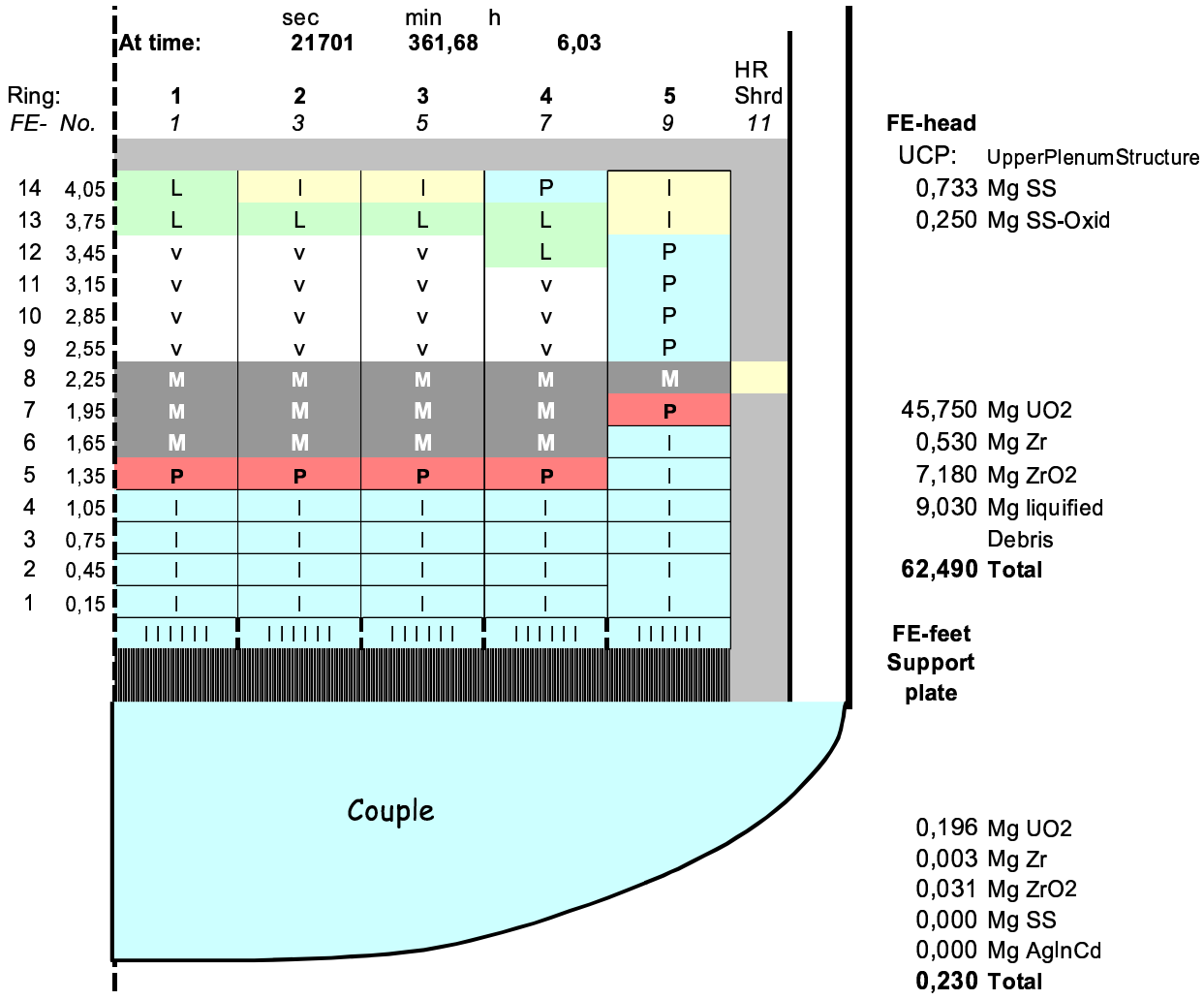

Figure 4.9 Final state of SBLOCA analysis with S/R5m32, characterised by nodal properties such as: intact fuel rods (-I-), porous debris (-P-), molten pool (-M-), voided region (-v-), and partially liquefied debris (-L-).

4.7 Discussion

One general characteristics of this scenario is the strong dependency of the time scales on thermo-hydraulics mainly caused by counter-current flow in the hot leg of the primary system (to be discussed in detail in section 4.8). Core heat-up is initiated when primary system pressure drops below 0.25 MPa so that natural convection cannot transport decay heat to SG secondary side.

That reflux-condensor mode, which extends from the fast cool-down of SG secondary side up to core heat-up, constantly refills the core by condensed water, so that sufficient steam for oxidation is available up to end of the calculation. As a consequence, highest hydrogen mass of all scenarios discussed in this report are calculated as discussed in section 7.1. The molten pool grows within 0.5 h up to app. 60 Mg until the lateral crust contacts the HR at app. 2.25 m elevation, whereas the lower crust is situated around 1.4 m, app. 0.3 m above water level.

4.8 Comparison of different SBLOCA analyses

In total several analyses have been performed for the SBLOCA scenario and from the successful analyses four cases (Table 4.2) have been analysed in detail and will be discussed with respect to the influence of thermohydraulics on the event timing. Results from MELCOR /2/ and MAAP /3/ are available but not considered here. The results with S/R5 mod 3.2 ß are discussed in /14/ in detail. Analyses with S/R5m31 for the EPR in the design basis configuration (P_{th} = 4.25 GW) are not used here but documented in /23/.

From the four cases shown in Table 4.2, case C1 is a recalculation with the old version of S/R5 mod 3.1.f including some FZK/IRS extensions and uses the same input deck as case C2 calculated with original release of S/R5 mod 3.2. The case C3 was calculated with a special S/R5 version which includes some RELAP5 mod 3.2.2.β improvements with respect to non-condensable predictions in subcooled water.

Generally the implemented extension worked well for the accumulators, however, it undefinebly influences also the interface terms between liquid and vapour phase. In the actual RELAP5 version (R5 mod 3.2.2.γ) released in 2000, this formulation was corrected. Later-on it was found that most of the numerical problems arise if more than one surge-line injects non-condensables into one RELAP5 volume. In a first approach the accumulator surge-lines were distributed along several sub-volumes of the cold leg. Finally, the three accumulators were merged again into one 3-fold accumulator in case C4, calculated with S/R4 mod 3.2.irs as described in the Appendix (Table 10.1).

As explained in section 4.1 this thermohydraulic phase of this scenario is rather long, mainly due to the assumed EFWS supplying SG1 with water. In Table 4.3 time of the most relevant events as well as the duration of the different phases are given for all cases.

Table 4.2 Raw initial and boundary conditions of S/R5 analyses for SBLOCA

Case	C1	C2	C3	C4
Input Deck	Ex5B2x50.mar	Ex5B2x50.mar98	Ex5C2x5.Sep99	Ex5B2kx5.J2k
Data source	Ex5B2x5.m32. oct.dmx	Ex5B2x50. mar98.dmx	Ex5C2x5.Sep99. dmx	Ex5B2kx5.J2k.dmx
Code version	SR5m31f	SR5m32	SR5m32β	SR5m32.irs
Most significant difference to Reference calculation.				Reference
RCSL	Accumulator valves kept open after emptying	Accumulator valves kept open after emptying	Accumulator valves kept open after emptying	Accumulator valves kept open. Volume control-system deactivated when leak detected
RELAP	Radiation calculation in the Upper head ***Special adaptation to R5 mod 3.1.F***	Radiation calculation in the Upper head	Radiation calculation in upper head (UH). **Reduced primary system coolant mass** Containment simulated by different R5 volumes with only one pressure boundary	No radiation calculation in UH Primary coolant inventory adapted to BDOP data **Combine three Accus of Loop 2 into one**
SCDAP	RDB-wall as SCDAP shroud component Slumping into HR-Bypass **Ring to ring radiation**		RDB-wall as R5 heat structure Slumping into DC Only intra-ring radiation	RDB-wall as R5 heat structure Slumping into DC Only intra-ring radiation
COUPLE	No Couple Input		Initial volume temperature too high	Input deck revised

4.8.1 Thermohydraulic phase

As start time for the thermohydraulic phase the voiding of the accumulators is considered and the end time is the onset of hydrogen production. In this interval the driving heat source is only decay heat and the heat sink is the SG1 secondary side until primary system depressurisation is assumed. Due to different code versions and input decks the four cases show different timing behaviour and the duration varies between 183 min (C2) and 391 min (C3). For a more detailed discussion the most relevant results are outlined in Figure 4.10 and Figure 4.11. For an explanation of the different timing behaviour in the primary system, interface conditions in the SGs to the secondary side given Figure 4.12 a and b have to be considered too. Between the scenario starting first with core heat-up (C1, Figure 4.10a) and the last (C3) a difference of app. 3 h is calculated. Within this time the decay heat decreases by app. 20%.

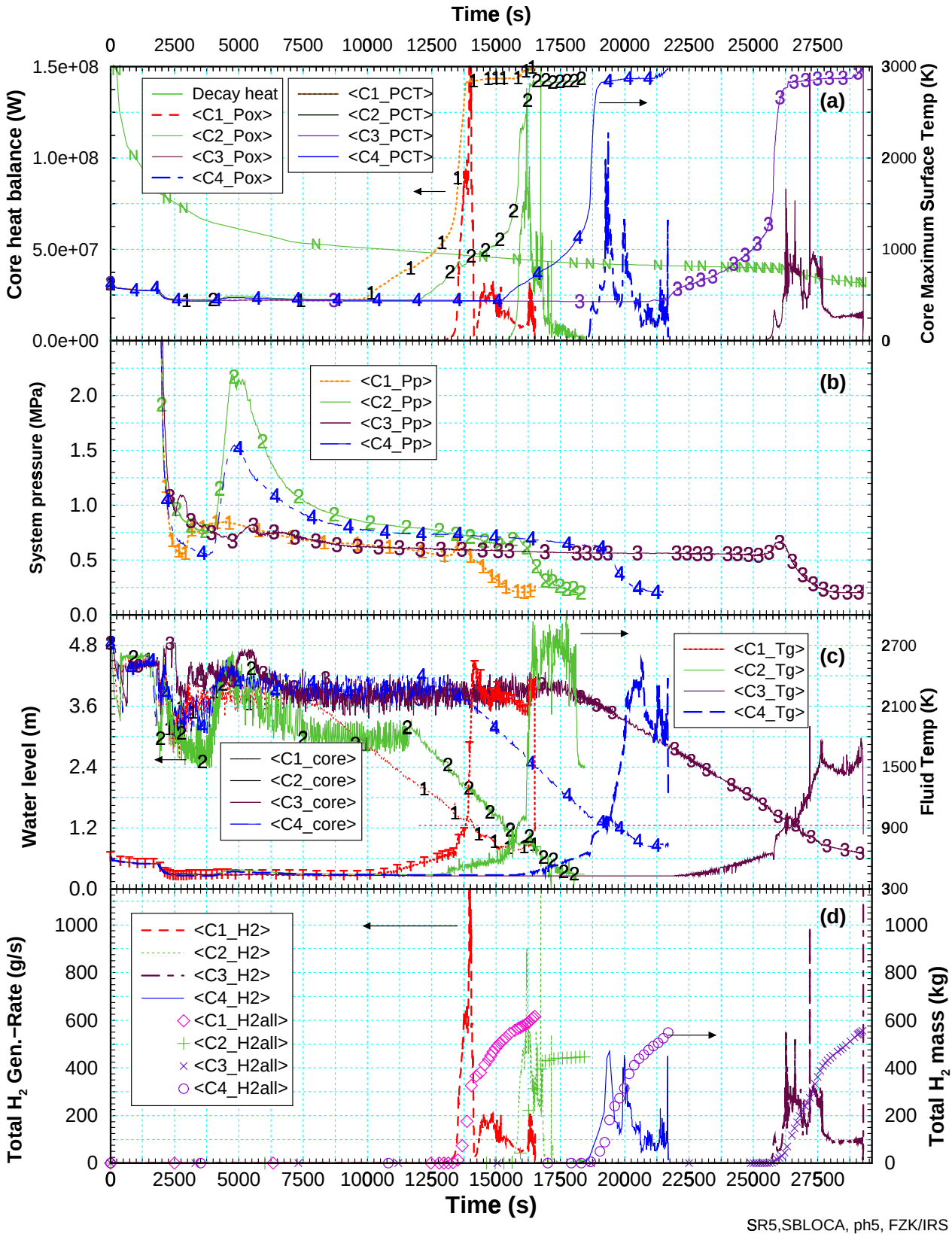

Figure 4.10 Comparison of SBLOCA accidents analysed with S/R5m31 and S/R5m32: (a) nuclear and chemical power (left scale) and peak core temperature (right scale), (b) primary system pressure, (c) core water level (left scale) and core outlet vapour temperature (right scale, with 926 K line), and (d) hydrogen production rate (left scale) and total H_2 mass (symbols, right scale).

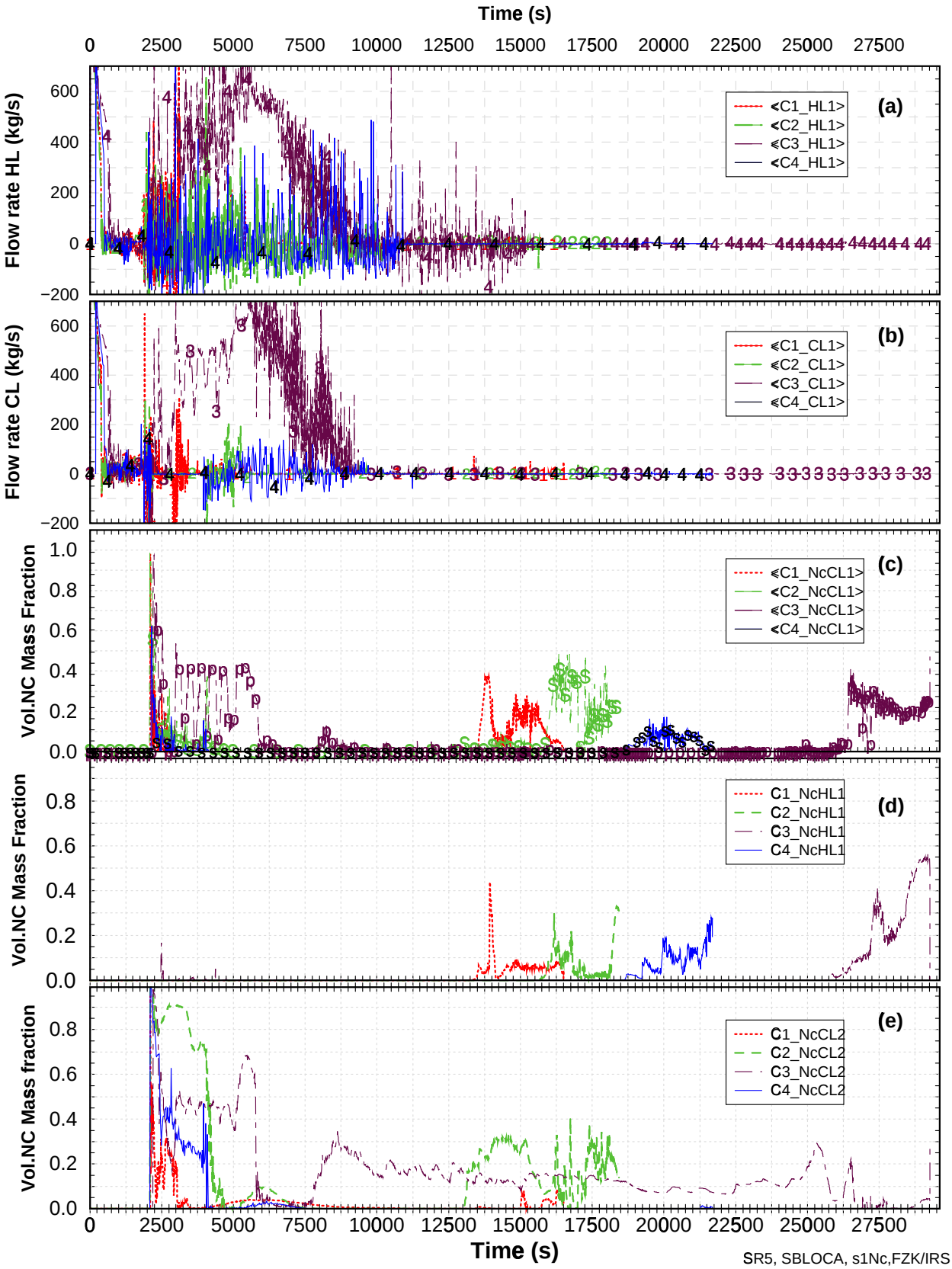

Figure 4.11 Comparison of primary system data: (a) mass flow rate driven by natural convection in the hot leg and (b) in the cold leg, (c) amount of non-condensable in the primary system fluid at leak position in the cold leg of loop 1, in the hot leg (d), and in the cold leg of loop 2 (e) which is connected to loop 1 by downcomer entrance.

All primary system pressure curves given in Figure 4.10 b show similar shape, especially C1 and C3. In case C2 and C4 a steep pressure increase is calculated mainly due to fluid mixture at the leak position. This behaviour can be explained for C1 with code version S/R5 mod 3.1, which had some problems to simulate the specified lateral leak position at the cold leg pipe. The natural convection scheme in the cases C1, C2, and C4 is restricted to the hot leg of loop 1 (Figure 4.11a, b) only, establishing a reflux condensor mode of vapour flowing to the SG1 and water flowing back to the upper plenum. The re- flow of the liquid water can be seen in Figure 4.12 e as negative fluid velocity prior to primary side depressurisation.

In case C3 a loop circulation is established between 2500 s (42 min) and 9000 s (150 min), the vapour also condensates at the downcomer side of the SG1 tubes. So water is flowing into the main coolant pumps (MCP) and than back to the downcomer. After 9000 s the mass flow rate in the cold leg of loop 1 drops to values observed in the three other cases (Figure 4.11 b).

This causes different core dry out rates, which become obvious in Figure 4.10 c. An average dry-out rate is calculated for C1 to –1.5 m/h, for C2 –2 m/h, C4: -1.8 m/h, and C3: app. –1 m/h. Except for case C2, which shows a higher evaporation rate mainly due to the higher primary system pressure between 4000 s and 12000 s as shown in Figure 4.10 b (-2-), this dependence can be explained by the decay heat decrease.

In all cases the total heat flux to the SG1 secondary side (Figure 4.12 a) ranges between 50 MW and 25 MW so that nearly the whole decay heat is transferred to secondary system. Core heat-up starts when the collapsed water level drops below app. 3.0 m in the core as can be seen comparing Figure 4.10 a and c. The ongoing water evaporation in the core leads to heat up rates in the upper part of the core of < 0.3 K/s. At that time primary system pressure varies between 0.6 and 0.7 MPa. App. 70 min later core outlet vapour temperature exceeds 926 K and primary depressurisation is initiated (Figure 4.10c). When the cladding temperature reaches 1000 K the oxidation model is activated influencing the course of the accident in releasing of additional energy.

4.8.2 Core degradation phase

The duration of this phase varies between 28 min (case C2, C4) and 38 min (C3) as given in Table 4.3. Driven be the energy release of cladding oxidation the peak core temperature increases rapidly leading to peak heat-up rates between 5 and 9 K/s. As a consequence, a few minutes after onset of oxidation, the fuel rod cladding of the central ring bursts after ballooning by exceeding maximum strain in all cases.

Within the next 20 min absorber rod failure is calculated in the central ring, followed by the first release of U-Zr-O melt after oxide layer failure. The core damage during early core melt phase influences all parts of the core which are app. 1 m above collapsed water level transforming the cylindrical geometry into a localised debris configuration. Such a configuration is considered to be coolable unless a cluster of sub-channels is closed by subsequent melt relocation events. In such a situation the embedded decay heat increase inner temperature up to melting of the U-Zr-O mixture, so that liquid nest are formed inside the debris. If cooling is reduced further on, such a configuration is the starting point of an in-vessel molten pool of corium.

Table 4.3 Comparison of the SBLOCA event timing calculated with different S/R5 versions.

Nr	Scenario type (General) Event	C1	C2	C3	C4
1	Code specification	mod 3.1.F	mod 3.2	mod 3.2β	mod 3.2.irs
2	EPR input deck	Ex5B2x50	Ex5B2x50	Ex5C2x5. Sep99	Ex5B2kx5.J 2k
3	Data source (documentation)	/23/	---	/14/	section **4**
4	Reactor scram	1	1	0.5	0.5
	Thermohydraulic phase events	Time (min)	Time (min)	Time (min)	Time (min)
5	Accumulator injection period	32-35	32-35	33	31-35
6	Fast cool-down of SG – 2nd side	31	31	32	32
7	SG2 – 2nd side dry-out (no EFWS)	65	48	75	---
8	Onset of core heat-up	162	194	357	253
9	Primary side depressurisation	229	264	435	317
10	Onset of hydrogen production	242	218	424	307
	Late Phase events				
11	Onset of clad failure (balloon., rupture)	259	220	425	310
12	Onset of Absorber rod failure	263	227	431	312
13	Clad oxide failure -> first U-Zr-O melt	266	230	443	318
14	Melting of upper core plate (R1-R5)	277	242-251	459	334
15	Onset of pool formation	272	246	462	335
16	Debris/Molten pool crust contacts HR	---	275	487	362
	Phase duration				
17	Thermohydraulic phase (10 – 5)	207	183	391	272
18	Initial core degradation (15-10)	30	28	38	28
19	Molten pool spreading (16-15)	----	29	25	27
	Reason of termination	***User stop***	***SCD error***	***SCD error***	***SCD error***

4.8.3 Molten pool spreading

The in-vessel late phase is determined by the axial and lateral spreading of the molten corium pool as shown in Figure 4.13. In each pictures the growth of the molten pool is shown by the equivalent pool radius of a hemisphere completely filled with corium (-P-). The axial position of the supporting crust is outlined for each ring by solid/dashed lines.

Except for the different initiation times listed in Table 4.3 the duration until end of calculation is similar. The end of this phase is defined by the code failure time of S/R5 mod 3.2 due to numerical problems in case of melt slumping into the lower plenum. All four cases show an onset of molten pool formation in the centre ring at app. 3.3 m core elevation, one node above the supporting rubble debris.

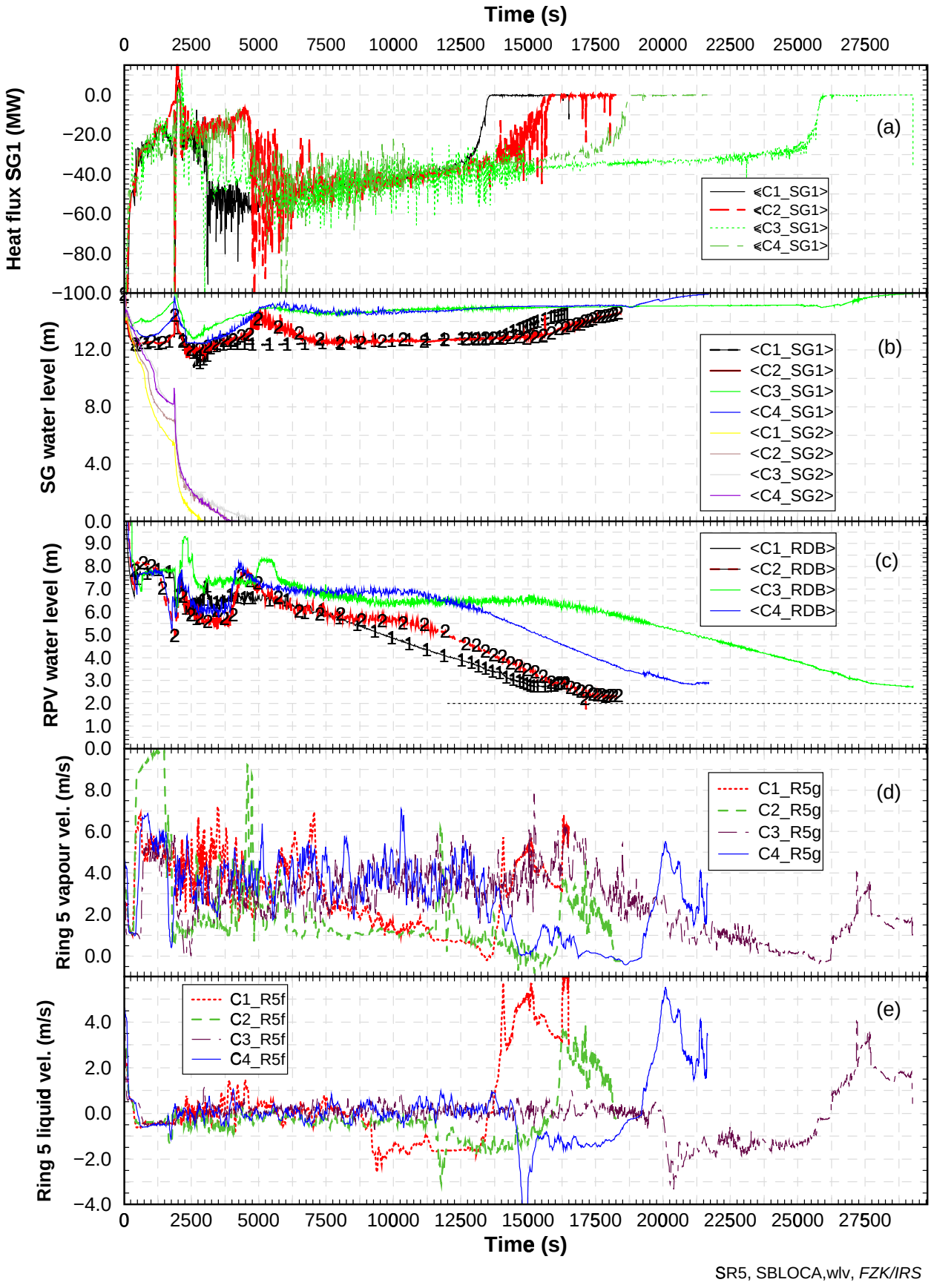

Figure 4.12 Comparison of system data: total heat flux in SG1 to secondary side (a), water level in SG1 and SG2, water level in the reactor pressure vessel (c), vapour (d) and liquid (e) velocity in the outermost (5) ring at to of active core height.

Unfortunately for case C2 the axial position of the supporting crust was not available, so that only the equivalent pool radius is given. In the other cases the molten pool spreads axially down to app. 1.5 m until contact between lateral crust and HR is calculated. This indicated a molten pool sink velocity of app. 0.07 m/min (= 4 m/h). Assuming that this velocity is maintained also in the lower third of the core, the lower end of the active core is reached within app. 22 min. Taking into account the results of the detailed HR melt down analyses /14/ a complete penetration of the HR is possible during this time. Taking into account the uncertainties discussed above and in /14/, as well as the structure of the LCSP, an axial failure of the molten pool crust is highly unlikely.

4.8.4 Discussion

From Table 4.3 an average duration of the thermohydraulic phase (line 17) is calculated to 263 min ± 37 %, to 31 min ± 5 % for the initial core degradation, and to 27 min ± 7 % for the molten pool spreading phase. With simultaneous consideration of different code versions and slightly differences in the input decks (Table 4.2) the time intervals calculated for each case in Table 4.3 are rather similar except for the thermohydraulic phase.

This indicates that the simulation of thermohydraulic effects such as natural circulation, counter-current flow, outflow conditions etc. has a strong influence on the event timing. On the other side, in the other phases critical decision points are controlled mainly by temperature levels (clad failure, onset of oxidation, formation of a molten pool, ...) so that the timing is strictly speaking only dependent on the heat-up rate which is caused by decay- and oxidation heat and by the pressure boundary condition.

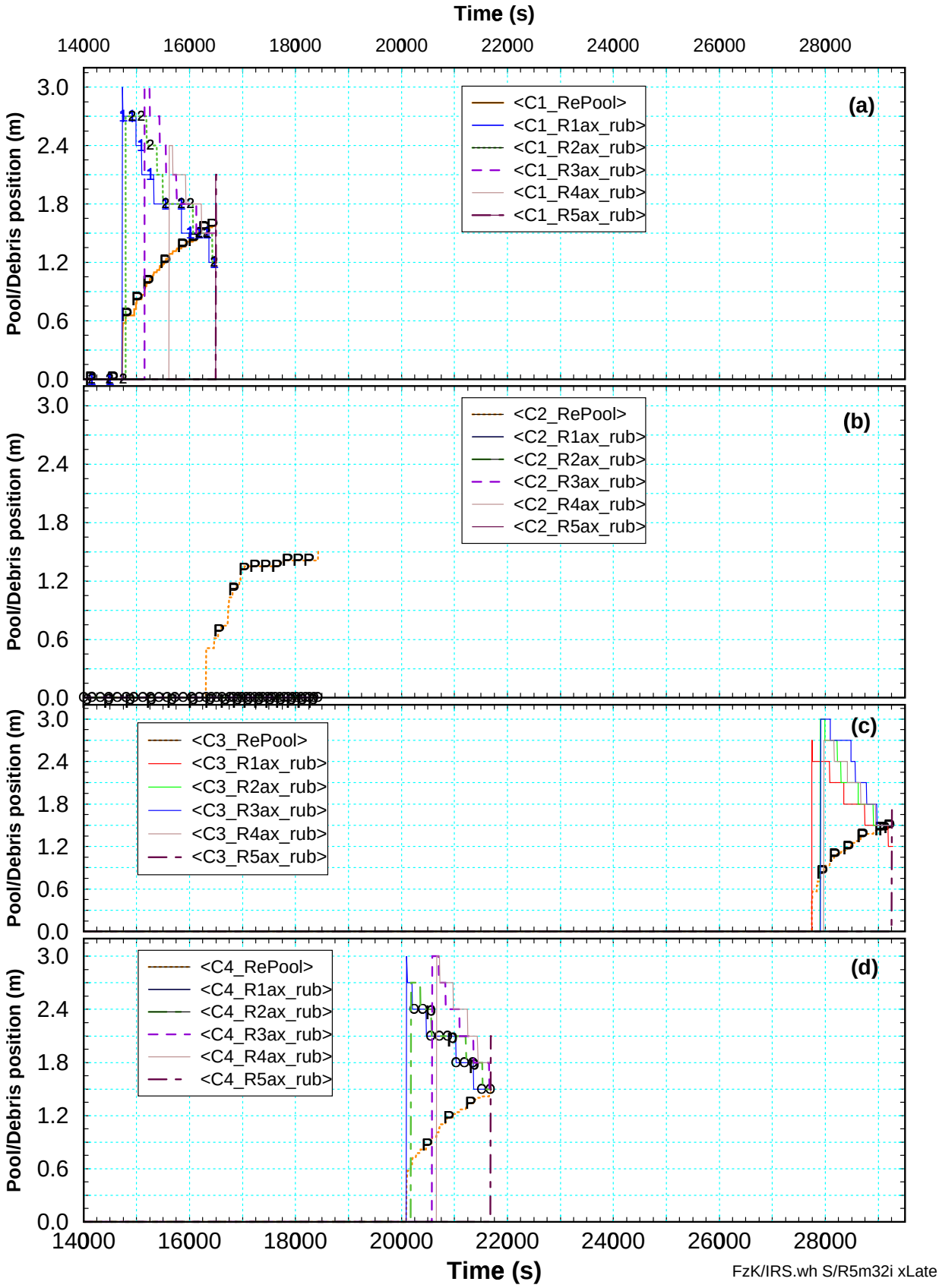

Figure 4.13 Comparison of core configurations in late phase: axial position of debris below molten pool in each ring and equivalent pool radius (-P-) for cases C1 (a), C2 (b), C3 (c), and C4 (d).

5 Loss of Power Scenario

The results of S/R5 mod 3.2 calculations for the scenario " LOOP" (this section) and the delayed LOOP reflood (section 6) will be discussed with respect to hydrogen source for containment analyses and corium source term with respect to in-vessel melt relocation into the lower head.

From different scenarios investigated with S/R5 the loss of off-site power (LOOP) scenario was selected to be representative for delayed reflood prior to onset of oxidation and core degradation. For this scenario, a loss of off site power with subsequent loss of emergency power supply driven by the small and large diesel generators is assumed. Only battery power is available for the, reactor control, surveillance and limitation system and to activate depressurisation valves.

5.1 Thermohydraulic phase

The thermohydraulic phase is subdivided into a natural convection period (section 5.1.1) at high system pressure and the refill and boil-down period (section 5.1.2) at low system pressure as can be seen in Figure 5.1 b.

5.1.1 Natural convection

At loss of off-site power, the absorber rods immediately drop into the core, shutting down the reactor (Table 5.1). Primary coolant pumps and main feed water coolant pumps slow down, and after 10 s main coolant pumps run out. Several seconds later the turbine valve is closed, turbine bypass valve is assumed to remain closed, so that no heat can be transferred to the steam condenser directly. Heat transported from the core to the SG - now by natural convection - increases secondary system pressure so that the set point of safety valves (9.1 MPa) is reached 20 s later. This relatively stable state of natural circulation (Figure 5.2 b) is maintained up to SG dry-out (Figure 5.3 a, b) at about 6000 s (1.7 h). Afterwards no feasible secondary side measure may affect the primary side effectively.

Up to 4500 s (75 min) the primary system pressure (Figure 5.1 b) is kept at normal operating pressure because natural convection is sufficient to remove the decay heat. PCT (Figure 5.1 a) and core outlet temperature (Figure 5.1 b) are at saturation level. The decreasing SG water inventory, however, inhibit vapour condensation in the SG tubes so that natural convection ceases. The primary system pressure increases up to the set point of the first safety valve (valve opens at 17.6 MPa). When the pressure drops below 16.6 MPa the safety valve closes and the cycle starts again, as can be seen in Figure 5.2 d. As can be seen in Figure 5.2 d the design mass flux of 300 kg/s is not reached during normal pressure control operation.

This cycling lasts up to about 9000 s (150 min) releasing heat but also coolant. As a consequence, the water level in the core shrinks very fast leading to a temperature increase in the upper part of the core (Figure 5.1 a). Consequently, the core outlet temperature increases and when 926 K is reached in the upper plenum, primary system depressurisation is initiated by opening the dedicated pressurizer safety valve (PZR valves 824+834).

When the declining primary system pressure falls below 11 MPa the ECC initiation signal automatically triggers secondary side depressurisation, as can be seen in Figure 5.1 b. However, at that time this measure doesn't influence primary system, since the SGs are already empty.

5.1.2 Refill and boil-down

About 600 s after initiation of primary system depressurisation, the pressure has dropped below 4.5 MPa and the accumulator check valves open. Four minutes later, the accumulators are empty and the core is refilled as can be seen in Figure 5.1 c. In this study manual depressurisation is simulated 1800 s (30 min) after ECC initiation too, so that the secondary system pressure reaches containment pressure level. After core refill the primary system pressure is sustained at about 1.0 MPa corresponding to the specified containment pressure of 0.2 MPa and the pressure losses along the flow path through hot leg, surge line, PZR, and depressurisation valve. The boil-down period starts at about 11520 s (192 min) with a collapsed water level of 4.5 m in the core.

Table 5.1 List of events calculated for the LOOP scenario.

	Type (General)	**Time (min)**	**Primary System Pressure (MPa)**	**PCT (K)**
1	Reactor scram (=time of LOOP occurrence)	0.1 sec	15.5	T_{sat}
2	Evaporation of SG 2nd side	100	16.9	T_{sat}
3	Primary side depressurisation	142	17.2	T_{sat}
4	Accumulator injection period	158	4.5	T_{sat}
5	SG 2nd side dry-out (w/o EFWS)	104	17.2	T_{sat}
6	Fast cool-down of SG 2nd side	192	4.0	T_{sat}
7	Onset of core heat-up	198	<4.0	T_{sat}
8	Onset of hydrogen production	228	0.9	1000
9	Onset of clad failure (balloon., rupture)	229	0.88	1205
	Type (Local) Localisation by: R=ring, Z=axial zone	**Time** (min)	Position in the core R-Z	PCT (K)
10	Onset of Absorber rod failure	233	R1 - Z11	2240
11	Clad oxide failure -> first Zr-U-O melt	235	R1 - Z11	2830
12	Onset of large debris formation	240	R1 - Z11	2840
13	Melting of upper core plate (R1-R5)	244	R2: 260 min	2860
14	Onset of molten pool formation	252	R1 – Z10	2870
15	Debris / Molten pool crust contacts HR	305	R5 – Z7	2890
	Duration of phases	**min**		
16	Thermohydraulic phase (line 10 - 4)	75		
17	Initial core degradation phase (line 14-10)	19		
18	In-core molten pool spreading (line 15-14)	53		

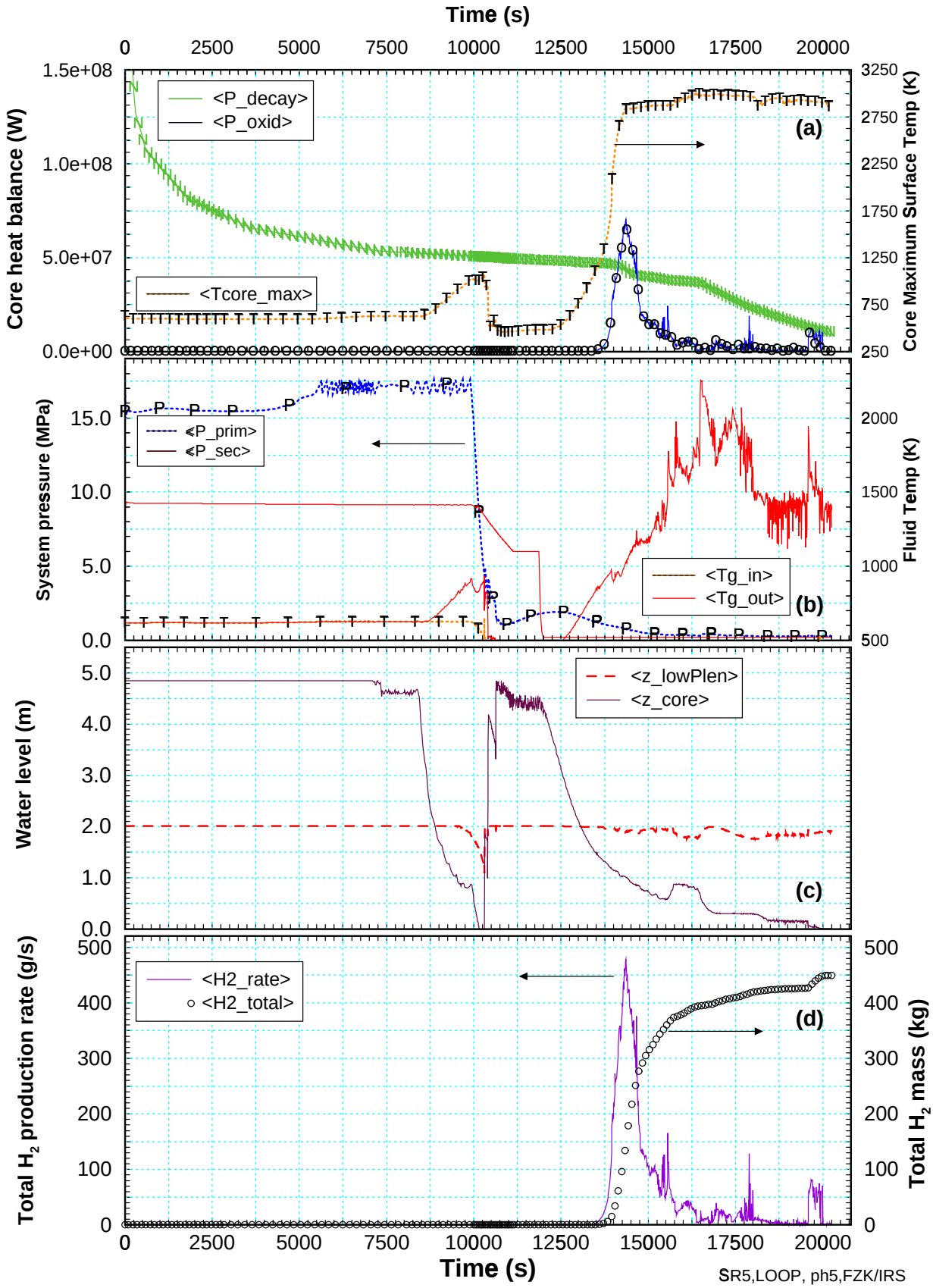

Figure 5.1 Results of LOOP with S/R5m32: (a) nuclear and chemical power (left scale) and PCT (right scale), (b) system pressure (left scale) core inlet and outlet fluid temperature, (c) collapsed water level of core and lower plenum (left), and (d) hydrogen production rate (left scale) and total hydrogen mass (-o-, right scale).

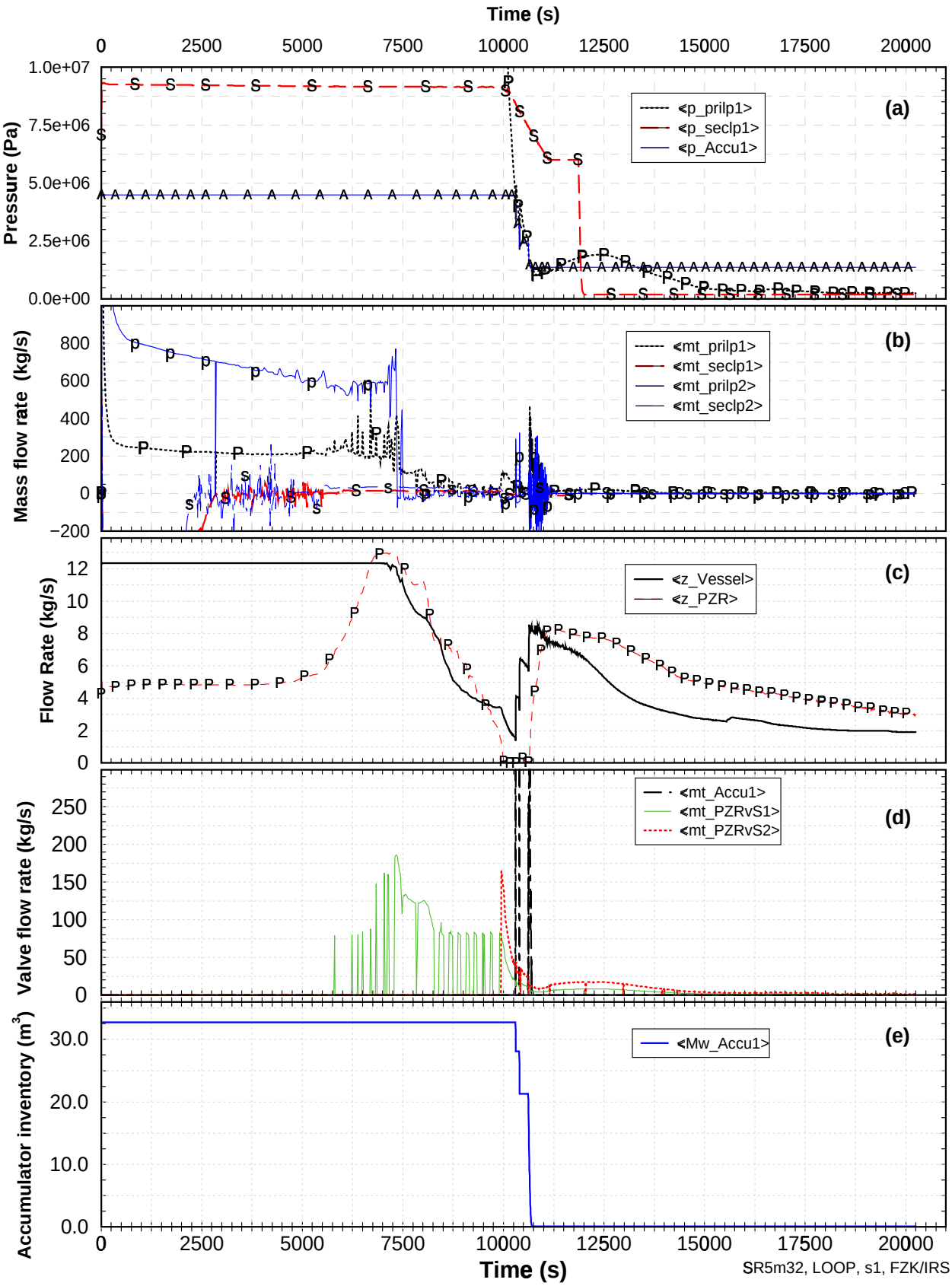

Figure 5.2 LOOP primary system behaviour: (a) system and accumulator pressure history, (b) mass fluxes in the primary system, (c) water level in pressurizer and reactor pressure vessel, (d) mass flow through accumulator stand pipes and PZR relieve valves, and (d) water volume inventory of the accumulator in loop 1.

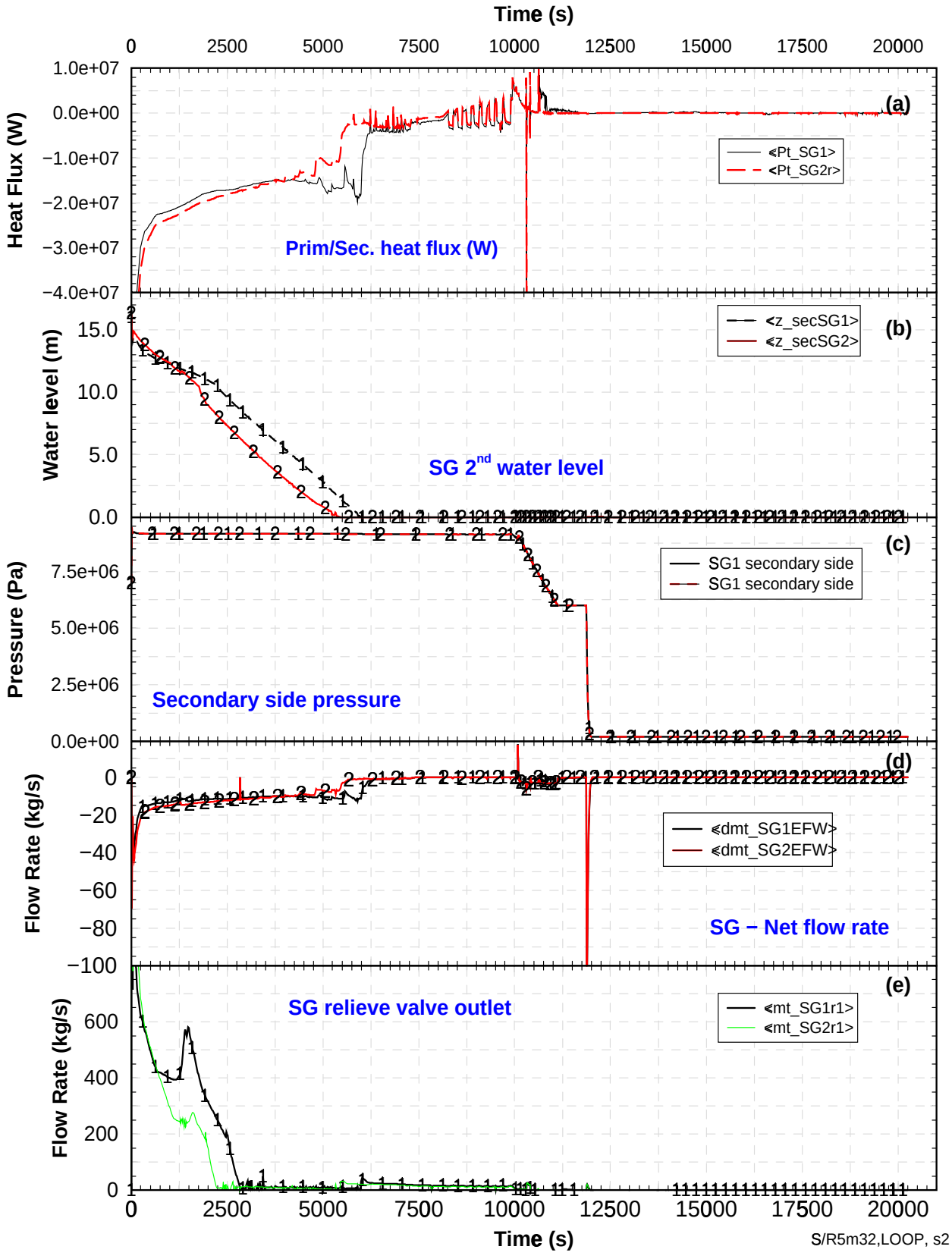

Figure 5.3 LOOP secondary side conditions: (a) heat flux to the SG 2nd side, (b) SG water level, (c) Secondary side pressure, (d) SG mass in-/out-flow balance, and (d) mass flow rate through SG relieve valves.

5.2 Core heat-up

As can bee seen in Figure 5.1 a at 11880 s (198 min) into the transient the core heat-up phase starts, the PCT rises with about 0.45 K/s for 1800 s up to 1300 K. For the next 35 min the heat-up is mainly driven by the decay heat, since a significantly contribution of clad oxidation is found after 232 min. In Figure 5.4 the cladding temperatures (left side) and the relevant oxide layer thickness (right side) are given for the five rings of the core (top-down). As can bee seen, the PCT temperature rise is caused by the centre ring, whereas the other ring are app. 300 s delayed in their temperature excursion.

The heat-up behaviour of the fuel rod in the outermost ring is totally controlled by the decay heat, no oxidation was calculated for this ring (Figure 5.4 k). The main reason is rather low steam production due to the low decay heat (Figure 2.6) released in this ring. Also the high temperature in the 4^{th} ring and the low inner surface temperature (< 1000 K) of the heavy reflector (HR, Figure 5.5 e) hinders oxidation. The additional heat transfer from the forth ring by radiation is not modelled (section 2.4.2).

5.3 Temperatures of RPV internals

In Figure 5.5 a survey of structural temperatures inside the reactor pressure vessel are given. For comparison, the fuel rod cladding temperatures of the centre ring (a) and the outermost ring (c) are given at indicated elevations (4m05 = 4.05 m). The temperatures of the heavy reflector are given for the inner surface (e), the centre line (at the inner interface to the simulated cooling borings (g)), and at the HR -CB interface (i). In all three pictures it is clearly indicated that the HR remains rather cold (<1500 K) up to contact with the molten pool crust. In the inner parts the steel temperature increase indicates contact mode, the outer side shows the influence of the heat conduction in the steel.

In the right row of Figure 5.5, the temperatures calculated for upper support plate and the upper dome wall in the upper head (b). Below the upper and middle sections (d) of the control rod drive support columns (CSC) are drawn and in Figure 5.5 f the lowest section is added. For all CSC structures the temperatures remain below 1400 K, no melting is calculated.

For the upper core plate (Figure 5.5 h) a complete melting of the inner four rings is calculated by R5 heat structures and SCDAP upper plenum structures. In this situation the steel melt is not added to the pool because of remaining fuel rods above the void (section 5.6).

The lower core support plate (Figure 5.5 k) is at saturation temperature up to app. 19500 s. Afterwards a steep temperature increase indicates that the water level has reached the lower end of the core, the foot section of the fuel elements.

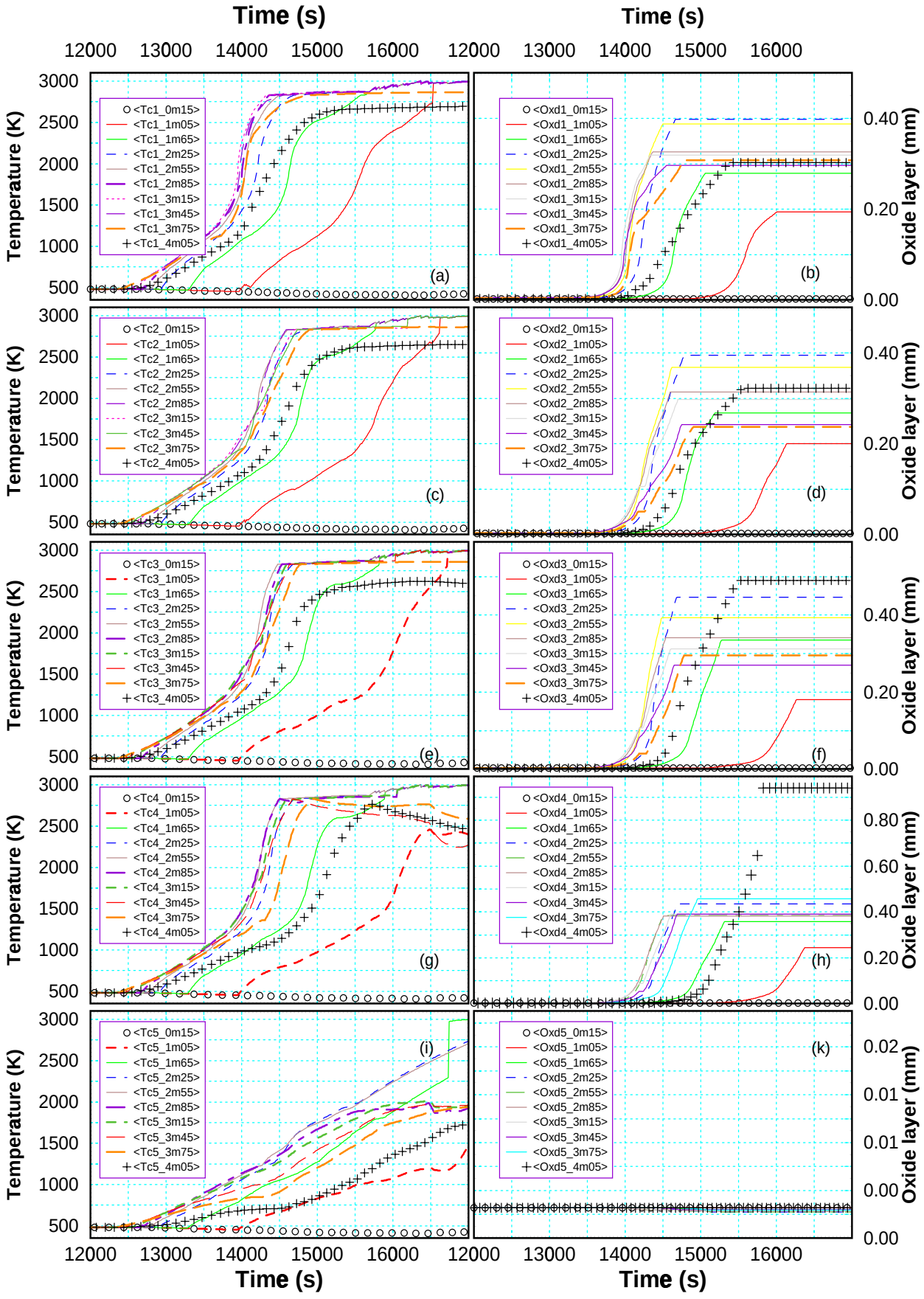

Figure 5.4 Temperature evolution in the core (left) and corresponding cladding outer oxide layer thickness (right) for the five rings in the core (top to bottom).

5.4 Core degradation

Clad ballooning and failure (breach) is calculated to occur in the four inner rings at 13750s (3.8h) and in the outer ring about 300 s later. This delay is mainly due to the HR which acts as an efficient heat sink because of radiative and convective heat transfer since its inner surface temperature is just above saturation temperature.

5.4.1 Component failures

At 14003s (3.9h), first absorber rod failure leading to melt relocation is calculated. The cladding of the fuel rod fails with subsequent melt release at 14105 s in the 12^{th} axial node of the central ring, and metallic melt relocates as droplets into the 11^{th} axial node. Within the next three seconds the same process is calculated to happen in adjacent rings up to the 4^{th} ring, the fuel rod in the 5^{th} ring follows 10s later.

At around 14195 s (3.9 h) the PCT reaches 2300 K, the core is only slightly damaged, and only limited melt relocations have occurred. After 14950 s a molten pool is formed in the centre channel of the core spreading in radial direction and relocating downwards. The collapsed water in the core still declines, and at about 16200 s (4.5 h), water remains only in the lower core support plate and the lower plenum.

5.4.2 Melt relocation

As a consequence of the five radiation enclosures in the core, axial melt relocation is more pronounce as radial core damage progression as can be seen in Figure 5.7. Within app. 50 min the lower crust of the in-core molten pool spreads out axially from app. 3.0 m to 0.9 m. It's outermost boundary extends to the outer ring finally contacting the HR at an elevation of 1.2 m. In Figure 5.7 the position of the lower crust is indicated for the five core rings. The molten pool starts in the centre ring of the 10^{th} axial zone with a mass of app. 7.0 Mg composed of UO_2 and ZrO_2. At that time the mass of partially liquefied debris amounts to 19 Mg, located in the vicinity of the molten pool. This amount will be reduced as the molten pool grows, spreading first radially into the second ring and then downwards 3 zones (app. 1.0 m). The next stage of axial relocation is initiated 7 min later when the pool covers all the inner three rings filling partially one axial zone (0.3 m). This is an unstable situation because the convective cooling of the lower crust in the inner two rings is rather low due to stagnant fluid. The procedure is repeated for each axial relocation until the molten pool contacts the radial boundary of the core at app. 303 min.

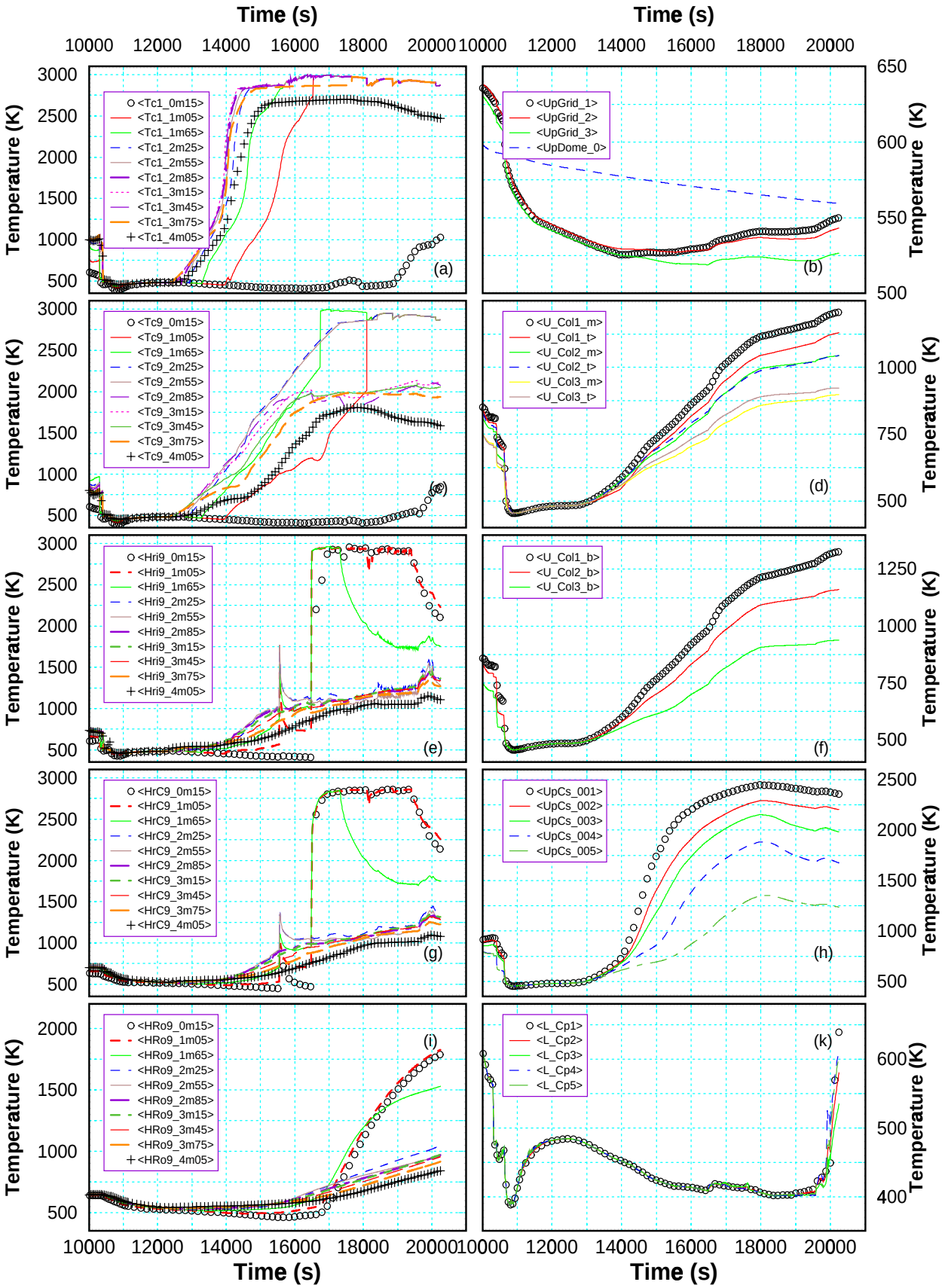

Figure 5.5 Temperature history of the LOOP base case scenario: core temperatures (left) (a) centre, (c) average, and (e) outermost ring, (g) HR inner surface and (i) CB outer surface temperature, RPV internals (right): (b) upper head, (d) USS, (f) upper part of CSC, (h) lowest part of CSC, and (k) LCSP temperature.

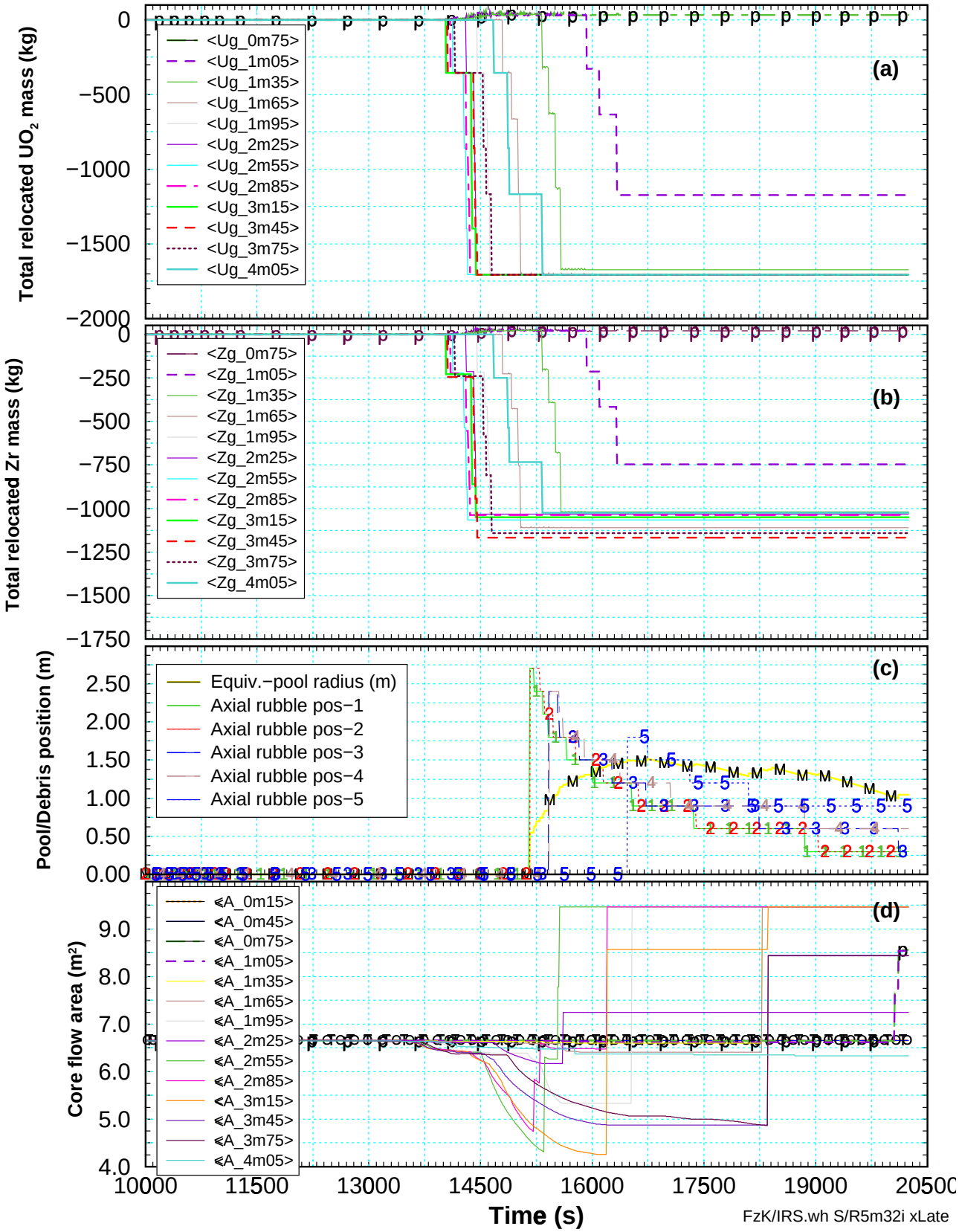

Figure 5.6 LOOP: Late phase metallic melt relocation for SBLOCA scenario: (a) UO_2 mass redistribution, (b) Zr mass redistribution, (c) axial position of porous debris (crust) and equivalent pool size, and (d) net flow area in the core.

5.5 Debris and Molten Pool

The molten pool is held in place by a crust of solidified melt and residues of fuel rods and guide tubes. The stability of this crust is decisive for the further development of the accident. In the best case, i.e. when the heat removal from the crust exceeds the heat generation inside the pool, the crust thickness increases. At the present time, only speculations are possible about the mechanical stability of the crust because of its largely unknown composition and the way in which the crust is supported by some fuel rods remaining in place. Prior to direct contact the core internals are heated by thermal radiation to such a temperature level that the steel is molten and relocates downwards.

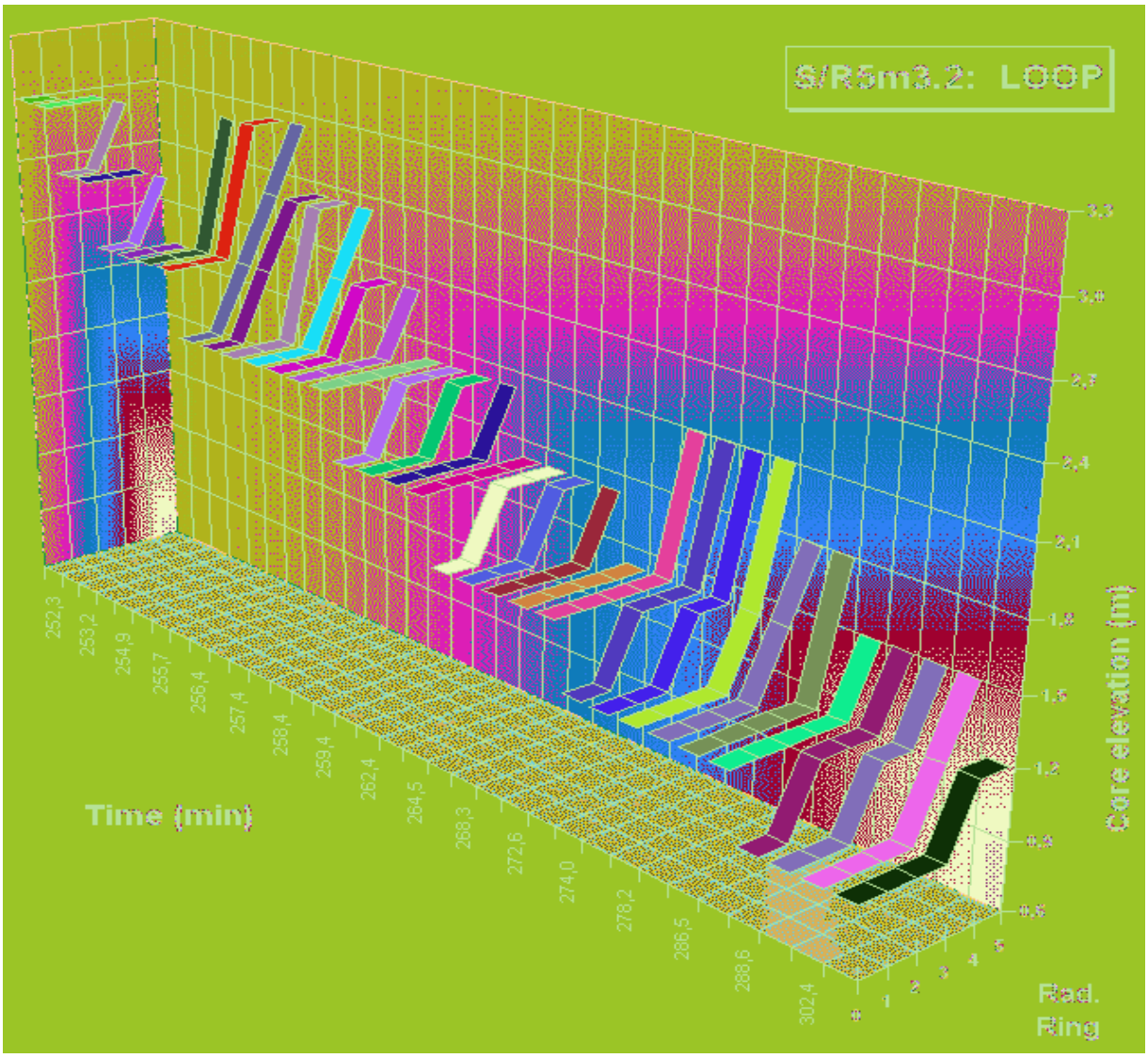

Figure 5.7 Axial and radial position of the lower crust of the in-core molten pool in the during LOOP base case for times at which relocation events were calculated in the time interval between 252 min and 304 min. The crust is situated on top of porous debris one zone below.

As indicated in Figure 5.8 the damaged fuel rods were molten above the molten pool and added to the molten pool inventory. Only the uppermost zone remains, based on the assumption that the claddings were backed together with structure material of the upper core plate, similar to findings of Phebus FPT0 test. However, taking into account results of Phebus FPT1 which are representa-

tive for medium burn-up conditions, this may be wrong for higher high burn-up situations because the pellets may mostly be disintegrated. S/R5 mod 3.2 only takes into account liquid relocation after the melting of the fuel rods; neither the influence of the burn-up on the pellet behaviour nor solid particle relocation is considered.

As a consequence the inventory of the uppermost zones has to be added to the molten pool inventory. The same holds for the intact fuel rod columns in the fifths ring shown in Figure 5.8. In other codes such as MELCOR the whole fuel stack above a molten zone collapses. However, this is the other extreme, adding too much mass to the molten pool by one event. In reality the fuel stacks will be destabilised and relocate more smoothly if support is ceasing.

5.6 Final state

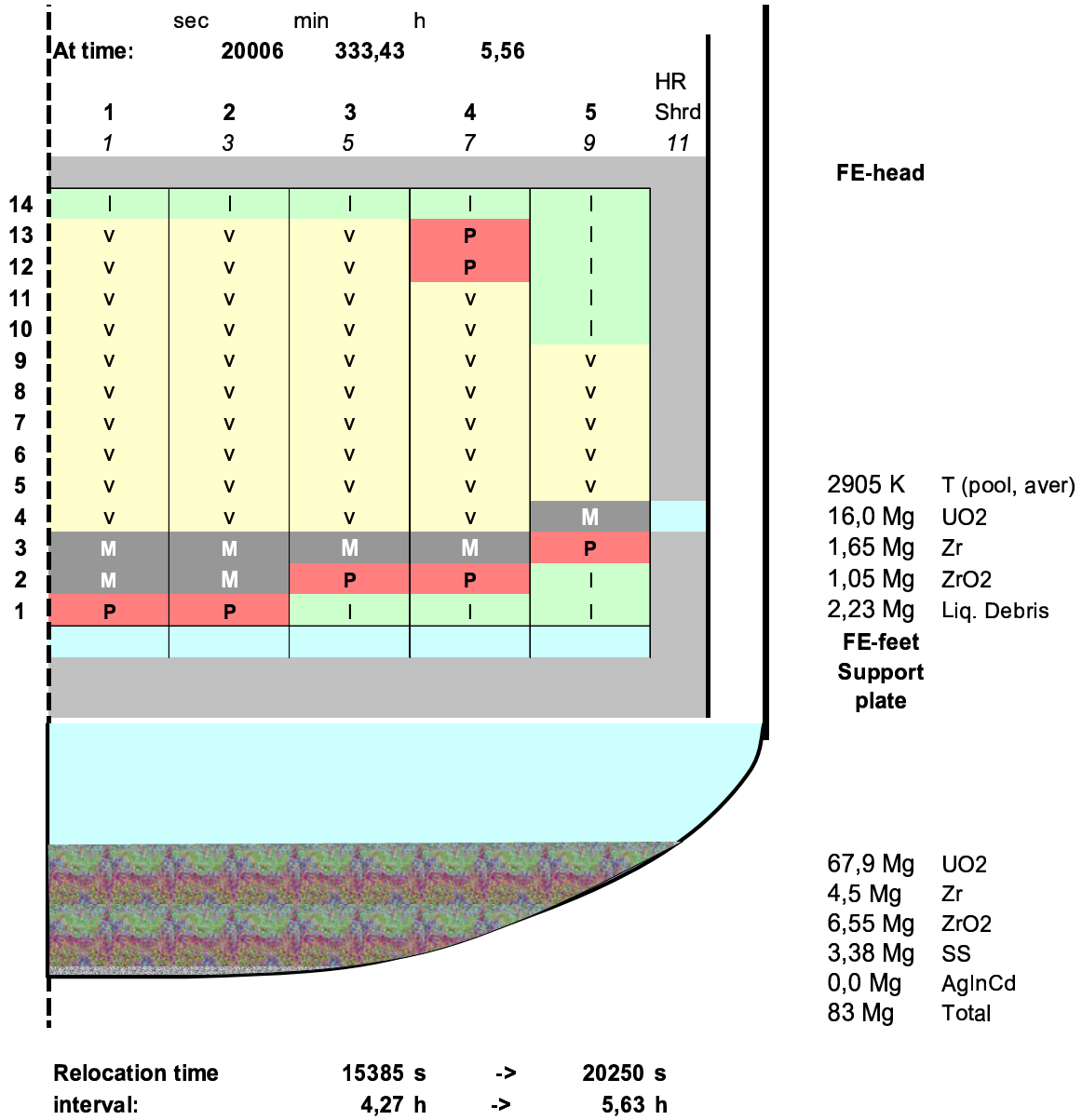

Figure 5.8 Final state of LOOP base calculation including melt slumping into lower plenum assuming failure of core enclosure. No interaction with the water is considered.

As can be depicted from Figure 5.7 the molten pool contacts the HR at app. 1.2 m elevation. In this calculation no interaction between core enclosure (HR) and molten pool was activated. Also no lower plenum model (Couple) was used. Therefore S/R5 only balances the material released through breaches assuming instantaneous failure of the enclosure.

Especially for failure analyses for the LCSP, the distribution of molten material in the core and lower plenum indicates, that no further cooling from the bottom could be assumed. This leads to boundary conditions for LOWCOR2 calculations assuming hot surfaces on both sides. In this stage of the accident, however, the risk of a fuel coolant interaction is rather low due to lacking water evaporated by melt dripping through the downcomer app. 0.3 h earlier.

Due to mass storage fault, the output file is not readable after 20006 s so that last relocation and slumping data are lost.

5.7 Discussion

In the loss-of-off-site power (LOOP) scenario no active system is assumed to be available, only valve actuation is possible e.g. for depressurisation. The scenario has two thermohydraulic phases, first the primary system stays at high pressure so that the decay heat is released by cycled depressurisation up to 142 min, and a low pressure phase up end of calculation, when molten pool crust contacts HR at 305 min. After SG dryout at 104 min no secondary side measure is feasible.

Hydrogen is generated from 228 min when PCT exceed 1000 K with a maximum in the early core degradation phase at app. 10 min later up to a total mass of app. 460 kg. The lower crust of the molten pool relocates within 85 min down to 0.6 m increasing size but from 317 min it looses mass to the lower plenum (drippling). Therefore mass balance is not assured, this scenario has to be rechecked with S/R mod 3.3.

For this scenario the time window for safe reflooding has to be assessed since the reflood capabilities have come from off-site. Core reflooding behaviour at different initiation times is investigated for this scenario in section 6.

6 LOOP REFLOOD SCENARIO

Formation of a molten pool in the core is calculated after app. 3.9 h (Figure 5.1 d) and a contact between crust of the molten pool and the heavy reflector at app. 4.5 h. For the reflood study, however, it is assumed that electrical power supply for ECC pumps can be re-established before the peak core temperature (PCT) exceeds 2800 K. Based on the LOOP scenario described in section 5 reflood calculation were performed assuming that either all four low head safety injection (LHSI) or all four medium low head safety injection (MHSI) systems can be activated (Figure 2.4).

Since the time of ECC system activation is rather arbitrary because nobody can predetermine the time of power-regain, the peak core temperature (PCT), was chosen to roughly define the core state. The study includes reflood calculations starting with a PCT of 1900 K, 2100 K, 2300K, 2500 K, and 2800 K. However, the PCT is a local value and dependent on simulation of decay heat and heat transfer mechanisms in the core, e.g. core wide radiation coupling.

6.1 Initial reflood conditions

The reflood calculations are based on the LOOP data up to the time of ECC initiation and water injection into the primary system. The reflood initiation temperatures mentioned above define a time window between 13905 s (T19) and 14280 s (T28).

This time window is shown in Figure 6.1 for the core temperatures and the oxide layer thickness. In Figure 6.2 the core condition prior to reflood is shown, extracted from the LOOP base case calculation (section 5). In Figure 6.1 b, d, f, h the minimum oxide layer thickness for the shattering model discussed in section 2.7.2.3 is given as dotted lines. An data extract of Figure 6.1 is listed in Table 6.1. In all cases below 2800 K only the fuel rod cladding in the centre ring comply with shattering criteria.

As indicated in Figure 6.2 c, d, e the core damage state is indicates in 5 different stages of rod damage: intact rod 0.0, rupture due to ballooning: 0.1, formation of local rubble debris or local fragmented pellet: 0.2, cohesive debris: 0.4, and molten pool: 1.0. No significant flow blockage e.g. by ballooning is calculated for the core as can be seen in Figure 6.2 f.

Two sets of calculations have been performed based on two different restart-plot files. Therefore, a slight discrepancy in the reflood initiation times was observed as indicated in Figure 6.3 and in Table 6.1. If heat-up rate is decreasing, e. E. after oxidation phase, this time difference can extend up to 70 s in case of T28. To overcome this difficulties relative time intervals are used, based on the reflood initiation time.

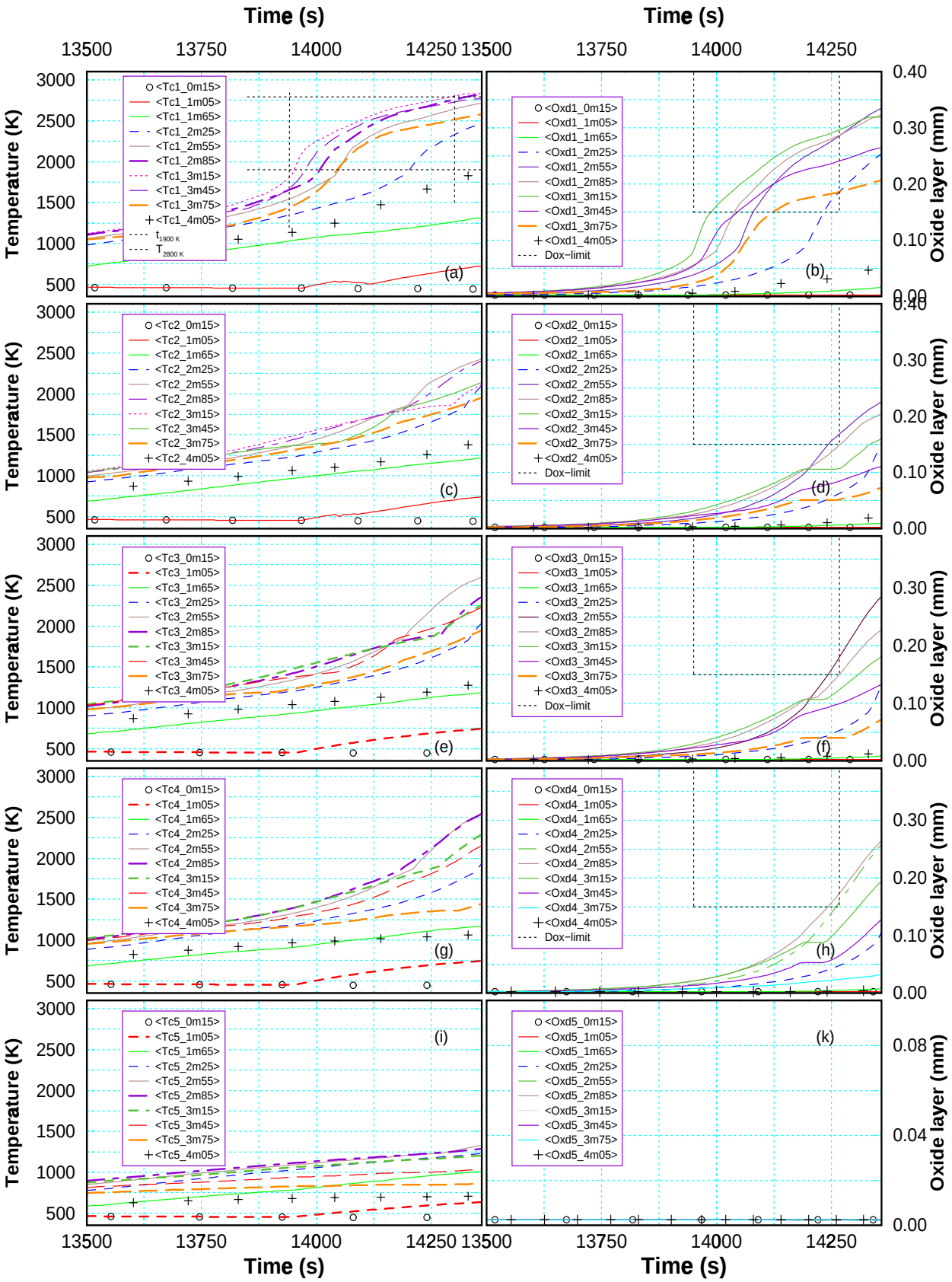

Figure 6.1 Temperatures and oxide layer thickness calculated for the base case (section 5) prior to reflood initiation. In (a) the region of the centre ring temperatures and times used for reflood initiation are outlined. For the oxide layer graphs the limits prerequisite for shattering activation are shown by straight dotted lines.

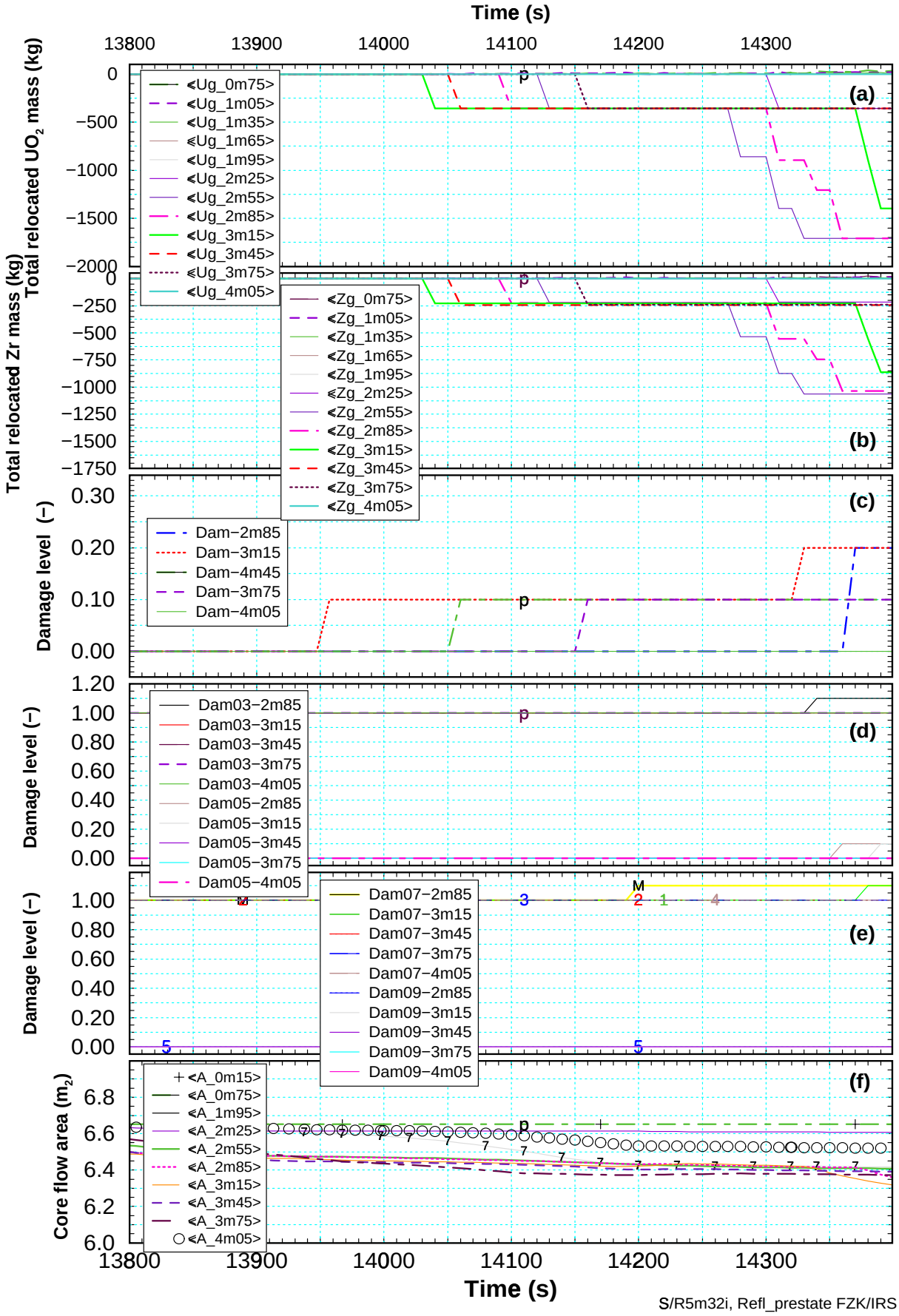

Figure 6.2 Overview of core damage state of the base case (section 5) prior to reflood initiation: (a) and (b) global relocated mass in the core, (c), (d), (e) fuel rod damage states, and (f) free fluid cross section.

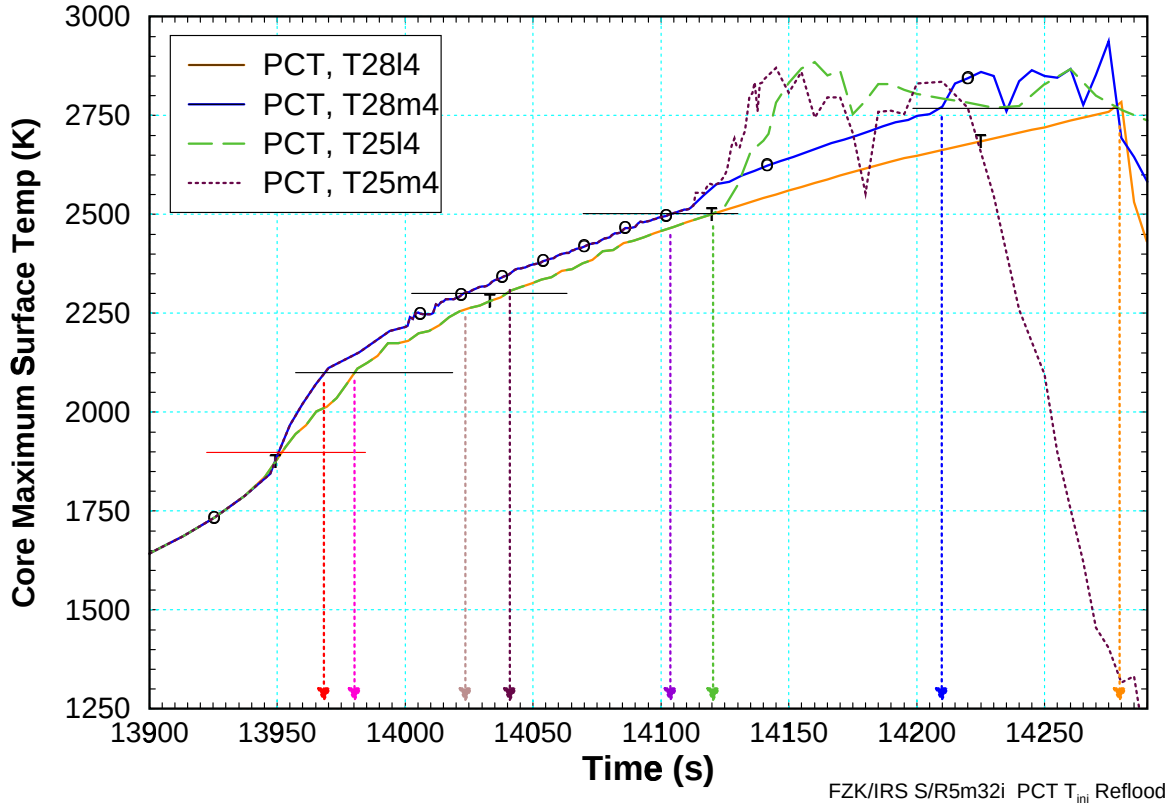

Figure 6.3 Reflood initiation temperatures and corresponding times for both types MHSI (upper curves) and LHSI (lower curves).

Table 6.1 Initial conditions for all reflood cases

	Case	Time		Pressure	Water level	Axial zones with oxide layer thickness δ_{ox}>150 µm at reflood initiation				
		sec	min	MPa	m	R1	R2	R3	R4	R5
1	T19l40/T19m4	13950	232	0.92	1.10	----	---	---	---	---
2	T21l4	13970	233	0.89	1.09	**11**	---	---	---	---
2	T21m4	13980	233	0.89	1.09	**11**	---	---	---	---
3	T23l4	14025	234	0.88	1.08	**11**	---	---	---	---
3	T23m4	14042	234	0.88	1.08	**11**	---	---	---	---
4	T25l4	14104	235	0.86	1.06	**9-12**	---	---	---	---
	T25m4	14122	236	0.86	1.06	**9-12**	---	---	---	---
5	T28l4	14267	237	0.86	1.05	**8-18**	**9-10**	**9-10**	**9-10**	---
5	T28m4	14200	239	0.86	1.05	**8-18**	**9-10**	**9-10**	**9-10**	---

6.2 Reflood scenarios

In the following both scenarios of each reflood initiation temperature will be discussed briefly using an overview graphics with four sections. In (a) the core heat balance is shown with the sources decay heat and oxidation power (left scale). The consequence, the peak core temperature (PCT) is shown using right scale. Below (b), the system pressure is given as well as core inlet and outlet vapour temperature (right scale). The lower two graphs show the behaviour of the activated ECC system, the mass flow rate (d) and the core and lower plenum water level. In section 7.2 the general results such as hydrogen production and damage state are discussed and compared.

General thermohydraulic behaviour

The differences in the common behaviour of either LHSI or MHSI activation are as follows:

As shown in Figure 2.4 the set pressure of the LHSI pumps is limited to 2.0 MPa. Therefore, pump ceasing is often observed due to the increasing primary system pressure. Depending on the core state, this can lead to a long period of ECC inactivity (section 6.2.3). But even in this case the cooling effect of the increased evaporation hinders further core damage.

The high set point of MHSI pumps is never exceeded in all calculations, the pumps are constantly activated. The spikes shown in several graphics are numerical artefacts caused be restart requests.

6.2.1 Analysis of case T19

As can be extracted from Table 6.1 no zone of the core has reached the criteria (oxide layer thickness > 150µm) required for the improved shattering model. Both T19 cases (T19l4 and T19m4) are very close to the design basis reflood conditions, so that only the case T19m4 will be discussed.

Globally the fuel rod temperatures in the core remain below any eutectic temperatures or melting points of fuel rod materials. Only one node exceeds melting temperature of the β-Zry (Figure 6.4 a) for a very short time period caused by single node shattering at 13983 s (Table 7.1). However, no further fuel rod damage is initiated, accident mitigation is achieved by activation of either all MHSI or all LHSI systems. At that time, the exothermal energy of Zry oxidation only exceeds slightly the decay heat for several seconds. The absorber rods of the inner ring fail in the 11^{th} zone, releasing all melt up to the 13^{th} zone (Table 7.2). Core outlet temperature calculated in the lowest volume of the upper plenum remains below 1250 K (Figure 6.4 b).

The primary system pressure shown in Figure 6.4 b increases up to 3.0 MPa and decreases within 12 min to base case pressure (Figure 5.2 a). Time interval required to refill the core completely is rather short (app. 2 min) and saturation temperature is reached for all fuel rods at 14100 s, app. 150 s after reflood initiation (Figure 6.4 c,d). The whole cool-down process is finished a 14080 s, only less than 3 min after reflood initiation as indicated in Table 7.1.

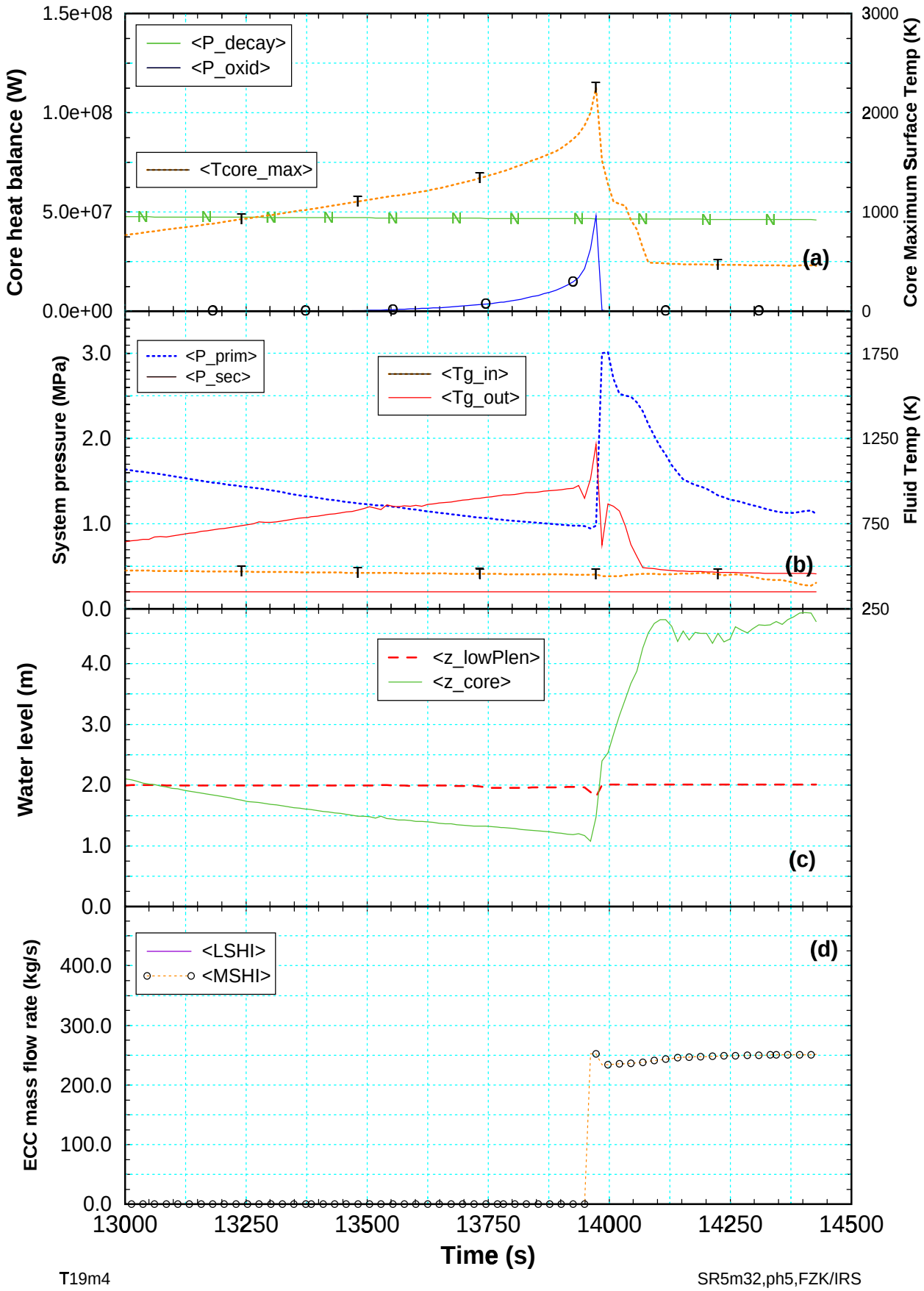

Figure 6.4 Overview of T19m4 case: (a) nuclear and chemical power (left scale) and PCT (right scale), (b) system pressure (left scale) core inlet and outlet fluid temperature, (c) collapsed water level of core and lower plenum, and (d) MHSI injection rate.

6.2.2 Analysis of case T21

At a first glance the system response of both T21 cases are comparable to those calculated for the T19m4 scenario, however, the higher temperatures in the core at reflood initiation time (13970 s /13980 s) drastically increase the time interval up to cool-down to saturation level.

LHSI: T21l4

Compared to the previous case T19m4 (Figure 6.4) no large difference are found with respect to PCT history and exothermal energy release shown in Figure 6.5 a. Only one difference is detectable, the increased duration of the temperature plateau between 1300 K and 1500 K, which lasts for 260 s. This is caused by a ceasing ECC injection (Figure 6.5 d) due to an increase in the primary system pressure to app. 3.5 MPa (Figure 6.5 b). However, during this short ECC injection period of 25 s app. 7.5 m³ ECC water is injected leading to a water level of 2.4 m in the core. At 14168 s the primary system pressure drops below 2.0 MPa and during this second injection period app. 24 m³ water is added, rising the core water level to 4.1 m until a second pressure increase at 14306 s caused by a water plug in the PZR depressurisation valves stops the reflood process. At that time PCT drops below 1000 K and at 14375 s (app. 400 s after reflood initiation) saturation conditions are reached. The exothermic energy only exceeds slightly the decay heat level (spike at 14000s, Figure 6.5 a).

Shattering and core damage remains localised, the detailed data are summarised in Table 7.1 and Table 7.2. Hydrogen production rate and total hydrogen mass are comparable. The core is kept rather intact, only metallic melt originate from the absorber rod in the innermost ring is calculated.

MHSI: T21m4

In the second case all MHSI pumps are activated so that an injection rate of app. 250 kg/s is achieved (Figure 6.6 d). This only 40 % of the LHSI makeup rate (app. 400 kg/s Figure 6.5 d) so the flooding rate is somewhat less in the beginning, but remains rather constant up to complete core refill at app. 14150 s, app. 170 s after reflood initiation. No pump ceasing is calculated, the primary system pressure increase ends at 2.7 MPa.

At 14000 s similar water mass is injected into the core, however, the collapsed water level in the core just reaches app. 1.2 m, compared to app. 2.5 m in case T21l4 (Figure 6.5 c). Consequently the steam production rate is lower. This allows the upper section of the core to continue to oxidise driving the PCT far beyond 2800 K reaching 2865 K at 14051 s (Table 7.1). During this peak the oxidation energy is as twice as high as the decay heat. After 14050 s cool-down due to ongoing water injection starts. During cool-down, shattering is calculated for three zones in the inner ring which increase the exothermal energy between 14080 s and 14110 s (Table 7.2). However, this process remains localised in the inner ring, so that in total only 3 kg hydrogen is added to the total hydrogen mass. At 14028 s, prior to shattering activation first fuel rod clad failure is calculated for the inner ring in the 11^{th} and 12^{th} zone at 14104 s, respectively. The core damage is terminated by the ongoing cool-down process. When the calculation was stopped at 14142 s, the PCT is below 1000 K so that no further damage is to be expected. At that time the collapsed water level in the core is at 4.4 m.

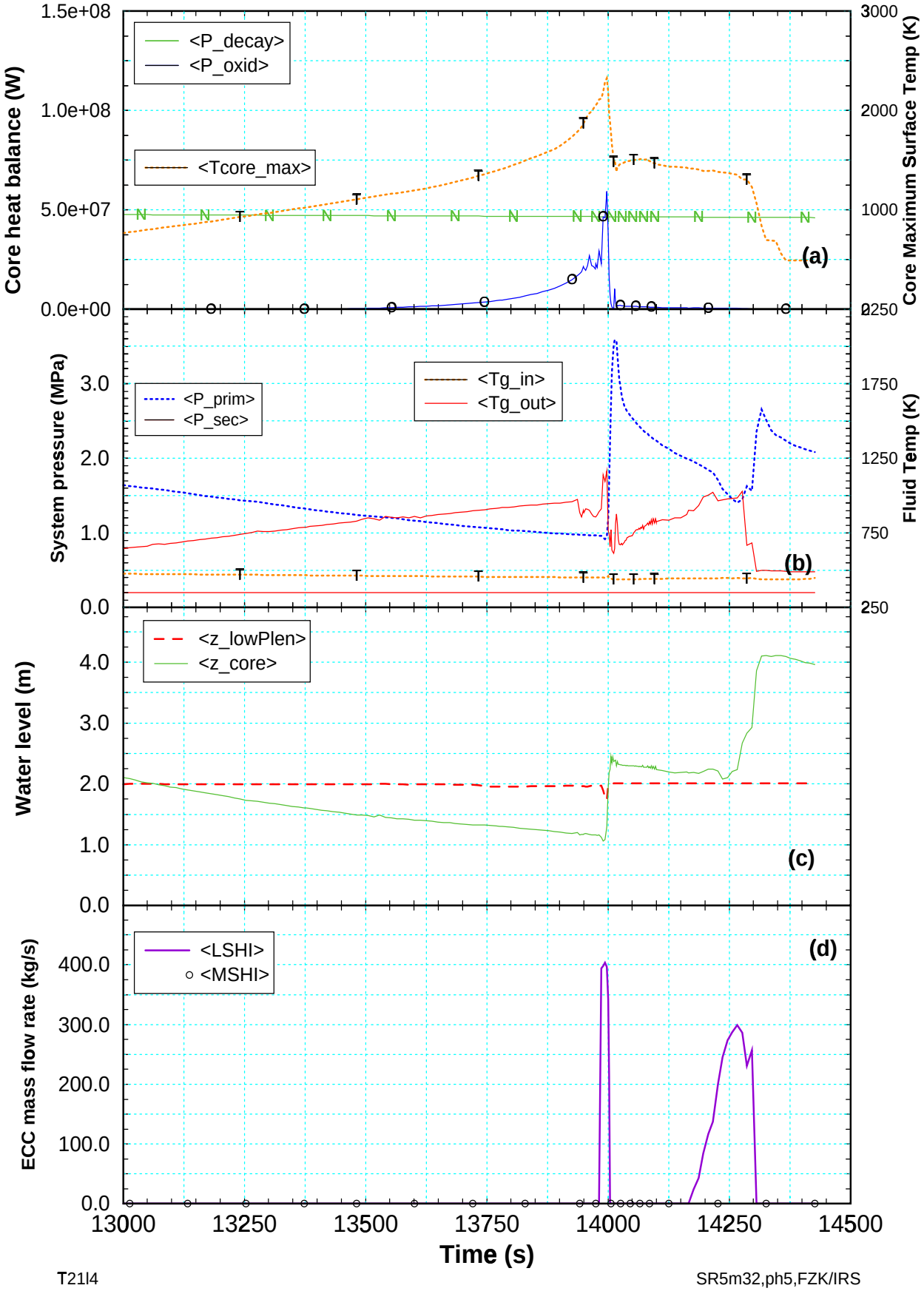

Figure 6.5 Overview of T21l4 case: (a) nuclear and chemical power (left scale) and PCT (right scale), (b) system pressure (left scale) core inlet and outlet fluid temperature, (c) collapsed water level of core and lower plenum, and (d) LHSI injection rate

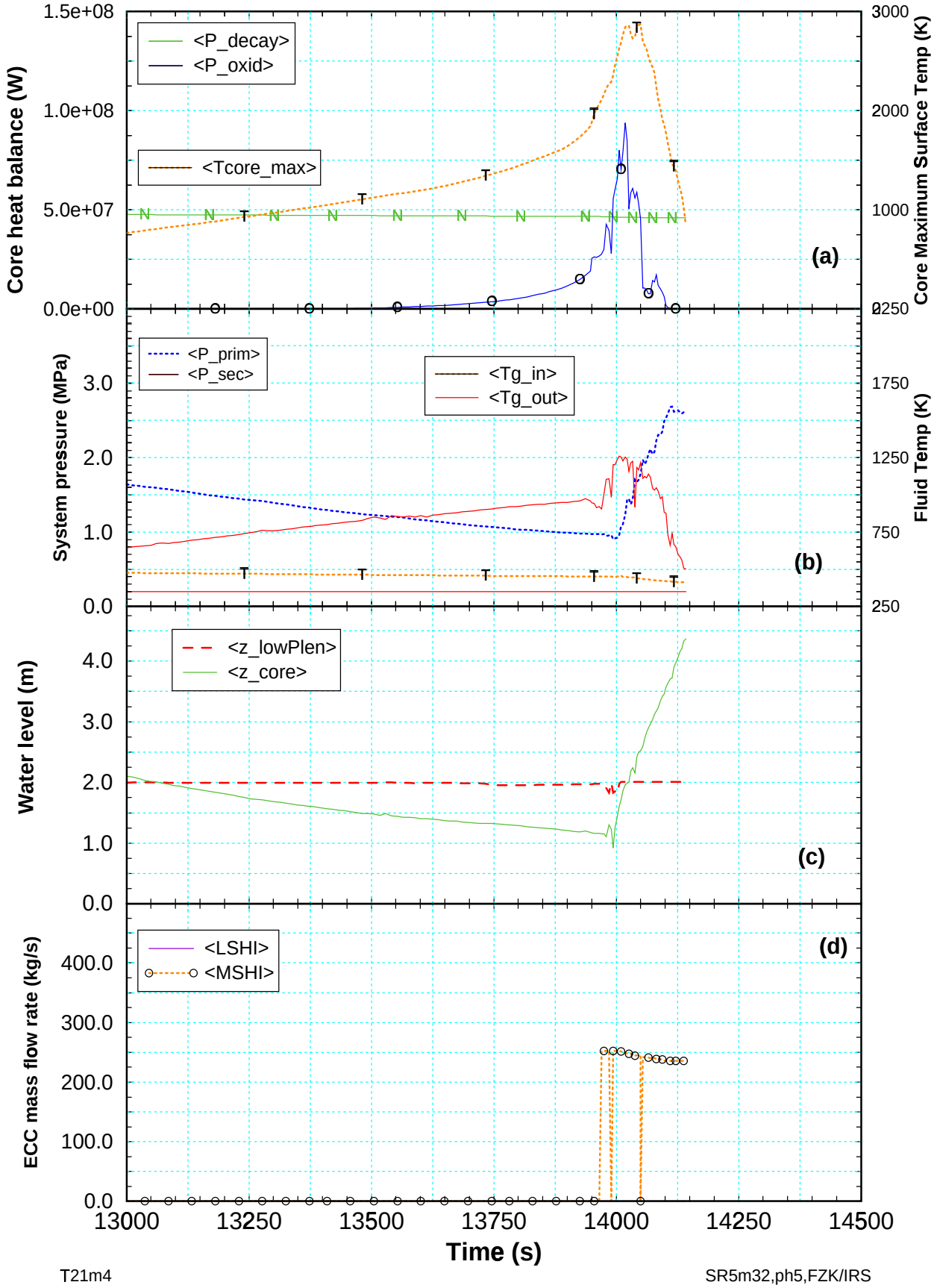

Figure 6.6 Overview of T21m4 case: (a) nuclear and chemical power (left scale) and PCT (right scale), (b) system pressure (left scale) core inlet and outlet fluid temperature, (c) collapsed water level of core and lower plenum, and (d) MHSI injection rate

6.2.3 Analysis of case T23

A fist glance on the results of the T23 case shown in Figure 6.7 a revealed two temperatures spikes separated by a long lasting temperature plateau. This non-prototypic case, called T23ml4, was not foreseen and was caused by an error in the restart input deck. The other case T23m4 was calculated as foreseen.

LHSI+MHSI: T23ml4

Normally the each pump group (LHSI and MHSI) is locked against the other. In this case, however, both pump groups, the LHSI as well as the MHSI feed in at 14025 s with their native pump characteristics, however with the set point limitation of the LHSI system. Furthermore, the LHSI pumps should continue to feed in when the pressure decrease below set point. In this case, however, the control logic for the pump refused restart (at 14250 s), so that only 7.2 m^3 ECC water is injected into the core (3.2 m^3 from the MHSI and 5.0 m^3 from the LHSI) as can be seen in Figure 6.7 d.

As a consequence, the core water level is only increased up to 2.5 m (Figure 6.7 c) as in case T21m4. The water injected within 15 s drives the primary system pressure up to 3.9 MPa (Figure 6.7 b) but stopped further core degradation reducing the PCT from 2300 K down to 1500 K as can be seen in Figure 6.7 a. Up to this time app. 36 kg hydrogen was released, the core remained intact except for the absorber rod failure in the innermost ring (Table 7.2) as calculated for previous cases. For the next 800 s the PCT remains at around 1500 K.

At 15000 s heat-up starts again and it was decided to continue this case with a second reflood initiated also at a PCT of 2300 K. This time, the pump set point were corrected. The reflood initiation conditions were reached at 15260 s and at 15300 s primary system pressure exceeds 2.0 MPa so that the LHSI ceases and only the MHSI continues to support the core with ECC water. This time the core has a more uniform radial temperature profile so that shattering conditions were reached in four rings (Table 7.1). Within 20 s starting from the 2nd ring nearly all fuel rod claddings in the upper quarter of the core reach conditions for shattering.

Fast core reflood driven by both ECC systems keeps the time window for further core damage rather short, so that after 15300 s the PCT decreases below 1500 K stopping all material interactions. At 15400 s the LHSI system ceases but the core is refilled completely. But in this short time interval of this second reflood period the core is massively damaged and blockages are formed in 2.25 m elevation (Figure 6.8 b). The absorber rods of all four inner rings were damaged in the upper third of the core. Also the representative fuel rods in the inner ring and in the 4th ring were damaged in the 12th level and below.

From the total hydrogen mass of 81 kg (Figure 6.8 a) only 37 kg are produced up to 14100 s during first reflood period. Prior to second reflood app. 74 kg hydrogen is produced during 2nd heat-up. Hydrogen produced by simulated reflood effects (shattering model) is rather small, app. 10 kg.

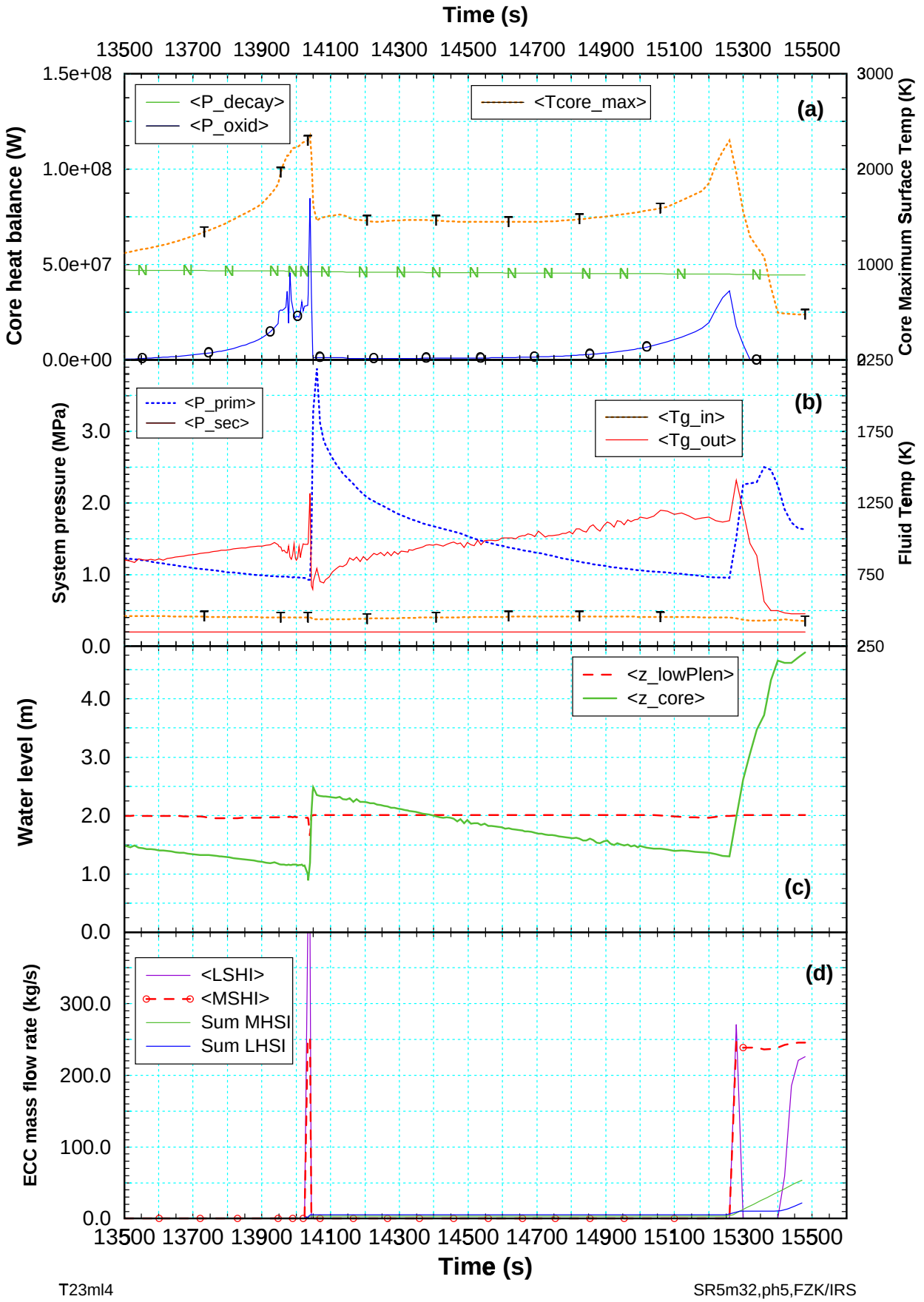

Figure 6.7 Overview of T23ml4 case: (a) nuclear and chemical power (left scale) and PCT (right scale), (b) system pressure (left scale) core inlet and outlet fluid temperature, (c) collapsed water level of core and lower plenum, and (d) LHSI injection rate

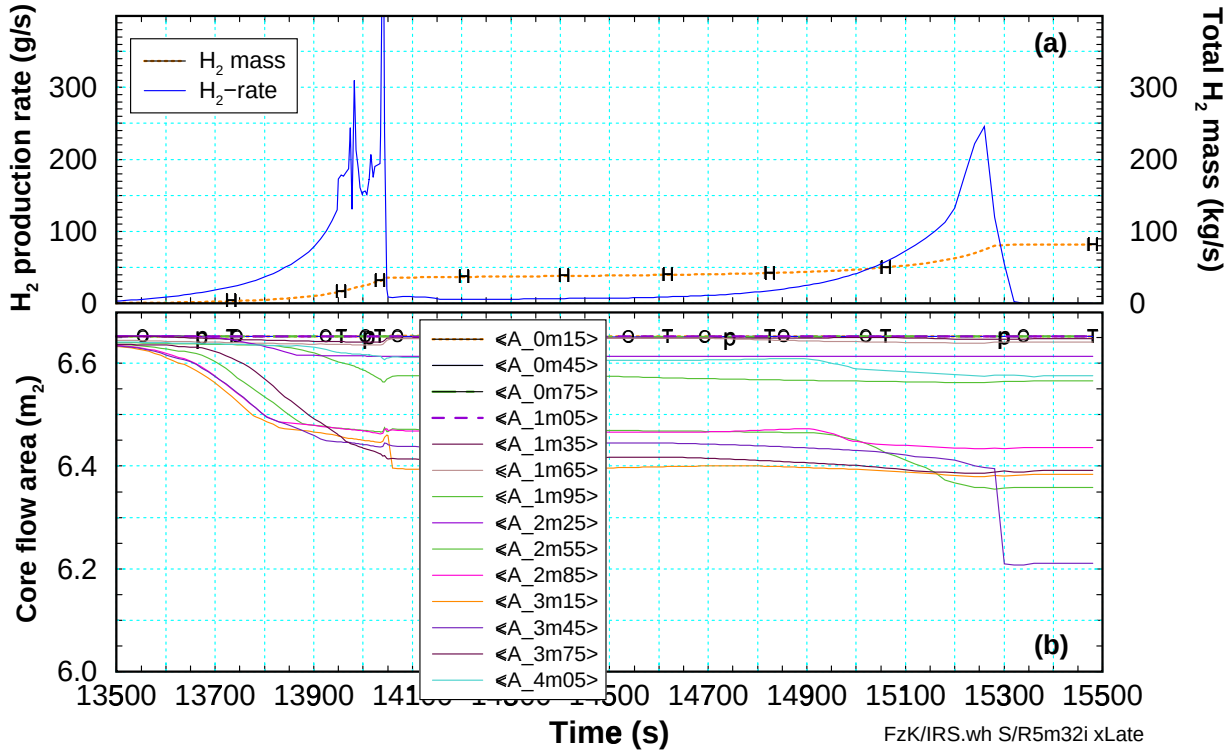

Figure 6.8 Hydrogen (a) and blockage history of T23ml4 case: (a) Hydrogen production rate (left scale) and total hydrogen mass (right scale) and (b) flow cross section area in the core.

MHSI: T23m4

In the second case, T23m4, the activation of all MHSI pumps at 14025 s worked correctly as foreseen (Figure 6.9). As mentioned above (Table 6.1), at reflood initiation the conditions for shattering exist only in one node (3.15 m, axial zone 11).

At 13980 s all MHSI pumps start to inject (Figure 6.9 d) increasing the collapsed water level in the core with app. 0.02 m/s until complete core refill at 14225 s (Figure 6.9 c), so that the time interval is only 245 s. The spikes shown in the LHSI curve in Figure 6.9 d are due to restarts of S/R5. In this case primary pressure increase is limited to 2.8 MPa reached when the collapsed water level reached the upper end of the active core.

The PCT as well as the energy release shown in Figure 6.9 a, show a fast increase as steam is produced by water evaporation in the lower third of the core, similar to conditions calculated for the T21m4 case (section 6.2.2).

In total app. 65 kg hydrogen are produced, composed of 22 kg before reflood initiation, app. 40 kg during steam cooling, and app. 3.5 kg due to shattering (Table 7.2). The latter contribution is the relative small peak in the falling edge starting at 14150s. Main reason of this relative small energy release is the fast cool-down due to forced MHSI injection (Figure 6.9 d). removing efficiently the excess exothermal energy by cold steam. Core damage remained limited to the inner ring and the upper third of the core. Localised porous debris, caused be metallic melt relocation, was formed prior to shattering activity.

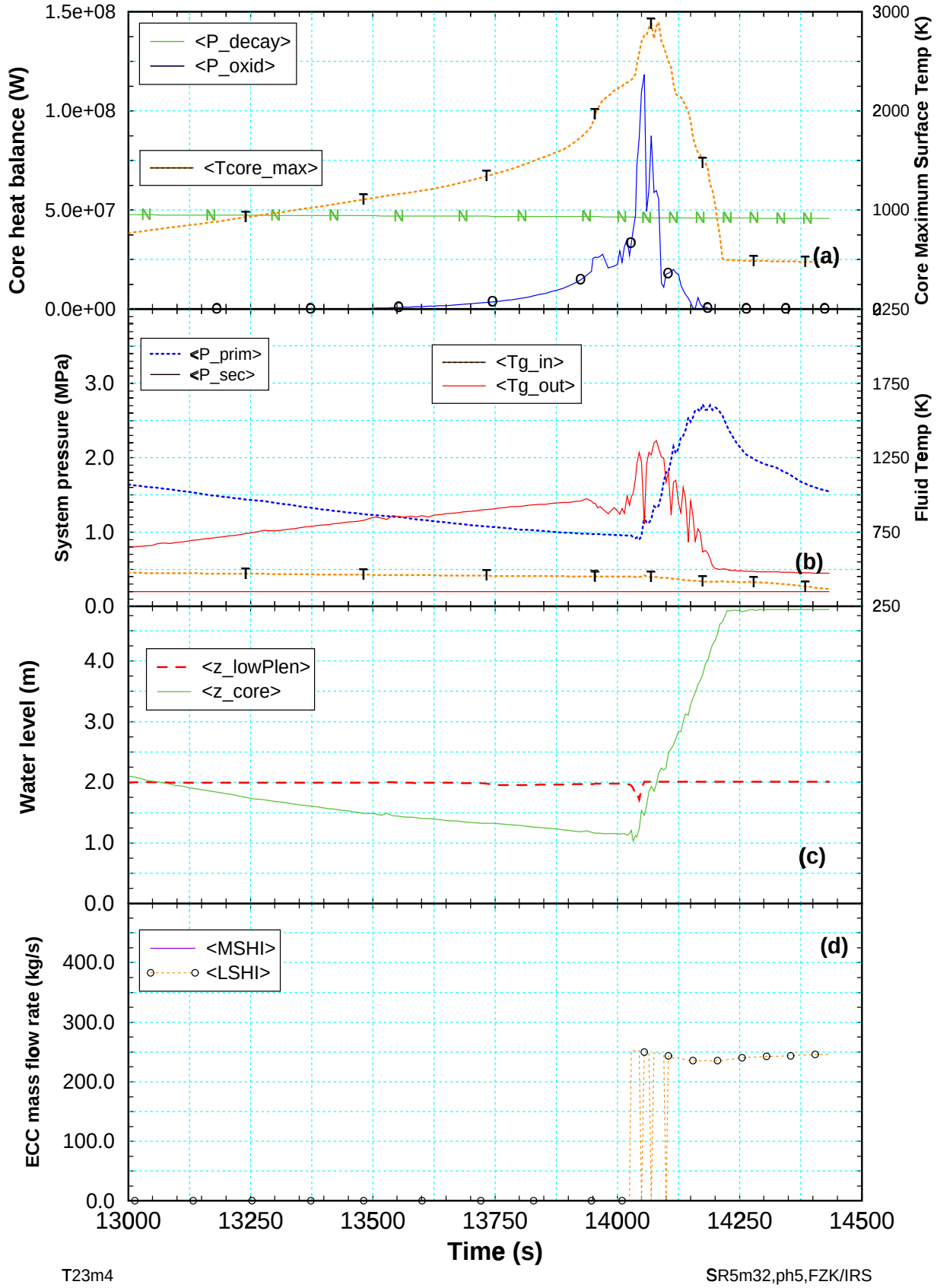

Figure 6.9 Overview of T23m4 case: (a) nuclear and chemical power (left scale) and PCT (right scale), (b) system pressure (left scale) core inlet and outlet fluid temperature, (c) collapsed water level of core and lower plenum, and (d) MHSI injection rate

6.2.4 Analysis of case T25

When the PCT reached 2500 K (Table 6.1), the conditions for shattering is extended to four axial nodes (Table 7.1), in an elevation between 2.55 m and 3.45 m. At that time the ECC systems were activated a system pressure of 0.86 MPa (Table 6.1). In previous cases only localised damage was calculated after reflood initiation, mainly due to clad failure and metallic melt release of less than 750 kg U-Zr-O melt in the whole core. In this and the following scenarios, however, damage and debris formation were calculated, so that a more detailed discussion is required. From the comparison of PCT shown in Figure 6.3 the differences between unmitigated and T25 cases is obvious.

LHSI: T25l4

At reflood initiation (14104 s) the LHSI pumps start (Figure 6.10 d) but ceases at 14160s, only 56 s later due to system pressure increase. 30 s later LHSI injection is regained, but due to the high primary system pressure near 2.0 MPa (Figure 6.10 c) with rather low make-up rate of app. 100 kg/s.

During the first injection period app. 10 Mg water is injected into the core, so that the collapsed water level rises to app. 2.1 m and the evaporated water initiates at 14130 s a steep temperature increase (Figure 6.10 a, b). PCT rises to app. 2900 K and remains there for 300 s. A typical reflood behaviour as calculated for earlier reflood scenarios (Figure 6.7 or even Figure 6.5) is not found. Here a rather smooth temperature decrease with a cool-down rate of < 3 K/s after 14350 s was calculated. Nearly all fuel rod temperatures above 3.0 m shown in Figure 6.11 left side show this smooth cool-down behaviour.

In the outermost ring (Figure 6.11 i), radiative heat transfer to the inner side of the HR prevents temperature increase above 1200 K and hence hinders fuel rod oxidation (Figure 6.11 k). Up to app. 3.0 m core elevation cool-down to temperatures < 1000 K can be found, only the upper third of the core, and here preferentially the 2-4 suffer due to additional heat-up (Figure 6.11 e, g).

The steep temperature rise triggers oxidation (Figure 6.10 a) and rod failure (Table 7.2) leading to local debris formation. Between 14127 s and 14140 s the absorber rods of ring two and three fail. In the same time interval massive melt relocation occurred as can be seen in Figure 6.12 a, b.

During 2nd injection period 5 Mg water rises the core water level to app. 2.5 m and the increased steam production triggers another oxidation escalation (Figure 6.10 a). Water injection and oxidation is correlated up to 14400 s. Afterwards, fuel rod oxidation in the inner three rings (Figure 6.11 b, d, f) is stopped due to lacking metal, while oxidation continues in ring four increasing fuel rod temperatures (Figure 6.11 g).

At 14249s first shattering event is calculated in the inner ring at 2.55 m and at 14300 s metallic melt relocation is finished. Relocation of debris is still ongoing leading to massive blockages at app. 14430 s in 3.15 m core elevation in ring 2 (app. 20 %) and ring 3 (app. 36 %) as indicated in Figure 6.12 d. In this calculation the pool formation conditions (T> 2873 K) were not met (Figure 6.12 c), however, the uncertainty in this field is rather large due to different possible initiation conditions.

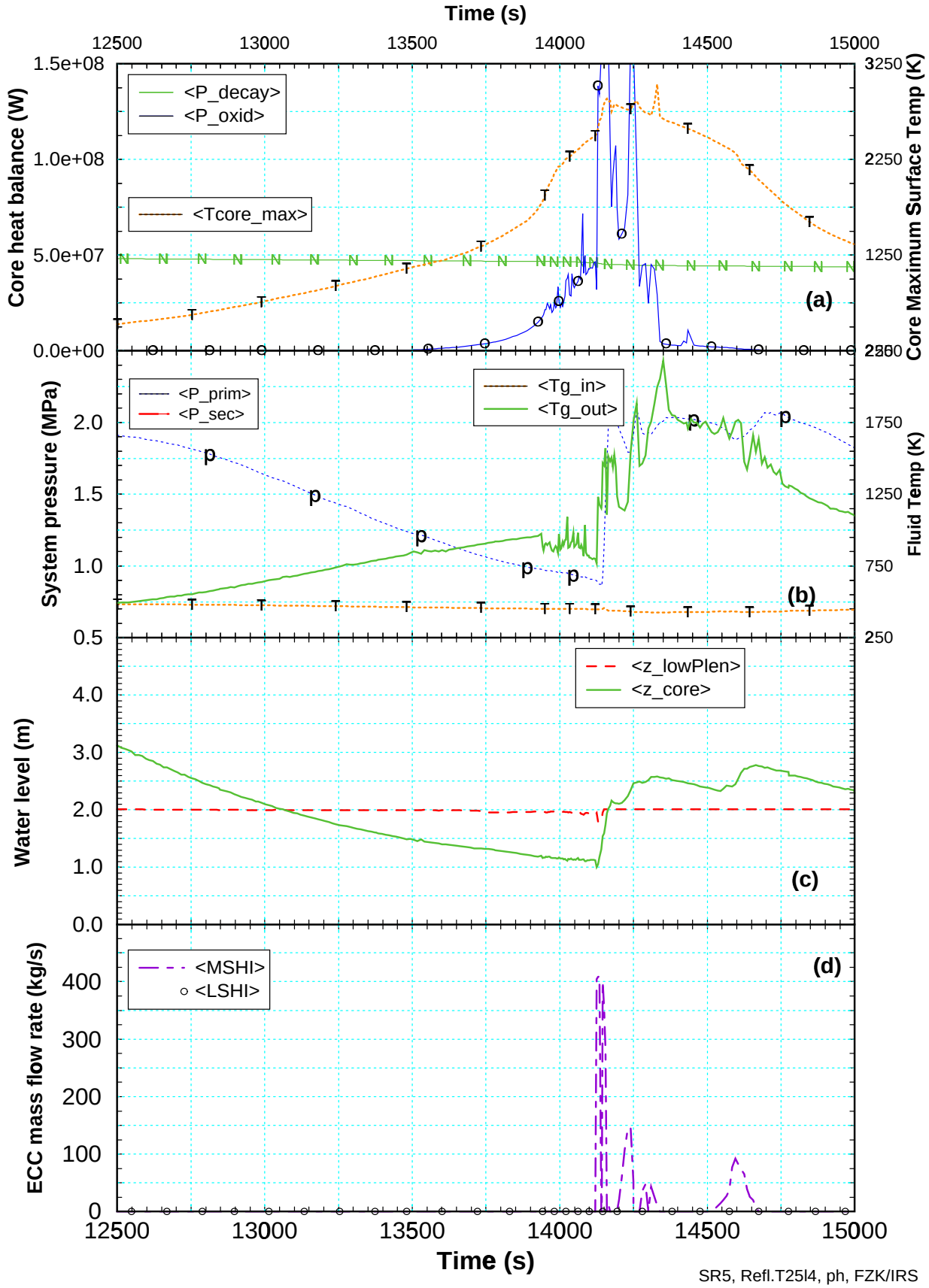

Figure 6.10 Overview of T25l4 case: (a) nuclear and chemical power (left scale) and PCT (right scale), (b) system pressure (left scale) core inlet and outlet fluid temperature, (c) collapsed water level of core and lower plenum, and (d) LHSI injection rate.

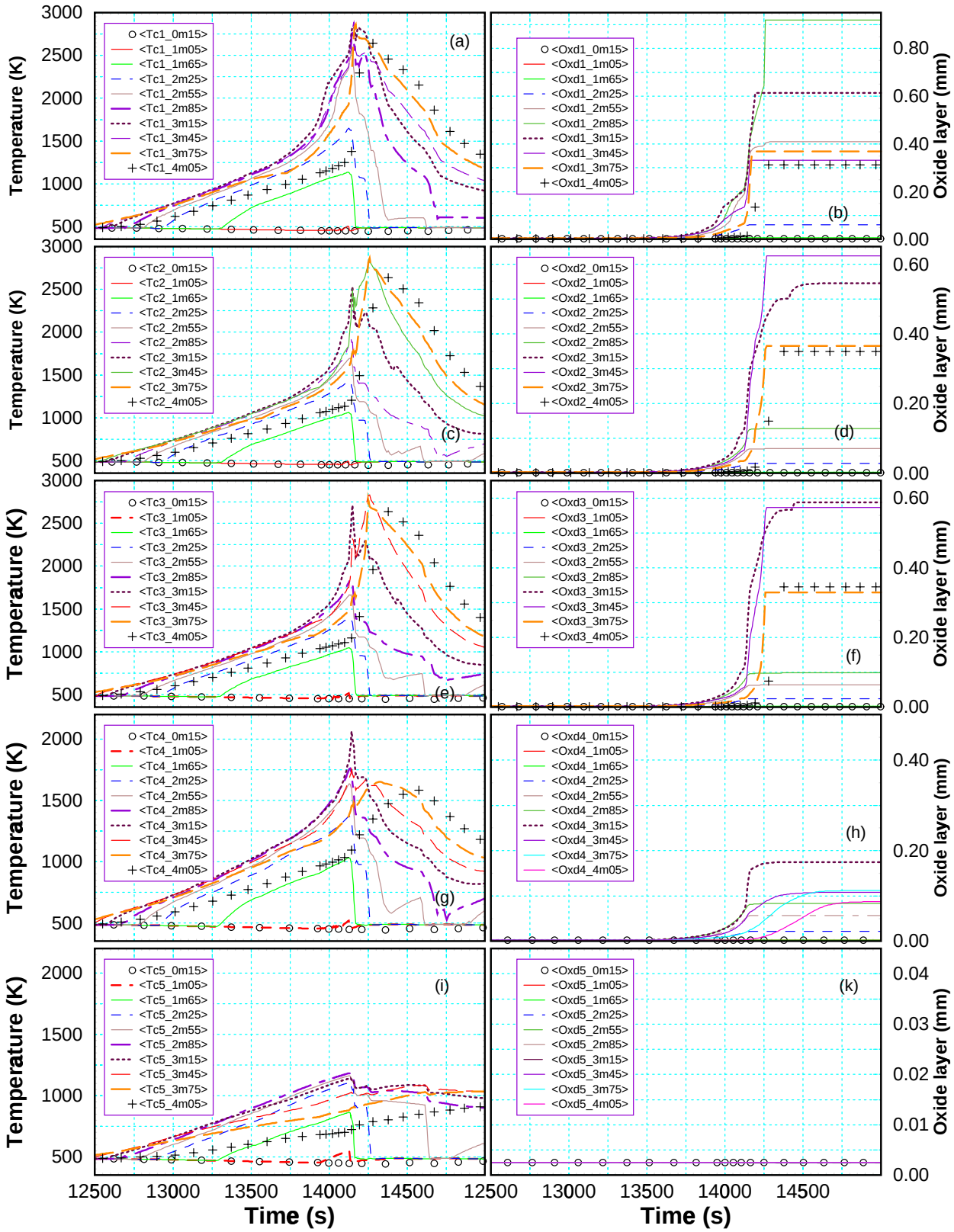

Figure 6.11 Temperature evolution for the reflood case T25l4 in the core (left) and corresponding cladding outer oxide layer thickness (right) for the five rings in the core (top to bottom).

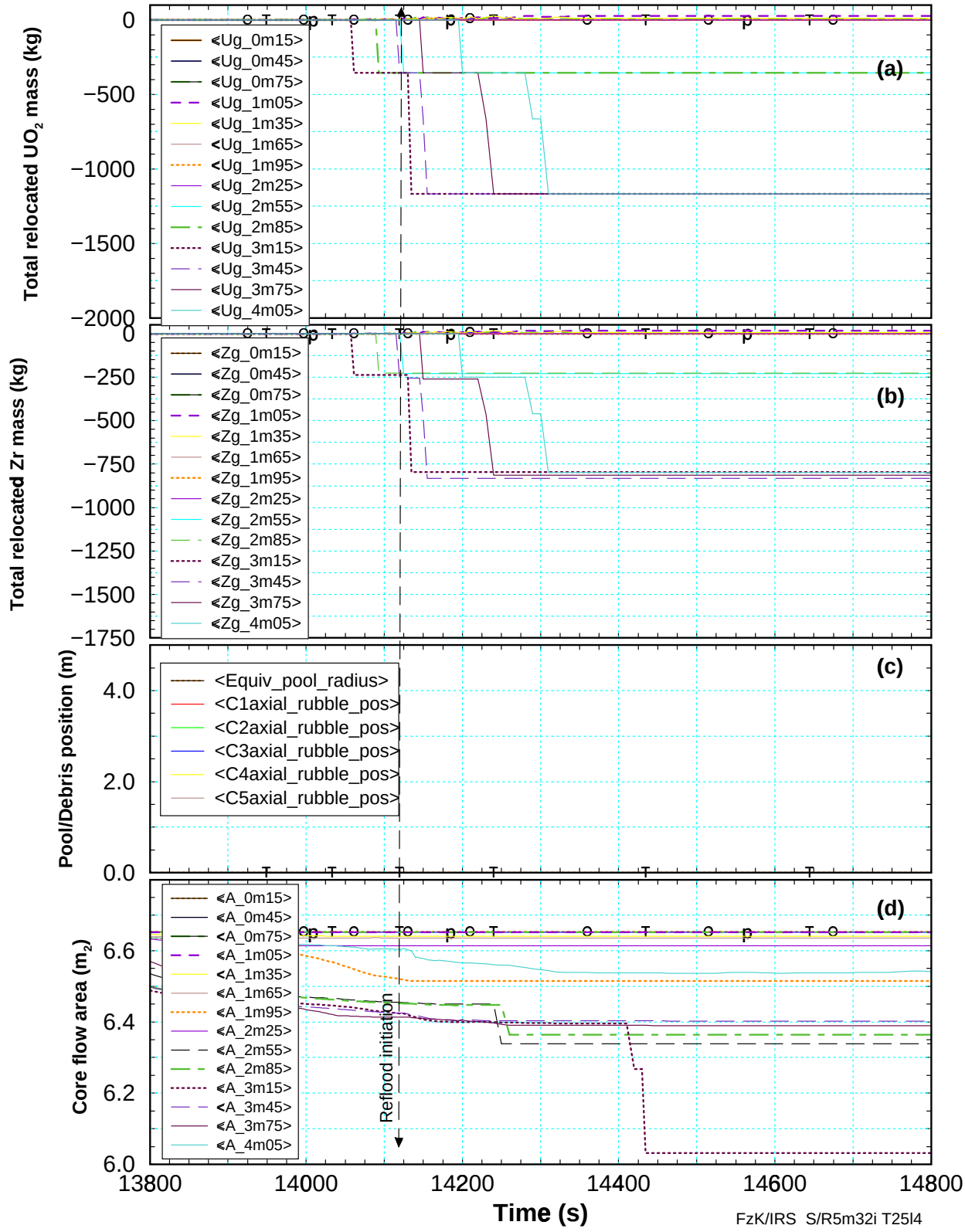

Figure 6.12 LOOP Reflood T25l4: Late phase metallic melt relocation: (a) UO_2 mass redistribution, (b) Zr mass redistribution, (c) axial position of porous debris (crust) and equivalent pool size, and (d) net flow area in the core.

Between 14610 s and 14740 s shattering is calculated for ring 1 and 2 extending from 2.85 m up to 4.05 m (Table 7.1), but no hydrogen production was calculated because of lacking metal due to previous melt relocation between 14160 s and 14260 s as indicated in Table 7.2. Such a situation was not considered in the "shattering" model which was based on QUENCH experiments, but has to be included to avoid misinterpretation.

The calculation was terminated when the PCT (Figure 6.10 a) drops below 1372 K and the system pressure decreases below 2.0 MPa at app. 15000 s. Indeed, due to a restart problem, the reactivation of the LHSI system was locked after 14850 s, but at that time it was obvious that no further oxidation has to be expected due to core state and temperature level, so no recalculation of this restart was performed.

For case T25l4 a debris reflood model should have been used to continue calculation because at 14500 s the LHSI starts again to fill the core. However, such a model is not available and not under discussion.

MHSI: T25m4

In this case all MHSI pumps are activated so that the whole core is flooded completely within 118 s (app. 0.02 m/s), cooling down efficiently the whole core to saturation level almost three minutes after MHSI pump activation (Figure 6.13 d). From Figure 6.13 a, an effective PCT cool-down rate can be determined to 10 – 20 K/s. Such a behaviour also can be seen in the individual cladding temperatures of all axial zones and radial rings shown in Figure 6.14 a, c, e, and i.

At 14188 s the core collapsed water level has just reached 2.5 m, first shattering event is calculated for inner ring in 2.55 m core elevation (Table 7.1) leading to a hydrogen spike in the falling edge of the oxidation power (Figure 6.13 a) and releasing U-Zr-O melt (Figure 6.15 a, b). Between 14213 s and 14266 s the inner two rings experience shattering in the upper third of the core, however, without significant hydrogen release due to efficient cooling by the two-phase flow with subsequent quenching as indicated in Table 7.1.

The clad oxidation and metallic melt relocation (Figure 6.15 a, b) is stopped after 14200 s while some debris relocations continued up to 14261 s as indicated in Table 7.2 and Figure 6.15 d. The latter relocations (in ring 2) are due to a rudimentary debris fragmentation model, included in the S/R5 mod3.2 set of late phase models. However, this model has not been validated sufficiently so that a reliable discussion of these results is not reasonable.

At app. 14300 s the PCT dropped to saturation level, that means within 3 min after pump start. Primary system pressure decreases below 2.0 MPa at app. 14700 s. The calculation was terminated when the upper plenum has been filled and the PZR water level extends to app. 12.0 m.

The most significant difference between T25m4 and the previous case T25l4 is that the continuous flooding process even with a reduced make-up rate of the MHSI is more efficient that the high make-up rate of the LHSI, which ceases after app. 1 min, leaving the core under boil-down conditions. The total hydrogen amount (Table 7.2) indicates a higher value for the T25m4 because of the shattering (Figure 6.14 b) and less metallic melt relocations (compare Figure 6.12 with Figure 6.14).

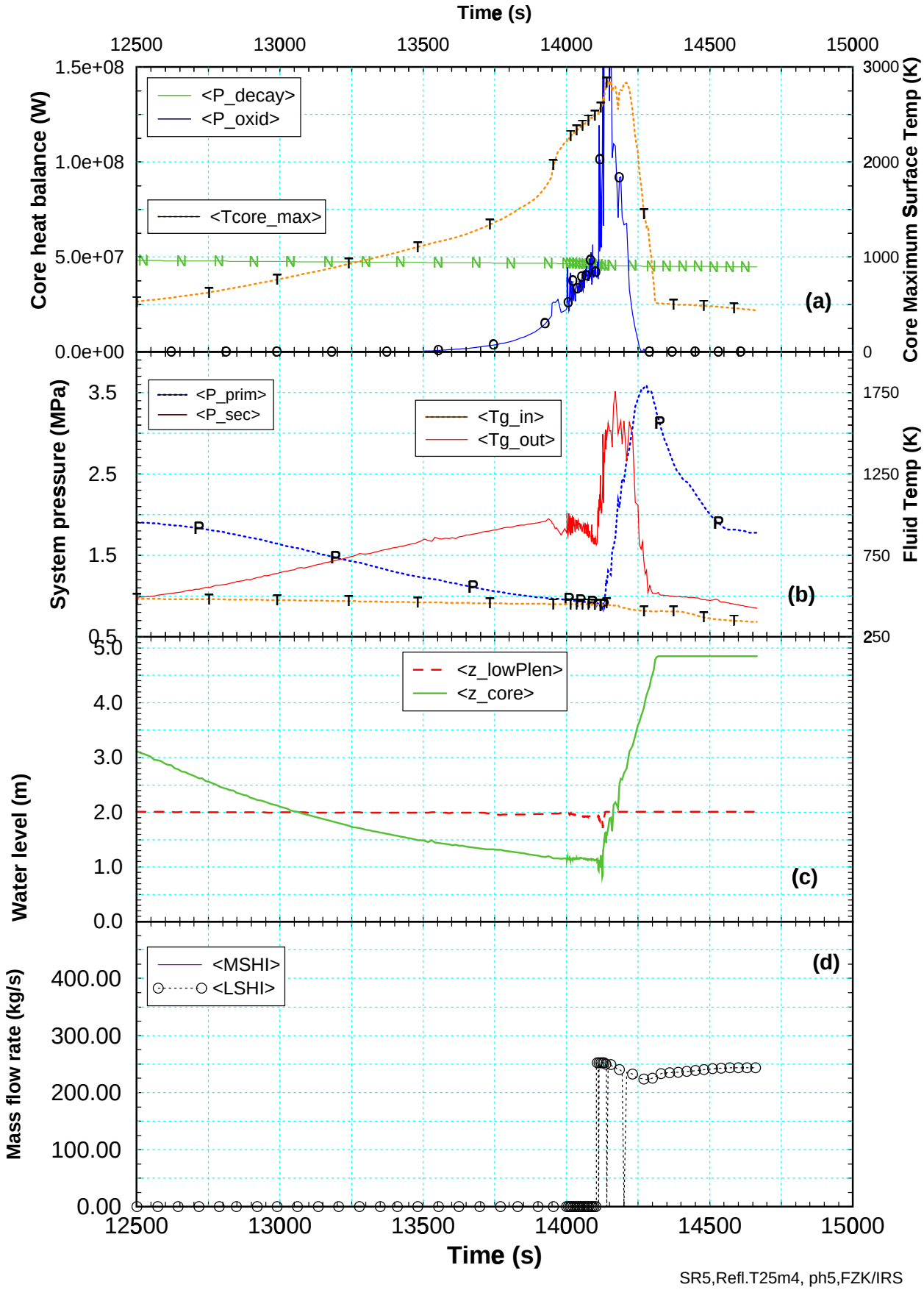

Figure 6.13 Overview of T25m4 case: (a) nuclear and chemical power (left scale) and PCT (right scale), (b) system pressure (left scale) core inlet and outlet fluid temperature, (c) collapsed water level of core and lower plenum, and (d) MHSI injection rate.

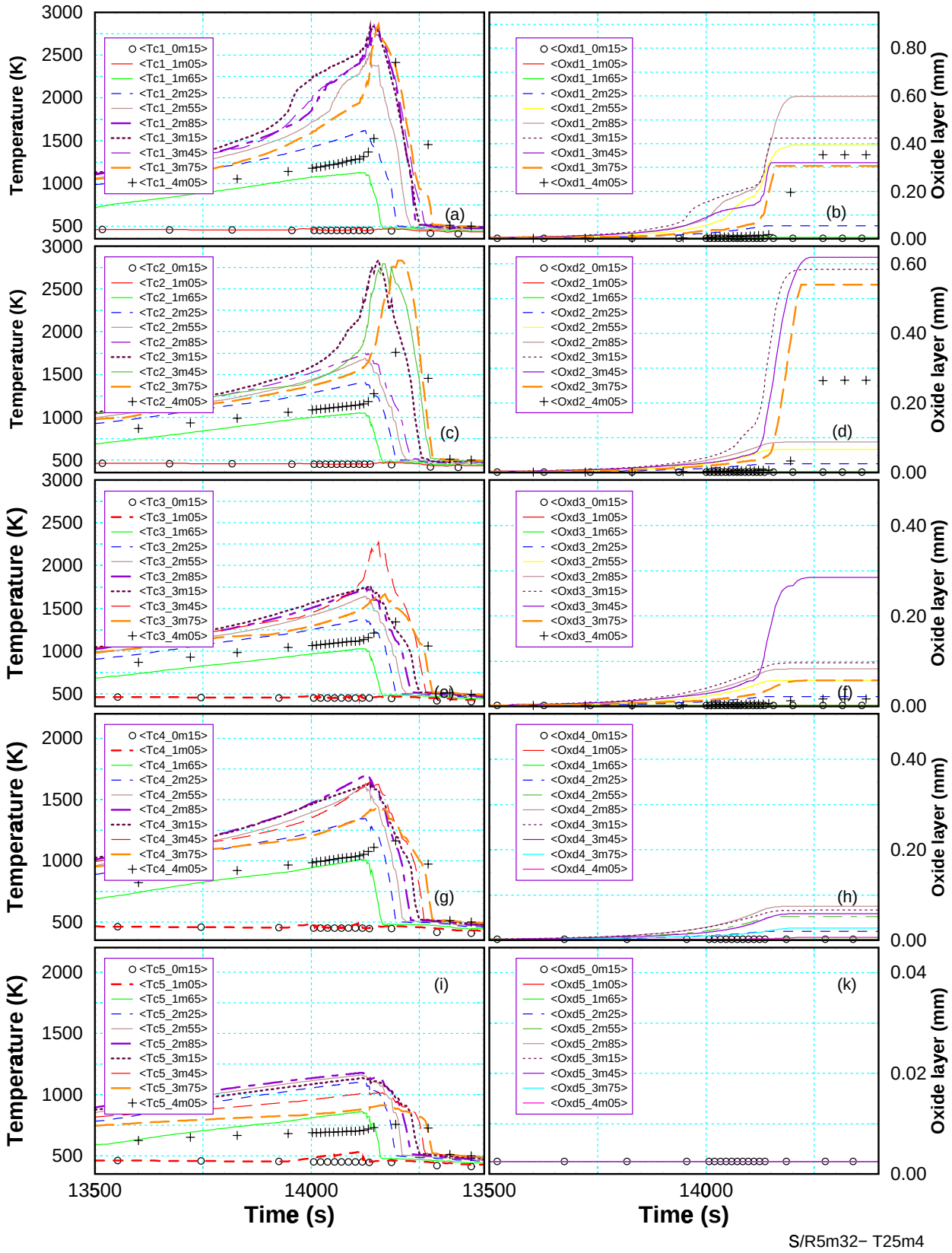

Figure 6.14 Temperature evolution for the reflood case T25m4 in the core (left) and corresponding cladding outer oxide layer thickness (right) for the five rings in the core (top to bottom).

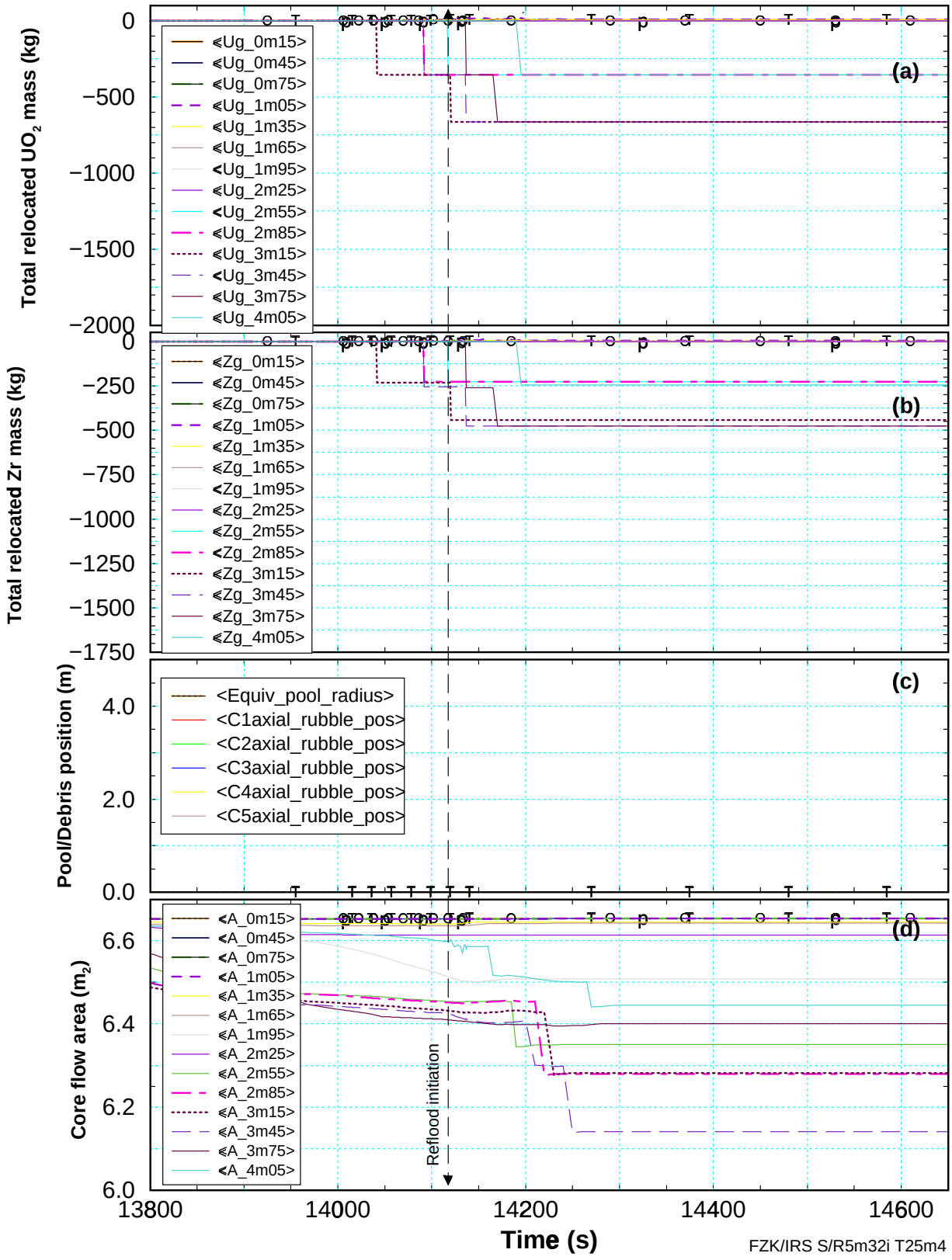

Figure 6.15 LOOP Reflood T25m4: Late phase metallic melt relocation: (a) UO_2 mass redistribution, (b) Zr mass redistribution, (c) axial position of porous debris (crust) and equivalent pool size, and (d) net flow area in the core.

6.2.5 Analysis of case T28

As mentioned in the pervious section, the influence of cladding failure, formation of blockages, or porous debris can not be considered with S/R5mod 3.2.irs. Also the last reflood scenario T28 had to be initiated when the PCT exceeds app. 2760 K due to unstable conditions at higher temperatures. Moreover, due to high non-linearity in the simulation of the phenomena such as melt release and blockage formation, the reflood initiation time differs between 14267 s for T28l4 and 14200 s for T28m4. Due to these restrictions the following cases will only discussed briefly. For a profound analysis, thermohydraulics as well as material behaviour models have to be improved to suffice best estimate criteria.

MHSI: T28l4

At 14267 s (Table 6.1) the ECC pumps were activated to inject water at a system pressure of 0.86 MPa. After a short period of ECC injection the increasing system pressure stops the pumps, so that only 4 Mg water were added to the core water inventory.

At 14280 s the calculation crashed due to water property errors. Neither time step reduction, which normally helps to overcome such difficulties, nor an earlier restart time were successful. Obviously the increased damage may enhance code instability if two phase flow conditions have to be calculated with high differential velocities.

MHSI: T28m4

Additionally to problems mentioned above the reflood initiation logic was faulty as can be seen in Figure 6.17 d. The first activation is originated to the 2500 K case, however, its contribution to the T28m4 case seems to be negligible because neither damage progression nor hydrogen production is affected. Only 1.7 Mg ECC water is added to the core increasing collapsed water level by app. 0.10 m (Figure 6.17 c). From the PCT curve in Figure 6.17 a only a small delay is detectable.

The ECC pumps start at 14200 s injecting for app. 100 s filling the core to app. 2.8 m but increasing the primary system pressure to app. 4.0 MPa. As mentioned above, restart input deck errors delay ECC injection for app. 80 s.

At 14381 s the ECC system is activated again for 60 s filling the core up to 3.6 m. After this injection period evaporation rate is sufficient to cool down the core below 1200 K.

Such a type of intermittent ECC injection if rather pessimistic and somewhat unrealistic. But is indicates, that maximum damage and hydrogen is produced by adding sufficient water at high core temperatures and allowing the core to react for a certain time.

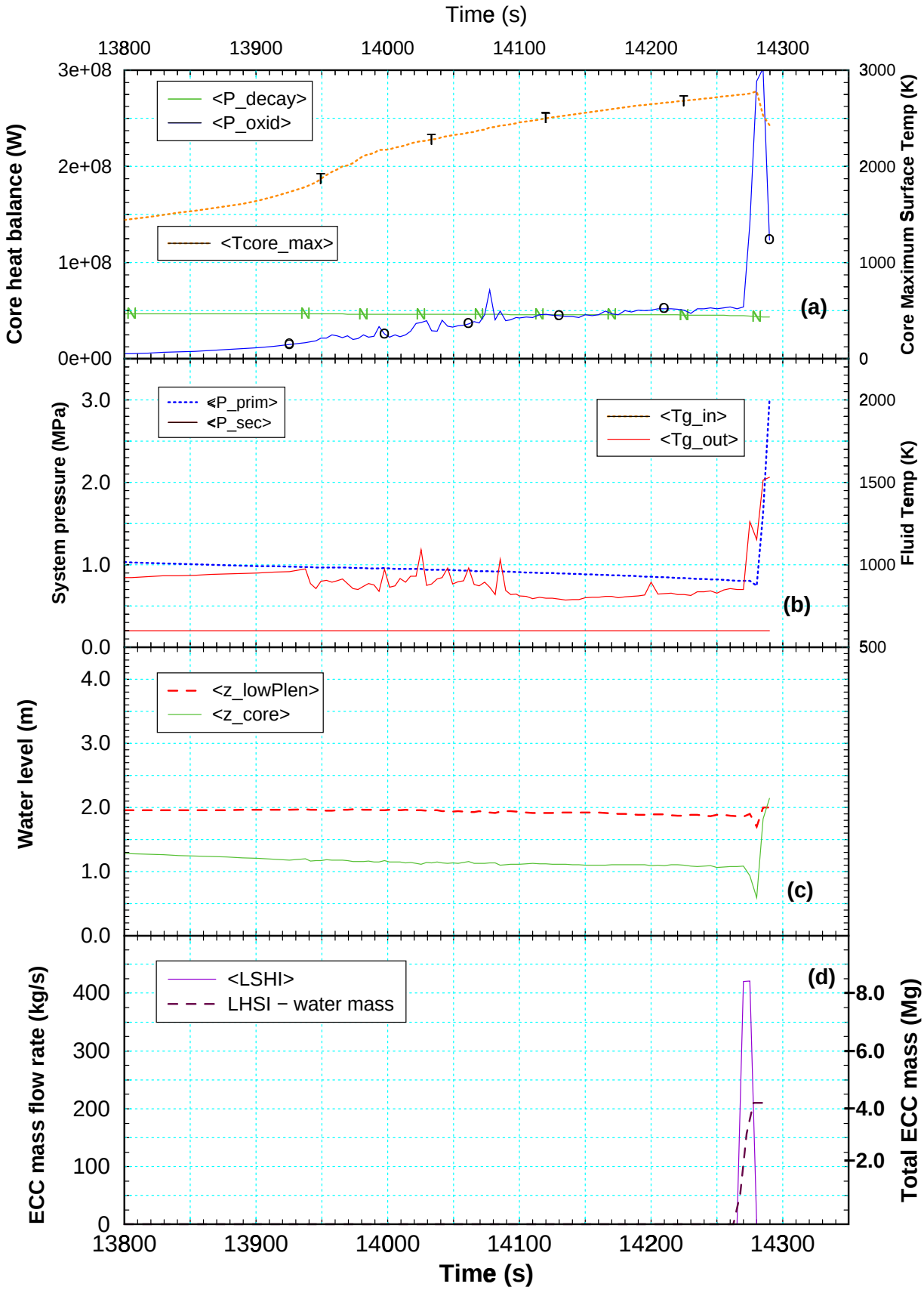

Figure 6.16 Overview of T28l4 case: (a) nuclear and chemical power (left scale) and PCT (right scale), (b) system pressure (left scale) core inlet and outlet fluid temperature, (c) collapsed water level of core and lower plenum, and (d) LHSI injection rate and total water mass.

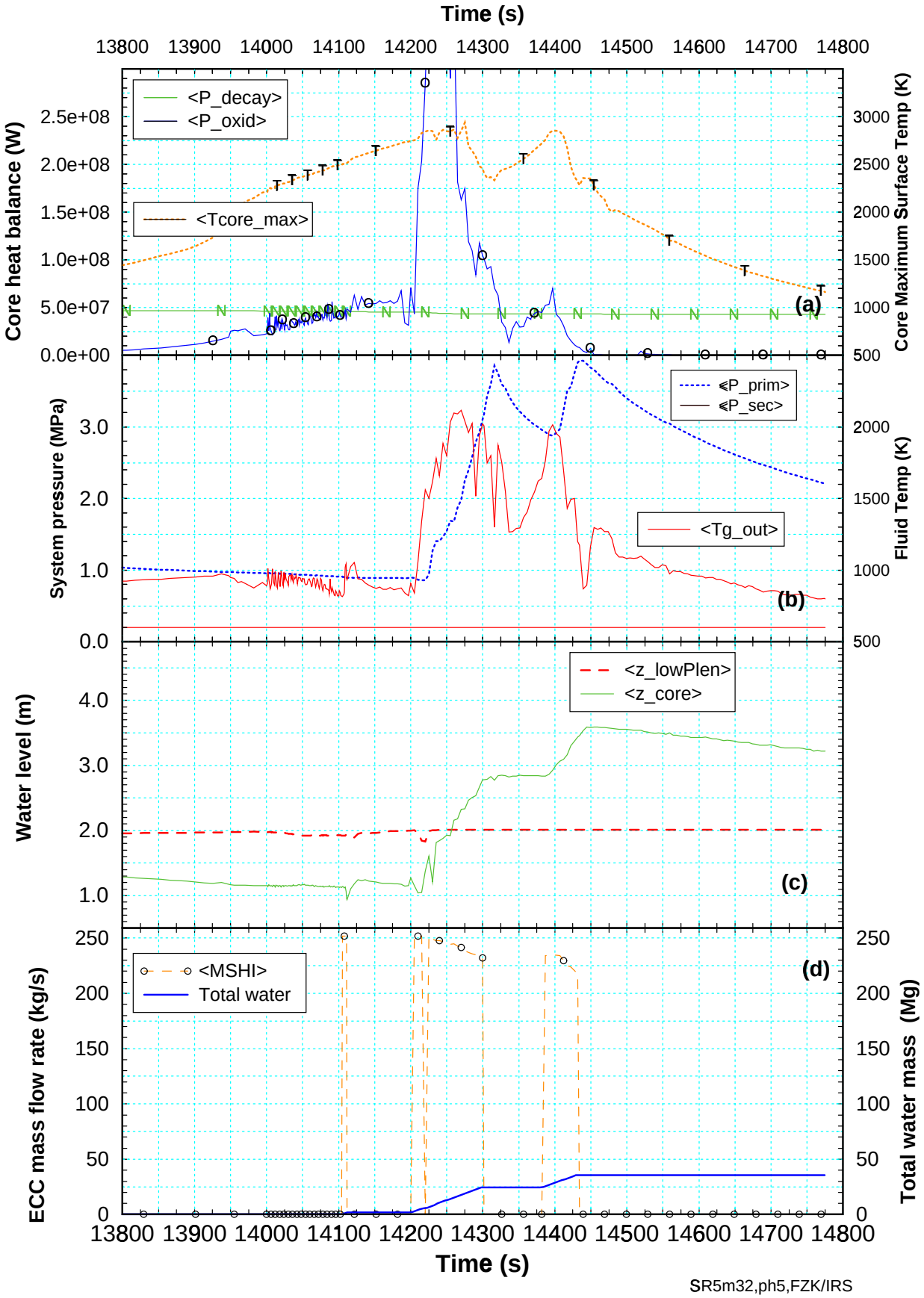

Figure 6.17 Overview of T28m4 case: (a) nuclear and chemical power (left scale) and PCT (right scale), (b) system pressure (left scale) core inlet and outlet fluid temperature, (c) collapsed water level of core and lower plenum, and (d) MHSI injection rate

7 DISCUSSION OF RESULTS

In this section the main integral results will be discussed and compared for unmitigated accident scenarios (surge line (SL) rupture, loss-of-offsite power (LOOP), an small break loss of coolant accident (SBLOCA)) leading to severe core damage (section 7.1) and reflood scenarios for the LOOP scenario (section 7.2).

7.1 Accident scenarios

In this study several unmitigated accident scenarios have been investigated with the best estimate code system S/R5 mod 3.2. Main objectives was to compute in-vessel damage propagation in axial and lateral direction, hydrogen production and release into the containment. As can be seen in Figure 7.1 the total hydrogen mass differs between individual calculations in magnitude and time. From different calculations for one scenario a rough estimation of scatter of the results (uncertainty) can be obtained.

The SL-rupture scenario, a typical large break loss of coolant accident (LBLOCA) is characterised by low system pressure. Such low pressure reduces time step and core stability, especially under low mass flow rates and high temperature conditions. So the total hydrogen mass is strongly dependent on the evaporation rate. The hydrogen mass calculated by the four calculations performed with S/R5 varies between 80 kg (very low evaporation rate) and app. 220 kg until code fails (section 3).

The result of an ICARE2v2 calculation is added for comparison, however, the calculation used S/R5 results for the primary circuit to deliver at core inlet steam conditions (mass flow rate, temperature) and the primary system pressure at the upper plenum, since ICARE2v2 is restricted on the core itself.

The investigated LOOP scenario starts as a high pressure sequence until primary system depressurisation is initiated. The total hydrogen calculated for the three cases varies between 439 kg and 450 kg in a time window of app. 3000 s. Time variation at onset of oxidation (PCT=1000 K) of app. 4500 s, is mainly caused by an early onset of oxidation prior to primary system depressurisation as can be seen in Figure 5.1. The hydrogen masses calculated for the reflood cases (section 7.2) are within the variations of LOOP results.

Compared to other scenarios the SBLOCA scenario shows a large time interval of app. 12500 s. Since time interval at onset of oxidation is nearly the same (12400 s) the reasons are due to thermohydraulic conditions in the primary system. Up to onset of oxidation this scenario is characterised by a reflux – condensor mode in one loop of the hot-leg, so that the simulation of countercurrent flow strongly influence the time of core uncovery. Details are discussed in section 4.

In nearly all cases the calculation was terminated by one code error . When the molten pool contacts the HR melting is initiated with subsequent relocation of molten corium masses into the lower plenum. Therefore, data from the end-state of the calculations were used as input for spe-

cialised codes such as MC3D (FCI, /27/) or LOWCOR2 (HR failure/28/). That code error should be removed in the next version S/R5 mod 3.3, which will be released end of 2000.

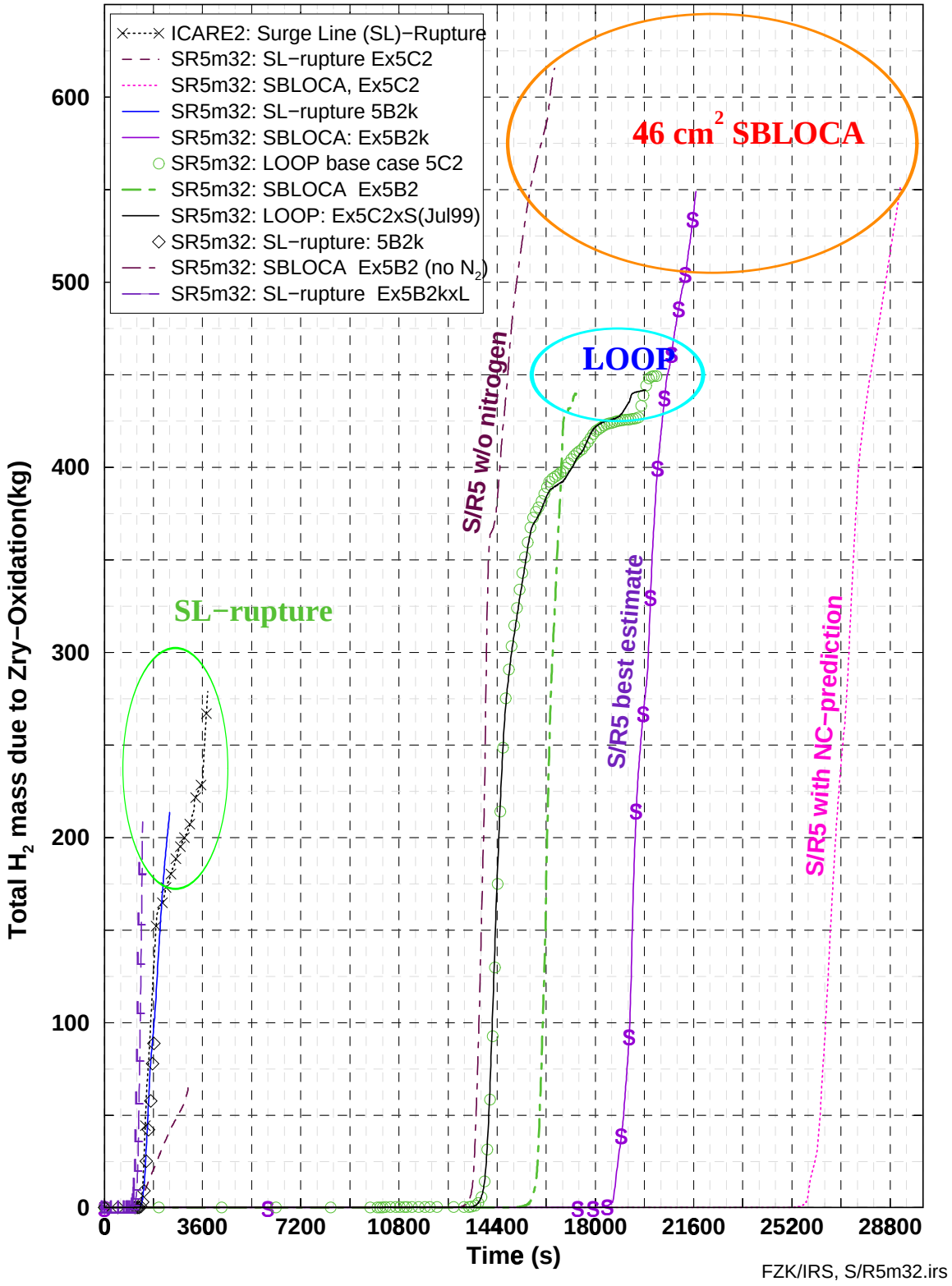

Figure 7.1 Total hydrogen mass calculated for the accident scenarios SL-rupture(left), LOOP (centre), and SBLOCA (right) calculated with S/R5 mod3.2 and ICARE2V2.

7.2 LOOP reflood scenarios

In Figure 7.2 the results of various LOOP reflood calculations with the best estimate code system S/R5 mod 3.2 are given for total hydrogen mass (top) and hydrogen source term (bottom). In the cases "MHSI" a complete activation of all medium head safety injection (MHSI) pumps was assumed and for cases "LHSI" all low head safety injection (LHSI) pumps, respectively. The local shattering model was used, however, improved as described in Section 2.7.2.3. All calculations were performed successfully, except for reflood cases T28l4 (T=2800K LHSI) and T28m4 (T=2800K, MHSI). In both scenarios numerical problems associated with very high surface temperatures and formation of local debris hinders a complete calculation ending with saturation temperatures.

1. As discussed in section **2.4.2** no ring to ring radiative heat transfer was considered. The consequence is that at the rather low system pressure of < 1.0 MPa the convective heat transfer is not able to transfer enough heat to adjacent rings. This results in a rather steep radial temperature profile especially after onset of oxidation. If in this time reflood is initiated (cases T19-T21) only the innermost rings show conditions supposed to be necessary for shattering during reflood. On the other side, in an earlier study /4/ ring to ring radiation was slightly overestimated so that four of the five rings achieved shattering conditions.
2. Due to computational restrictions (CPU time, data storage) the axial node length in the core has to be restricted to 0.3 m for this reactor simulation. This is somewhat larger than required for reflood analyses /24/. As a consequence, the conditions up- and downstream of the re-wetting zone (quench-front) may be averaged too much.
3. The model used to simulate the behaviour of the cladding under fast cool-down rates is still under development and the main effect has still not been isolated /24/. Also the behaviour of released metallic melt (in case T25l4) under highly oxidising conditions is still unknown.

Nevertheless, actually such investigations are the only feasible way to get rid of rather conservative extrapolation of experimental results /26/ which only allow to give upper limits of the hydrogen mass, but not the actual hydrogen production rate.

Except for the reflood scenario T28, the total hydrogen mass do not exceed those of the LOOP base case calculation (Figure 7.2 top). Generally, for MHSI cases hydrogen production rate is about two to four times higher than the base case (Figure 7.2 bottom). For LHSI cases transient oxidation starts with a peak value caused by fast reflood and levels down caused by ceasing of LHSI pumps as observed earlier /4/.

Compared to former study /4/ in which large parts of the core were heated-up by the oxidation, only the centre part of the core complies with the "shattering" conditions. Since the basic phenomena has not yet been pinpointed by the QUENCH program, this has to be assumed as the lowest possible hydrogen production during reflood. The other extreme is the not-physical global shattering option, which removes all protective oxide scales in the whole core leading to maximum possible hydrogen (such a model is used in the MAAP reflood calculations).

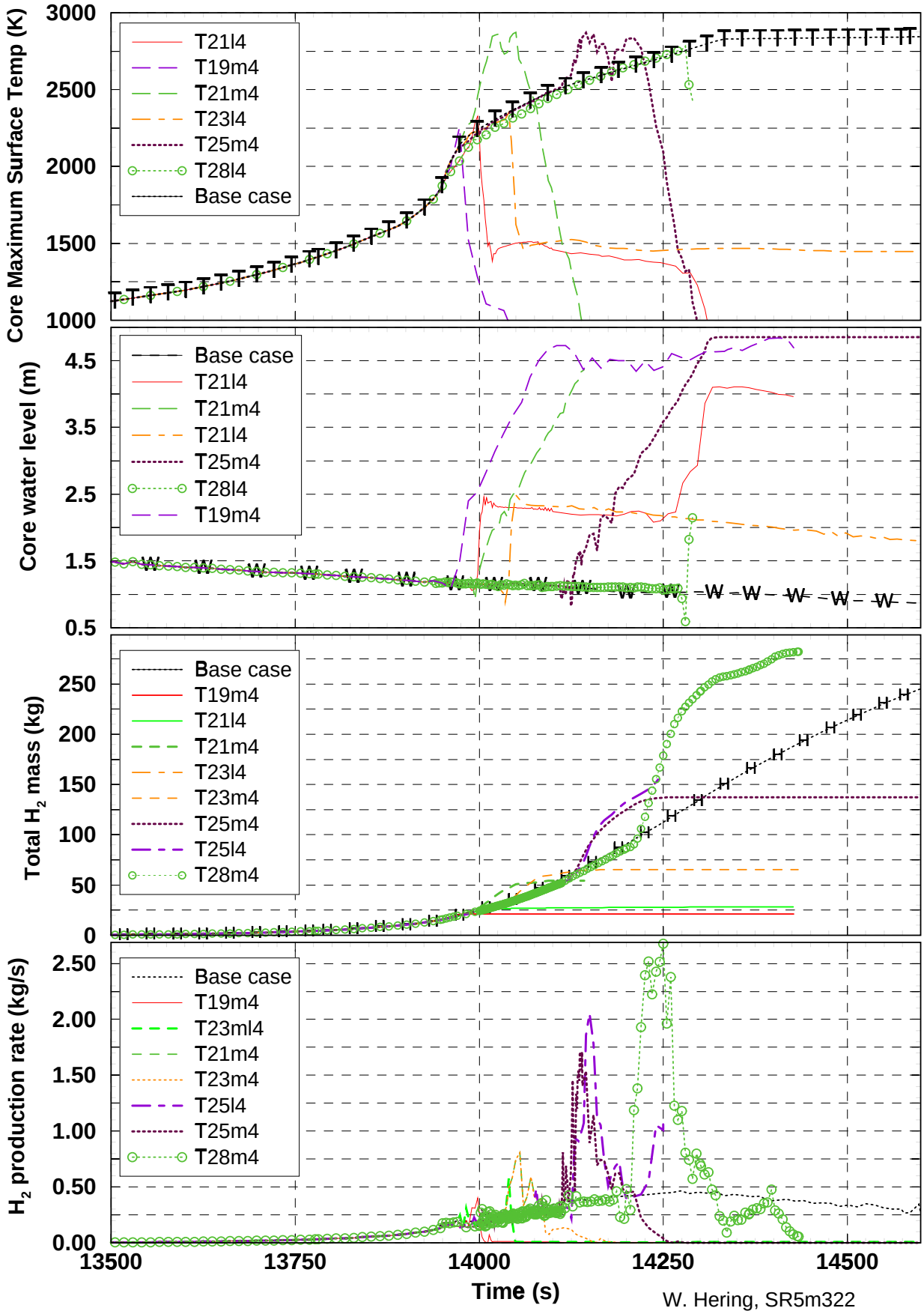

Figure 7.2 Overview of reflood scenarios: PCT history (top), core water level (below), hydrogen mass, and predicted hydrogen source term (bottom) between 1900 K and 2800 K compared to base case values (-b-).

Table 7.1 Summary of main results of reflood calculations: cool-down efficiency

	Case	**Pressure span (MPa)**		**ECC freq.**	**Core refill (>4m)**	**Calcula-tion end state**	**max PCT at time**	**Node with shatter-ing conditions** (bold: node shattered)	**Nodal shattering time**
		initial	max	-	sec	T sat	K / sec	Ring-Zone	sec
1	T19m4	0.92	3.5	1	14080	14080	2250 / 13975	r1z11	13983
2	T21l4	0.88	3.5	2	14315	14366	2325 / 14000	**r1z11 - r1z12**	14166
	T21m4	0.88	2.6	1	14123	> 14150	2865 / 14051	**r1z11, r1z12 r1z13**	**14080, 14089 14100**
3	T23ml4	0.86	3.8	3	15370	15400	2330 / 14050	r1z10 - r1z11 **r1z12**	14049 14051
	T23ml4 2nd re-flood						2340 / 15305	r2z12 r1z14, r3z13, r4z13 **r3z12**, **r4z12**	15274 15281 **15291**, **15294**
	T23m4	0.86	2.7	1	14184	14218	2890 / 14040	**r1z10**, **r1z12 r1z13, r1z14**	**14128, 14135 14145, 14162**
4	T25l4	0.86	2.2	4	2.7 m	> 15500	3030 / 14330	**r1z9**-z10 **r1z11, r1z12 r2z12, r3z12 r1z13, r2z13, r3z13**	**14249 14612, 14627 14640, 14646 14694- 14740**
	T25m4	0.86	3.5	1	14300	14310	2860 / 14144	**r1z9, r3z12 r1z11, r1z10 r1z12, r1z13, r2z11, r2z12, r2z13, r2z14**	**14188, 14205 14213, 14218 - 14225 14244 - 14266**
5	T28l4	0.86	2.9	---	2.1 m	failed	2795/ 14285	--	--
	T28m4	0.86	4.0	3	3.5 m	> 15000	2930 / 14275	**r3z10, r1z12 r2z10-r2z12, r1z13 r3z11, r3z12, r4z11, r2z13 r4z12, r3z13, r4z13 r4z14, r2z14, r3z14**	**14303, 14304 14309 - 14319 14395, 14409 – 14410 14414 – 14424 14440 - 14604**

Table 7.2 Summary of main results of reflood calculations: source terms

	Case	End of Calc.	Absorber rod damage	Fuel rod damage (porous debris)	Hydrogen source term	
		Time (s)	Ring, Zone Time (s)	Ring, Zone Time (s)	Rate kg/s	Total kg
1	T19m4	14080	r1, z11-13, 13996	----	0.40	21
2	T21l4	14366	r1, z11-14, 14010	----	0.57	28
	T21m4	>14150	r1, z11-14, 13987	r1, z12, 14028 r1, z11, 14104	0.80	54
3	T23ml4	15500	r1, z11-14, 13993		0.56	37
	T23ml4 2nd reflood	at 15260s	r2, z11-14, 14787 r3, z11-14, 14773 r4, z11-14, 14867	r1 z11-z12, 15337 r4, z12, 15357	0.25	81
	T23m4	14218	r1, z11-14, 13993 r2, z11-14, 14104	r1z11-z12, 14070	0.80	66
4	T25l4	>15500	r1z9-14, 14005 r2z10-14, 14130 r3z10-14, 14127 r4z11-14, 14196	r1z9-z14, 14160 r2z12-z14, 14261 r3z12-z14, 14259	2.05	137
	T25m4	14664	r1z9-z14, 13993 r2z11-14, 14104 r3z12-14, 14159	r1z9-z14, 14147 r2z11-z13, 14216	1.75	161
5	T28l4	14298	r1z8-z14, 14050 r2z9-z14, 14155 r3z9-z14, 14131 r4z9-z14, 14228	----		
	T28m4	>15000	r1z9-z14, 13993 r2z9-z14, 14104 r3z10-z14, 14159 r4z11-z14, 14238	r1z9-13, 14223 r2z9-13, 14251, r3z10-13, 14250 r4z11-14, 14262	2.7	282
	LOOP	20250			0.46	461

8 Summary and Conclusion

With the best estimate severe fuel damage code SCDAP/RELAP5 mod 3.2 accident analyses have been performed for the European Pressurised Water Reactor (EPR) scenarios such as: the surge line rupture (SL), the loss of onsite and offsite power (LOOP), and a 46 cm² small break loss of coolant accident (SBLOCA). For the LOOP scenario a series of delayed reflood cases have been calculated. The reflood initiation time was selected after onset of oxidation and before massive formation of debris in the core, in the range between 1900 K and 2800 K peak core temperature.

Generally all calculations of unmitigated accidents were performed up to contact of an in-core molten pool with the EPR specific heavy reflector (HR). At time of HR failure the code fails too, at calculation of melt relocation into the water-filled lower plenum. Actually, the simulation of the following accident phase, including estimation of fuel coolant interactions (FCI), is not possible with S/R5 mod 3.2.

Therefore, data from the end-state of the calculations were used as input for specialised codes such as MC3D (FCI) or LOWCOR2 (HR failure). The database includes the status of debris and corium in the molten pool, temperature of internal structures in core and reactor pressure vessel, as well as temperatures of primary system pipe walls. Also the hydrogen source term has been calculated for various cases of the scenarios mentioned above.

Generally, reflood calculations could be performed successfully up to 2500 K peak core temperature without large numerical difficulties. Above 2700 K (T28 scenario), however, the core damage state shows some blockages and local debris formation triggers numerical instabilities which hinders a complete calculation with cool-down to saturation temperature. Also the hydrogen production during reflood was calculated using a rather coarse simulation since the basic process is still under investigation in the QUENCH programme at Forschungszentrum Karlsruhe.

The plant calculation should be repeated if an improved code version (S/R5 mod 3.3) is available also considering new experimental results.

9 References

/1/ The SCDAP/RELAP5 Development Team: SCDAP/RELAP5/MOD 3.2 Code Manual, NUREG/CR-6150, INEL-96/0422, Idaho Fall, Idaho, USA, 1997.

/2/ Summers et al.: MELCOR Computer Code Manuals, Vol. 1 - 2 (Vers: 1.8.3), NUREG/CR-6119, SAND93-2185, March 1995. On-line: http://melcor.sandia.gov/.

/3/ MAAP4 - Modular Accident Analysis Program for LWR Power Plant - Computer Code Manual", 1-4, principal investigators, R. E. Henry, C. Y. Paik, and M. G. Plys, EPRI Research Project 3131-02, Fauske & Associates, Inc., Burr Ridge, IL (May, 1994)

/4/ Hering W., Reflood Calculations for the Projected European Pressurized Water Reactor Using SCDAP/RELAP5 mod3.1, FZKA Report 6299; December 1999. http://bibliothek.fzk.de/zb/berichte/FZKA6299.pdf

/5/ Elias E., Sanchez V.H., Hering V.; Development and validation of a transition boiling model for RELAP5/MOD3 reflood simulations, NEDEA 183 177-332 (1998).

/6/ Allison Ch., ISS, private communication, 1999.

/7/ Baumann W., Jacobs G., Lau M., Meyer L., "Druckaufbau bei spätem Fluten in einem 'Station Blackout' " Projekt Nukleare Sicherheitsforschung Jahresbericht 1996, FZKA 5963, p.182-201, Forschungszentrum Karlsruhe, 1997.

/8/ Plank, H., private communication 1999.

/9/ Plank, H., private communication 1998.

/10/ Hagen S., Hofmann P., Noack V., Sepold L., Schanz G., Schumacher G., Large Bundle PWR test CORA-7. Test results report , FZKA 6030, April 1998.

/11/ Van der Hardt P., Jones A.V., Lecomte C., Tattegrain A.:"Nuclear Safety Research: The Phebus Severe Accident Experimental Program", Nuclear Safety 35(2), 1994.

/12/ Smit S.O., Sengpiel W.: Investigation of the Phebus FPT1 Bundle Degradation Experiment with SCDAP/RELAP5, FZKA 6294, in preparation (2001).

/13/ Hering, W. Homann Ch.: Improvement of the SCDAP/RELAP5 Simulator Model with respect to the FZK QUENCH Facility, FZKA Report 6566, in preparation (2001).

/14/ Hering W., Messainguiral Ch., Sengpiel W.: Investigation of the Meltdown Behaviour of Massive Radial Core Enclosures during LWR Accidents, FZKA-Report 6315, Aug. 2000.

/15/ Haste T.J. et al.: Design Studies for FZK Degraded Core Bundle Quench Experiments, Report AEAT-1360, May 1997.

/16/ Hiles R. P. et al.: Scaling Studies and Support of FZK Bundle Quench Experiments, Report AEAT – 4484 Issue 1, November 1998.

/17/ Hering W., Homann Ch., Sanchez V.H., Accident mitigation analyses for the EPR using SCDAP/RELAP5, Jahrestagung Kerntechnik, 18.-20.5.1999, S.267-270.

/18/ Homann Ch., Hering W., Analytical Activities for the QUENCH Facility Using the Mechanistic Code System SCDAP/RELAP5, Jahrestagung Kerntechnik, 18.-20.5.1999, S.263-266.

/19/ Kronenberg J., private communication, 1999.

/20/ Sanchez V.H., "Validation of the Reflood Model Implemented in the Code RELAP5/MOD3.2.2γ the Integral Test LOFT-LP-LB-1, FZKA Report 6426, in preparation.

/21/ Cathcart J. V., et al., Zirconium Metal Water Oxidation Kinetics VI Reaction Rate Studies, ORNL/NUREG-17, August 1977.

/22/ Urbanic V.F., Heidrick T.H. , High temperature oxidation of Zircaloy-2 and Zircaloy-4 in steam, Journal of Nuclear Materials 75,(1978) pp. 251-261.

/23/ Hering W., Results of Accident analyses for the projected European Pressurized Water Reactor Using SCDAP/RELAP5 mod 3.1, PSF Report; December 2000.

/24/ Frepoli C., Hochreiter L.E., Mahaffy J., Cheung F.B., A noding sensitivity analysis using COBRA-TF and the effect of spacer grids during core reflood, ICONE-8711, Proceedings of ICONE 8, 8^{h} International Conference on Nuclear Engineering, April 2-6, 2000, Baltimore, MD, USA.

/25/ Miassoedov A., Homann P., Leiling W., Piel D., Schmidt L., Sepold L., Steinbrück M., Hering W., Homann Ch., Flooding Experiments on the Investigation of the Hydrogen Source Term (Quench Test Results), Annular Meeting on Nuclear Technology '2000, p. 203-206.

/26/ Kronenberg J., Gandrille P., Hering W., Hydrogen production during reflood of a hot PWR core, Annular Meeting on Nuclear Technology '2000, p. 207-211.

/27/ Struwe D., Jacobs H., Imke U., Krieg R., Hering W., Böttcher M., Lummer M., Malmberg T., Messemer G., Schmuck Ph., Göller B., Vorberg G., Consequence Evaluation of In-Vessel Fuel Coolant Interactions In The European Pressurized Water Reactor, FZKA Report 6316, July 1999.

/28/ Hering W., Messainguiral Chr., Sengpiel W., Investigation of the Melt-down Behaviour of Massive Radial Core Enclosures during LWR accidents, FZKA-6315, November 2000.

10 APPENDIX

Table 10.1 Detailed description of FZK code improvements used for EPR calculations

S/R5m32.irs:
Code includes error correction from AEAT and FZK and uses PSI/FZK reflood model

Date	Subroutine	Description.
Jan 15 13:06	relap/dtstep	R5 and SCD output modified
Mar 29 09:51	relap/htadv	R5 radiation pointer calculation corrected
Jan 15 13:06	scdap/scdad3	void depend. fluid temperature T fluid = T(vapour + gas)
Jan 15 13:06.	scdap/iscdap	Pointer for innermost shroud corrected (shqin/shqout)
Jan 15 13:06	scdap/scdad7	shqin/shqout corr
Mar 15 17:15	scdap/scddat	header data space increased for more materials
Mar 15 17:14	scdap/fstate	allow ZrO2 pellets for QUENCH modelling
Mar 15 17:15	scdap/heatc2	material properties for copper
Mar 08 12:55	scdap/preint	pointer corrected
Jan 15 13:05	scdap/zone.	correct bug for more than 10 axial zones, no melt leverage
Feb 24 16:24	scdap/majscd	output for fuel rod heat-up rate
Aug13 09:04	scdap/shattr	FZK/IRS improved local shattering model
Feb 24 16:24	scdap/mxctmp	calculate T_{max}, dT_{max} (average Fuel rod)
Sep24 1998	relap/iradht	wrong limitation view * area ratio
Oct 13 10:40	scdap/rscdap	delete restart limitation for radiation

Table 10.2 SBLOCA: S/R5 code error

=<wh> epr-SLP32.irs Ex5Cx5 SBLOCA wo Reflood + 2Accu 032k

core degradation event: flow through embedded flow channels in shroud component blocked at axial node 1 time= .216822E+05 s, component no. = 11
RELAP5 control volume blocked = 101020000

```
0******** Thermodynamic property error with minimum time step, transient be-
ing terminated.
0******** Trouble, last advancement being repeated with  debug printout.
0******** Thermodynamic property failure,
         volno=   51060000,   p=     2.220059E+05,  ug =   2.191192E+06,
         uf =   1.225350E+04  quala=  7.323325E-01, voidf =   3.111715E-04,
         voidg =   9.996888E-01
```

```
0******** Thermodynamic property failure,
          volno=   51060000,  p =    2.220059E+05,   ug =   2.191192E+06,
          uf =   1.225350E+04 quala = 7.323325E-01, voidf =   3.111715E-04,
          voidg =   9.996888E-01
******** Vapor phase property call had error.
******** Extrapolation error.
```

Table 10.3 Overview of RELAP5 trips used for simulation of the most relevant parts of the RCSL system

Loop1	Loop2	Aux	Sum	Explanation / Action	Conditions
				Calculation control	
Transient initiation					
100			1100	time for break initiation	***USER value***
101			1101	time for surge line valve closure	***USER value***
102			**1102**	time for loss of off-site power	***USER value***
103			1103	SIS actuation (Tcore max exceeded)	T core > 4444
104				Primary system pressure	P prim <11.0 MPa
105			**1104**	PZR water vol < 10m³	1104 == 104 AND 105
				Primary system	
Reactor scram logic					
10			***11***	Primary system pressure	t == t(p prim < 13.0 Mpa) + 0.8s
12			***13***	Pump velocity too low	t == t(pmpvel < 101.1) + 0.8s
			1021	SG 2nd side pressure too high	t == t (304 OR 305) + 0.6s
			22	2nd side pressure in SG to high	t == t(1021) + 0.6s
31	32		1030	SG 2nd side water level too low	z < 13m
1030			***35***	Delay signal 1030 for 0.6 sec	t == t (31 OR 32) + 0.6s
1011	1012		**1099**	Reactor scram setpoint summary	First of (11 -13 - 22 - 35)
Accumulator control					
111	112			Accu initiation	p prim < 0.45 Mpa
115	116			Accu empty ?	Liq vol (accu) < 0.1 m³
1111	**1112**			Accu surge line valve open	== (111 / 112)
Decay heat					
199				Start decay heat calculation	Delay signal 1099 for 0.5 sec
RCP safety					
51	52			Void at main coolant pump entrance too sma	void > 0.1 in 332 / 432
			1050	General: void at main coolant pump small	51 or 52
1603	**1604**			RCp scram: void or LOOP	1050 or 1102
Primary side pressure control					
601			1601	Close PZR surge line if watervol < 0.5 m³	PZR wter vol < 0.5 m³
620		621		Pressure level valve 824: open/close	17,6 Mpa > P > 16.6 Mpa
630		631		Pressure level valve 834: open/close	18,0 Mpa > P > 17.0 Mpa
			1625	Actuation: valve 824 open	620 or 1623
			1626	Actuation: valve 824 close	Not 1623 and not 621
			1635	Actuation: valve 834 open	630 or 1623
			1636	Actuation: valve 834 close	Not 1623 and not 631
Primary side depressurization control					
622				Core outlet vapor temperature	T_F (202, 203) > 923 K
	623			Time delay avoiding spikes for actuation	t > t(622) + 30s
			1623	Both true: long term temperature level true	622 + 623
				Secondary system	
Secondary side insulation					
302	303			Delay signal 1099 for 2.0 and 2.5 sec	
			1301	MSIV open	== not 302
			1302	Turbine valve open: Normal operation	== not 1099
			1303	Turbine valve close: Transient	== 1099
		1304	1305	MSRV open	== 1099
			1401	MFW trip from 1099	
EFWS actuation					
511				Water level SG	t > t(1099) + 2.9 sec
1525				Not actuate in case of LOOP (-1102)	511 and not 1102
	1525			Not actuate generally (User input)	511 and not 511
SG safety					
304	305			2nd side pressure in SG to high	p sec > 9.15 Mpa
1304	**1305**			Activation of 2nd side	(304 / 305) or 1104

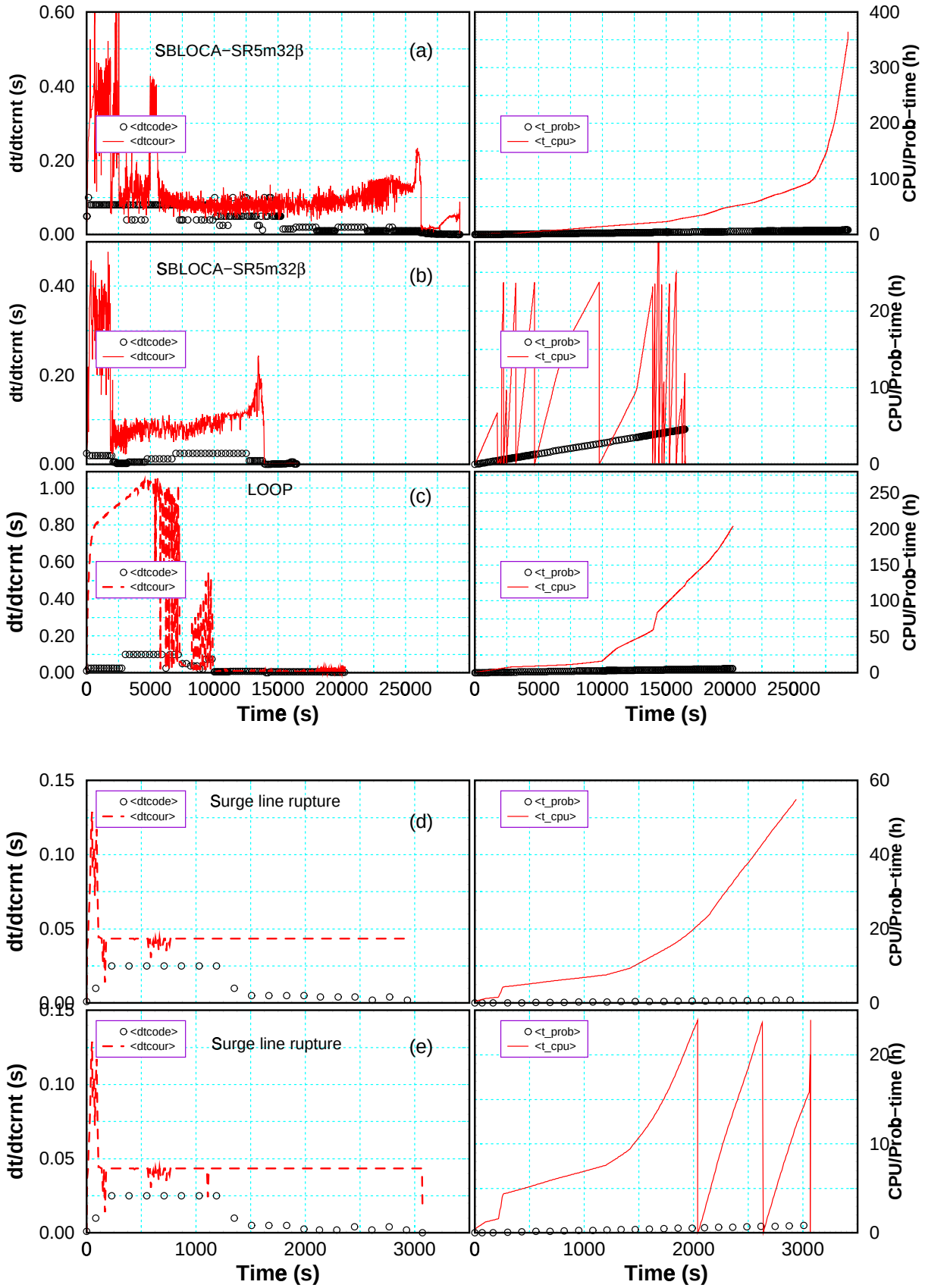

Figure 10.1 Used time step for stable calculations and Courant time step (left) and efficiency (right) for different calculations for the three scenarios SBLOCA, LOOP (top) and surge line rupture (bottom).

ACKNOWLEDGEMENT

The author would like to thank Victor Sanchez-Espinoza, Bruno Merk, Dankward Struwe, and Hermann Plank (Siemens Nuclear Power) for their thorough review of the paper and valuable suggestions.